U.S. Department
of Transportation

**Federal Railroad
Administration**

Parametric Analysis and Safety Concepts of CWR Track Buckling

Office of Research
and Development
Washington, DC 20590

G. Samavedam
A. Kish
A. Purple
J. Schoengart

DOT/FRA/ORD-93/26
DOT-VNTSC-FRA-93-25

Final Report
December 1993

This document is available to the public through the National Technical Information Service, Springfield, VA 22161

Notice

This document is disseminated under the sponsorship of the Department of Transportation in the interest of information exchange. The United States Government assumes no liability for its contents or use thereof.

Notice

The United States Government does not endorse products or manufacturers. Trade or manufacturers' names appear herein solely because they are considered essential to the objective of this report.

REPORT DOCUMENTATION PAGE

Form Approved
OMB No. 0704-0188

Public reporting burden for this collection of information is estimated to average 1 hour per response, including the time for reviewing instructions, searching existing data sources, gathering and maintaining the data needed, and completing and reviewing the collection of information. Send comments regarding this burden estimate or any other aspect of this collection of information, including suggestions for reducing this burden, to Washington Headquarters Services, Directorate for information Operations and Reports, 1215 Jefferson Davis Highway, Suite 1204, Arlington, VA 22202-4302, and to the Office of Management and Budget, Paperwork Reduction Project (0704-0188), Washington, DC 20503.

1. AGENCY USE ONLY (Leave blank)	2. REPORT DATE	3. REPORT TYPE AND DATES COVERED
	December 1993	Final Report February 1990-November 1992

4. TITLE AND SUBTITLE
Parametric Analysis and Safety Concepts of CWR Track Buckling

5. FUNDING NUMBERS
RR419/R4011

6. AUTHOR(S)
G. Samavedam*, A. Kish, A. Purple*, and J. Schoengart

7. PERFORMING ORGANIZATION NAME(S) AND ADDRESS(ES)
U.S. Department of Transportation
Research and Special Programs Administration
John A. Volpe National Transportation Systems Center
Cambridge, MA 02142

8. PERFORMING ORGANIZATION REPORT NUMBER
DOT-VNTSC-FRA-93-25

9. SPONSORING/MONITORING AGENCY NAME(S) AND ADDRESS(ES)
U.S. Department of Transportation
Federal Railroad Administration
Office of Research and Development
Washington, DC 20590

10. SPONSORING/MONITORING AGENCY REPORT NUMBER
DOT/FRA/ORD-93/26

11. SUPPLEMENTARY NOTES
*Foster-Miller, Inc.
350 Second Avenue
Waltham, MA 02154-1196
Under Contract to VNTSC

12a. DISTRIBUTION/AVAILABILITY STATEMENT
This document is available to the public through the National Technical Information Service, Springfield, VA 22161

12b. DISTRIBUTION CODE

13. ABSTRACT (Maximum 200 words)

The work reported here is part of a major investigation conducted by the Volpe National Transportation Systems Center for the Federal Railroad Administration on the thermal buckling of continuous welded rail (CWR) track in the lateral plane with the objective of developing guidelines and recommendations for buckling prevention.

This report presents results of the development and application of a personal computer (PC) software model for prediction of CWR track buckling strength. This model is based on the dynamic buckling theory previously validated by tests. The model accounts for all the important parameters influencing track buckling viz., rail size, curvature, lateral resistance,tie-ballast friction, fastener torsional resistance, track longitudinal stiffness, track vertical stiffness, misalignment amplitude and wavelength, and vehicle parameters. The sensitivity of the buckling temperatures with respect to each of the parameters is quantified, and critical parameters which strongly affect buckling strength are identified.

A basis for buckling safety evaluation is presented. An approach using the computer program for the development of safety limits in the form of allowable rail temperatures as functions of track peak lateral resistance, misalignment amplitude and curvature, is presented.

Conclusions of practical interest from the parametric study are presented.

14. SUBJECT TERMS	15. NUMBER OF PAGES
Track Buckling, Dynamic Buckling, Lateral Stability, Continuous Welded Rails, Buckling Safety Limits, Parametric Study	120
	16. PRICE CODE

17. SECURITY CLASSIFICATION OF REPORT	18. SECURITY CLASSIFICATION OF THIS PAGE	19. SECURITY CLASSIFICATION OF ABSTRACT	20. LIMITATION OF ABSTRACT
Unclassified	Unclassified	Unclassified	

PREFACE

This report presents a comprehensive study of continuous welded rail (CWR) track buckling strength as influenced by the range of all key parameters such as the lateral, torsional and longitudinal resistances, vehicle loads, etc. The work was performed under the OMNI Contract DTRS-57-89-D00009 awarded by Volpe National Transportation Systems Center (VNTSC), at Cambridge, MA. The work was done by Foster-Miller, Inc. under the technical direction of VNTSC, and sponsored by the Office of Research and Development, Federal Railroad Administration, U.S. Department of Transportation at Washington, D.C. Mr. William Paxton of FRA is in charge of this research program.

The parametric study presented here is based on the computer program jointly developed by VNTSC and Foster-Miller. The computer program is based on the dynamic buckling theory developed and validated by previous research efforts of VNTSC. On the basis of test data, the practical range of each of the parameters involved has been identified and computer runs have been made over this range to yield the buckling strength variations and the sensitivity with respect to the parameters. Critical parameters and their ranges have been evaluated through this process. Several conclusions of practical interest are drawn from this study.

SI* (MODERN METRIC) CONVERSION FACTORS

APPROXIMATE CONVERSIONS TO SI UNITS

Symbol	When You Know	Multiply By	To Find	Symbol
LENGTH				
in	inches	25.4	millimeters	mm
ft	feet	0.305	meters	m
yd	yards	0.914	meters	m
mi	miles	1.61	kilometers	km
AREA				
in^2	square inches	645.2	millimeters squared	mm^2
ft^2	square feet	0.093	meters squared	m^2
yd^2	square yards	0.836	meters squared	m^2
ac	acres	0.405	hectares	ha
mi^2	square miles	2.59	kilometers squared	km^2
VOLUME				
fl oz	fluid ounces	29.57	milliliters	ml
gal	gallons	3.785	liters	l
ft^3	cubic feet	0.028	meters cubed	m^3
yd^3	cubic yards	0.765	meters cubed	m^3
NOTE: Volumes greater than 1000 l shall be shown in m^3.				
MASS				
oz	ounces	28.35	grams	g
lb	pounds	0.454	kilograms	kg
T	short tons (2000 lb)	0.907	megagrams	Mg
TEMPERATURE (exact)				
°F	Fahrenheit temperature	5(F-32)/9 or (F-32)/1.8	Celcius temperature	°C
ILLUMINATION				
fc	foot-candles	10.76	lux	l
fl	foot-Lamberts	3.426	candela/m^2	cd/m^2
FORCE and PRESSURE or STRESS				
lbf	poundforce	4.45	newtons	N
psi	poundforce per square inch	6.89	kilopascals	kPa

APPROXIMATE CONVERSIONS FROM SI UNITS

Symbol	When You Know	Multiply By	To Find	Symbol
LENGTH				
mm	millimeters	0.039	inches	in
m	meters	3.28	feet	ft
m	meters	1.09	yards	yd
km	kilometers	0.621	miles	mi
AREA				
mm^2	millimeters squared	0.0016	square inches	in^2
m^2	meters squared	10.764	square feet	ft^2
m^2	meters squared	1.195	square yards	ac
ha	hectares	2.47	acres	mi^2
km^2	kilometers squared	0.386	square miles	
VOLUME				
ml	milliliters	0.034	fluid ounces	fl oz
l	liters	0.264	gallons	gal
m^3	meters cubed	35.71	cubic feet	ft^3
m^3	meters cubed	1.307	cubic yards	yd^3
MASS				
g	grams	0.035	ounces	oz
kg	kilograms	2.202	pounds	lb
Mg	megagrams	1.103	short tons (2000 lb)	T
TEMPERATURE (exact)				
°C	Celcius temperature	1.8C + 32	Fahrenheit temperature	°F
ILLUMINATION				
lx	lux	0.0929	foot-candles	fc
cd/m^2	candela/m^2	0.2919	foot-Lamberts	fl
FORCE and PRESSURE or STRESS				
N	newtons	0.225	poundforce	lbf
kPa	kilopascals	0.145	poundforce per square inch	psi

* SI is the symbol for the International System of Units

(Revised January 1992)

TABLE OF CONTENTS

TABLE OF CONTENTS (Continued)

Section **Page**

LIST OF ILLUSTRATIONS

LIST OF ILLUSTRATIONS (Continued)

LIST OF TABLES

LIST OF SYMBOLS AND ABBREVIATIONS

x	longitudinal distance from center of track
E	Young's modulus
A	rail cross-sectional area
I_{zz}	rail area moment of inertia about vertical axis
I_{yy}	rail moment of inertia about horizontal axis
ΔT	rail temperature increase (above the stress-free temperature)
$\Delta T_{B,MIN}$	lower critical temperature increase (above the stress-free temperature)
$\Delta T_{B,MAX}$	upper critical temperature increase (above the stress-free temperature)
ΔT_P	progressive buckling temperature increase (above the stress-free temperature)
w	lateral deflection
u	axial displacement in the buckled zone
U	axial displacement in the adjoining zone
v	vertical deflection
F	lateral resistance force
F_o	constant lateral resistance
F_P	peak lateral resistance
F_L	limiting lateral resistance
$2L$	buckling length
$2L_o$	length of initial misalignment
δ_o	initial misalignment amplitude
K_v	track modulus (units: lb/in.^{2} abbreviated as psi)
k_f	longitudinal stiffness
L/V	ratio of lateral to vertical load
α	coefficient of thermal expansion
μ_f	friction coefficient between ties and ballast
μ_1	stiffness parameter for lateral resistance
μ_2	stiffness parameter for lateral resistance
μ	stiffness parameter for torsional resistance
T	temperature
τ_o	torsional stiffness of track
$\bar{\tau}_o$	torsional stiffness per fastener
θ	rotation angle
Ω	energy required to buckle the track

LIST OF SYMBOLS AND ABBREVIATIONS (Continued)

A_m, a_m	numerical coefficients
b_m, c_m	numerical coefficients
$\bar{P}$	force in rails
Q	self weight
R	radius of curvature
R_V	ballast reaction force
V	vertical wheel load
V_1, V_2	strain energies
W	work done against resistance forces

EXECUTIVE SUMMARY

The increased utilization of continuous welded rail (CWR) tracks in the United States has resulted in a large number of accidents attributable to train derailments induced by thermal buckling of railroad tracks. In an effort to improve the safety of CWR tracks, experimental and analytic investigations were conducted by the Volpe National Transportation Systems Center (VNTSC) supporting the safety mission of the Federal Railroad Administration (FRA). These investigations included the development of a dynamic buckling theory which accounts for both thermal and vehicle effects in the evaluation of track stability. This theory has been used in the development of a PC-based software. This software can be used as an "expert" system by the railroad industry.

The computer program accounts for all the important parameters influencing the track buckling and provides a valuable tool for the generation of safety limits. The parameters include rail size, track curvature, lateral, longitudinal and torsional resistances, tie-ballast friction coefficient, track vertical stiffness, misalignment amplitude and wavelength, and vehicle loads and truck center spacing. A parametric study has been performed varying one parameter at a time, and fixing other parameters at their nominal values. Using the parametric study, the parameters are classified into primary and secondary groups, the primary group representing the most significant parameters that can be "controlled" in revenue service for buckling safety, and which can be used conveniently in the preparation of safety limits.

The report presents a basis for the safety evaluation and a procedure for the presentation of computer results in the form of safety limits for use by the industry. Alternative safety formulations are also briefly discussed, and the most promising approach is selected. A dynamic margin of safety of 10°F is recommended to give maximum flexibility to the railroad industry.

1. INTRODUCTION

Increased utilization of continuous welded rail (CWR) tracks and recent trends toward high speeds and heavier axle loads will require rigorous evaluation of track buckling safety under a wide range of track parameters. Significant experimental and analytic investigations have been carried out by the Volpe National Transportation Systems Center (VNTSC) supporting the safety mission of the Federal Railroad Administration (FRA). The VNTSC major research investigations include:

1. Development of a rigorous dynamic buckling model which accounts for all the important parameters.

2. Validation of the theory by carefully planned and controlled field tests.

3. Development of PC-based software for prediction of CWR track buckling strength, to be used as an expert system by the industry.

4. Development of safety concepts and specifications, generated by means of the computer software.

Research work on Items 1 and 2 was completed and presented in previous reports [1-4]. PC-based software for CWR track buckling evaluation has also been completed, and an interface to enable its use as an expert system has been developed. The computer software has the following features:

- It applies to tangent and curved tracks.

- Lateral alignment defects are included.

- It accounts for any nonlinearity in the lateral resistance. The individual contributions of tie bottom, crib and shoulder to the lateral resistance become important in the model.

- Linear or nonlinear torsional resistance can be incorporated.

- Linear or nonlinear longitudinal resistance can be incorporated.

- It considers vehicle load influences, and accounts for lateral resistance loss or variation under the cars. Car parameters such as truck center spacing and wheel loads are included as are track modulus and "tie-ballast friction" coefficient.

- It calculates the external energy required for an explosive (sudden) buckle and thus indicates the potential risk of buckling at a given rise in rail temperature.

- It can be run on a PC, with simple user-friendly inputs. It can be operated as an expert system, requiring no knowledge of the theoretical equations involved. The program has default options, and automatically supplies input not provided by the operator.

- The output can be in the form of buckling response curves, with printout of upper and lower buckling temperatures, energy and risk factors.

- Within the limitations of the physical assumptions, the model is extremely accurate, relying on differential equations and fast converging Fourier series solution.

This report deals with the safety concepts and specifications developed on the basis of numerical data generated using the computer program. The specific objectives of the report are presented here:

- Perform a parametric study using the computer program and validate the range of applicability of the program with respect to the input parameters.

- Quantify the sensitivity of the buckling temperatures/deflections with respect to the parameters.

- Identify critical or primary parameters which must be user defined and the secondary parameters which can be assumed at default values if not specified by the user.

- Develop a database for practical ranges of primary parameters. Use this data for safety specification charts.

2. CWR TRACK BUCKLING THEORY AND PARAMETERS

The purpose of this section is:

- To present theoretical concepts of the primary buckling mechanisms.
- To summarize the relevant equations and relationships involved in the theory.
- To identify key parameters and the mathematical idealizations used for their representation.
- To provide a theoretical basis for the evaluation of critical temperatures, radial breathing of curves, and the external energy required for precipitating buckling of the CWR track.

2.1 Buckling Mechanism

Several buckling mechanisms were presented in [1]. The most important mechanism analyzed here assumes that the buckling of the CWR track occurs in the lateral plane under the combined influence of vehicle and thermal loads. The tendency of the track to buckle laterally due to thermal loads is opposed by its lateral resistance (i.e., resistance offered by the ballast to tie lateral displacement) and also by the torsional resistance (generated in the fasteners holding the rail to ties). In addition the longitudinal resistance of the rail fasteners (resisting the relative longitudinal movement of rail with respect to ties) is also an important factor contributing to the track buckling strength (Figure 2-1).

Vehicle wheel loads influence the lateral buckling in two ways. The lateral wheel loads generated in curving or negotiation of rail lateral irregularities tend to move the track laterally. The vertical wheel loads produce nonuniform pressure on ties and thus change the distribution of the track lateral resistance. The tie bottom resistance increases at locations near the wheels and of course directly under the wheels. At some distance away from wheels, the lateral resistance can decrease from the original "static" values of the track with no vehicles. In fact, in some situations there can be "uplift" of the track, resulting in a total loss of the base friction. The central uplift zone occurring between the two trucks of the car is particularly vulnerable to buckling. Even without complete uplift, there will be significant loss of lateral resistance in this zone (Figure 2-2).

The vehicle lateral load is small at low speeds and L/V (the ratio of lateral to vertical loads) does not generally exceed 0.7 at such speeds. It has been previously shown [1] that the effect of such L/V on track buckling is small, although L/V may contribute to the generation and growth of misalignments.

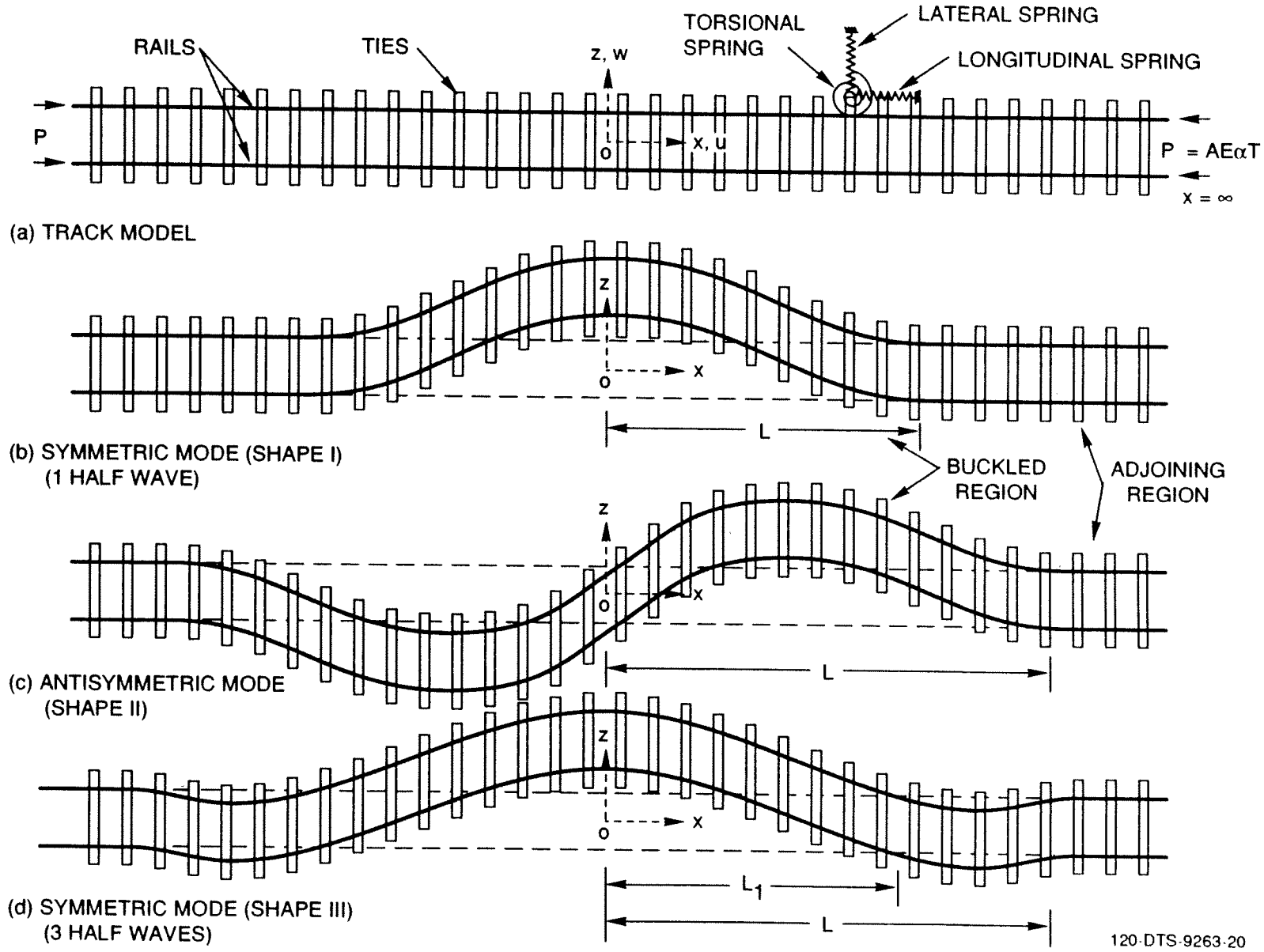

Figure 2-1. CWR Track Model and Possible Buckling Modes

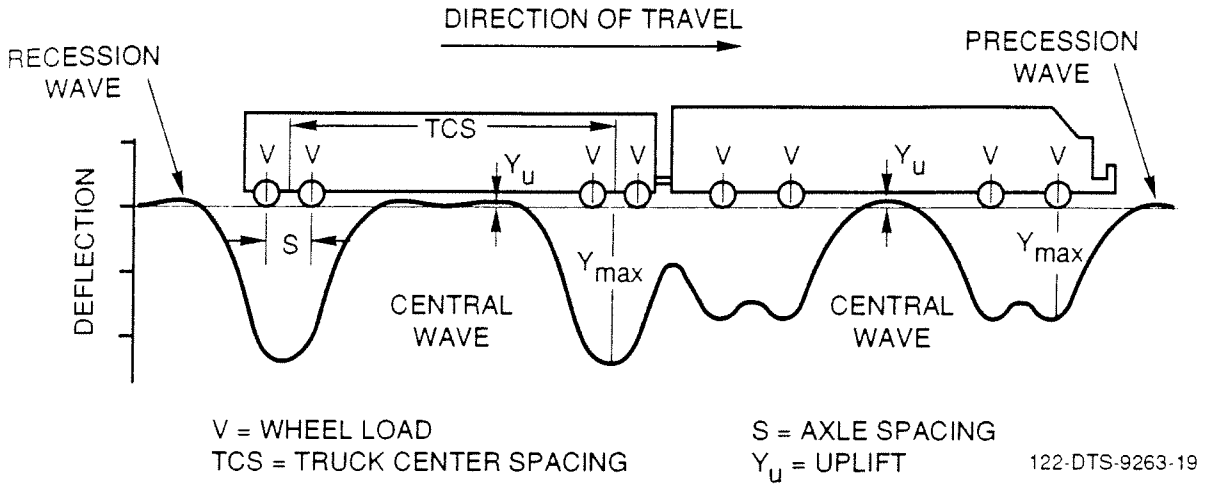

Figure 2-2. Uplift Phenomenon Under Vehicle Loads

Buckling Modes

Lateral buckling of CWR tracks can occur in symmetric or antisymmetric modes as illustrated in Figure 2-1. The resulting mode of buckling depends on the shape of the initial lateral misalignment. For symmetric misalignments, the tangent track tests conducted to date mostly showed Shape III buckling modes, whereas curved tracks showed Shape I modes. Calculations [6] have shown that the differences in buckling temperatures for all the modes are small. Shape I mode is assumed in the parametric study presented here as it simplifies the mathematical formulation.

2.2 Buckling Response Characteristic

The determination of track buckling response (temperature rise versus the lateral displacement) is carried out with the following steps:

1. Determine the vertical pressure increment/decrement on ties using the beam on elastic foundation theory, taking into account the rail size, the track foundation vertical stiffness, the vertical wheel loads and the axle and truck center spacing. The self weight of the track should also be taken into account.

2. Determine the lateral resistance distribution after accounting for the new tie bottom friction resulting from vertical load variation determined in Step 1.

3. Apply the nonlinear buckling theory [7] to determine the relationship between the temperature rise and the lateral displacement. The application of the buckling theory requires rail lateral moment of inertia, rail area, modulus of rail steel, initial track misalignments in terms of wavelength and amplitude, and idealized lateral, torsional and longitudinal resistances. In the case of curved tracks, the radius of curvature will also be a major input parameter.

4. Plot the relationship between the temperature rise and the lateral displacement which will yield a curve such as the one shown in Figure 2-3.

The buckling response characteristic shows two critical temperatures, in general. The upper critical buckling temperature $T_{B,MAX}$ represents a track position stable in the infinitesimal sense, i.e., with zero disturbance or energy input, the track will buckle out to the position C, which is stable. On the other hand, the track will buckle from position A into position S only with sufficient external energy input. Hence the minimum possible buckling temperature increase is $T_{B,MIN}$. The absolute temperatures are of course determined by the sum of the critical temperature rise and the rail neutral temperature (T_N, the force or stress free rail temperature). Clearly the two critical temperatures, the rail neutral temperature, and the energy required to buckle the track need to be included in the development of safety limits for CWR track buckling.

Progressive Buckling

In some extreme cases of weak CWR track, the buckling response can degenerate into the form shown in Figure 2-4, in which the two critical temperatures coalesce into one, which will be represented by T_P. The safety limit of such a track will be expressed in terms of T_P, and the track response temperature rise will be a progressive growth in lateral displacement, in contrast to the "explosive" response characteristic defined in Figure 2-3.

2.3 Buckling Theory

The equation to analyze the lateral stability of continuous welded rail (CWR) track can be derived by applying the principle of minimum potential energy [5,6]. Through the use of variational calculus, the equations of equilibrium are presented in the form of two highly nonlinear differential equations

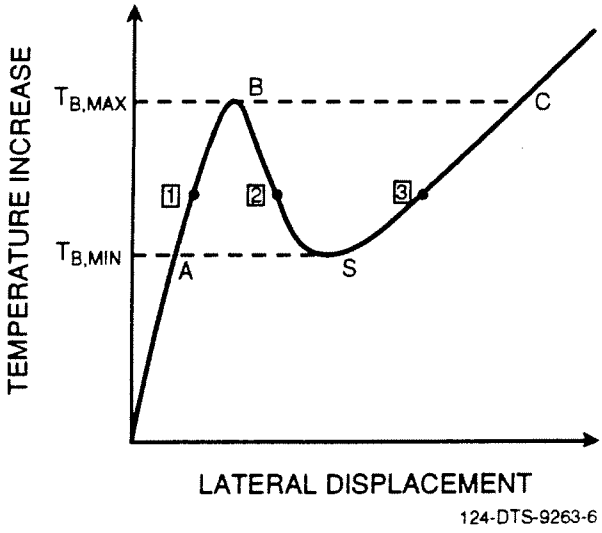

Figure 2-3. Typical Buckling Response

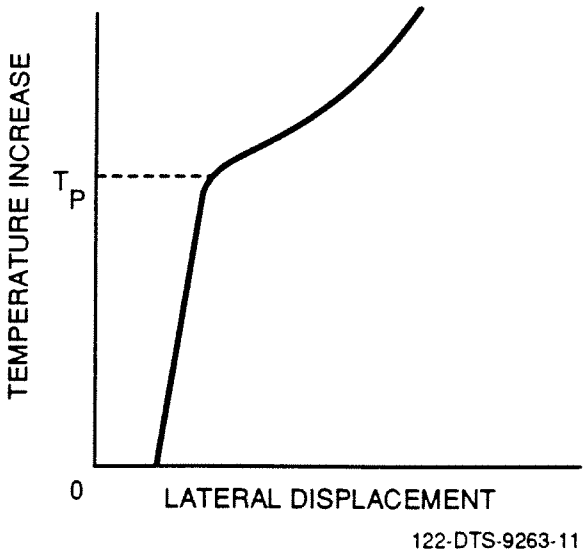

Figure 2-4. Progressive Buckling Response

for both tangent and curved tracks [6]. These differential equations become tractable by separating the infinite track domain into two regions: (1) a buckled zone where longitudinal displacement is neglected and (2) an adjoining zone that extends to infinity where lateral displacement is neglected (Figure 2-5). The equation for the two regions are coupled through another equation, which yields the temperature. For an assumed buckled length, 2L, the temperature increase, the lateral track deflection, and the compressive force in the rails can be calculated through the solution of the following differential equations.

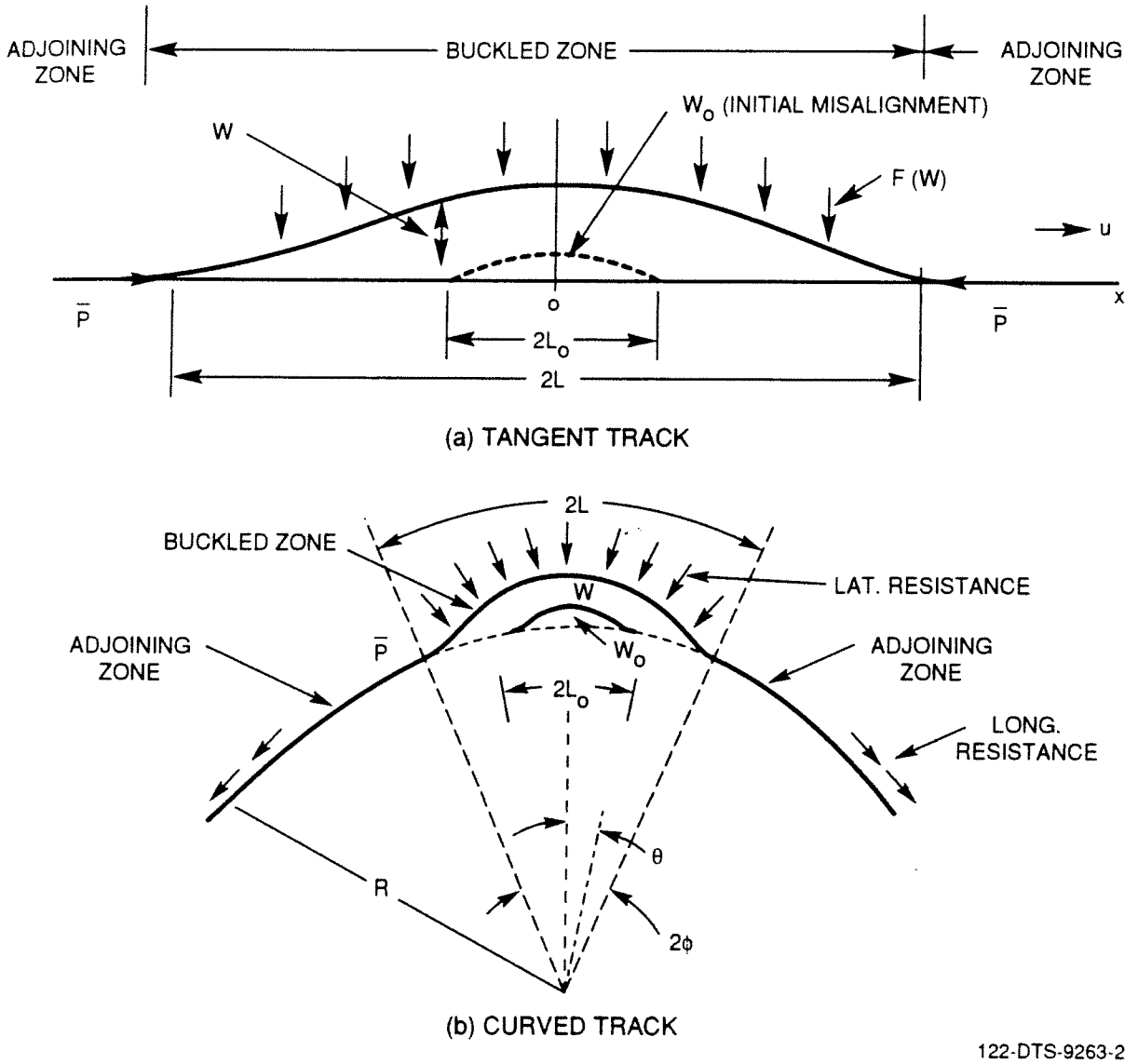

Figure 2-5. Geometry and Coordinates

Differential Equations

The governing differential equation in the buckled zone ($0 \le x \le L$) for tangent track is:

$$EI_{zz}\frac{d^4w}{dx^4}+\left(\overline{P}-\tau_o\right)\frac{d^2w}{dx^2}=-F[w(x)]-\overline{P}\frac{d^2w_o}{dx^2} \tag{1}$$

where E is the modulus of elasticity, I_{zz} is the area moment of two rails for lateral bending (i.e., about the vertical axis), $\overline{P}$ is the longitudinal force in the rails, F[w(x)] is the lateral resistance distribution function, τ_o is the linear torsional stiffness of fasteners (both the lateral resistance and the torsional stiffness are expressed here in terms of unit track length), w_o is the initial imperfection distribution, and w is the deflection in the lateral direction. The solution of this differential equation can be expressed in terms of an infinite trigonometric series as shown in References [1,6].

$$w(x)=\sum_{m=1,3,5,\ldots}^{\infty}A_m\cos\left(\frac{m\pi x}{2L}\right) \tag{2}$$

$$\frac{d^2w_o}{dx^2}=\sum_{m=1,3,5,\ldots}^{\infty}b_m\cos\left(\frac{m\pi x}{2L}\right) \tag{3}$$

$$F[w(x)]=\sum_{m=1,3,5,\ldots}^{\infty}a_m\cos\left(\frac{m\pi x}{2L}\right) \tag{4}$$

where,

$$A_m=\frac{-\left(a_m+\overline{P}b_m\right)}{EI_{zz}\left(\frac{m\pi}{2L}\right)^4-\left(\overline{P}-\tau_o\right)\left(\frac{m\pi}{2L}\right)^2} \tag{5}$$

The foregoing expressions satisfy the requirements of zero deflection, and curvature at the ends of the buckled zone. In addition, the zero slope condition will be satisfied by stipulating

$$\sum_{m=1,3,5,\ldots}^{\infty}mA_m\sin\left(\frac{m\pi}{2}\right)=0 \tag{5.1}$$

The foregoing equation which is solved by an iteration scheme, gives the relationship beween the assumed buckling length L, and the compressive load, $\overline{P}$.

The longitudinal resistance is assumed to be proportional to the longitudinal displacement. The governing differential equation in the adjoining zone (x>L) is derived from equilibrium considerations in the longitudinal direction. Thus, if proportional longitudinal resistance is assumed, then the differential equation in the adjoining zone is:

$$AE\frac{d^2U}{dx^2} = k_f U \tag{6}$$

where A is the cross sectional area of two rails, E is the modulus of elasticity, k_f is the slope of the longitudinal resistance versus longitudinal displacement curve i.e., longitudinal resistance stiffness, and U is the longitudinal displacement. The solution to this equation is:

$$U(x) = C_1 e^{\psi x} + C_2 e^{-\psi x}$$

where

$$\psi^2 = \frac{k_f}{AE} \tag{7}$$

However, the solution must be bounded for very large values of x. Then, U = U' = 0 in the limit as x approaches infinity, and $C_1 = 0$. Then after differentiation,

$$U'(x) = -\psi C_2 e^{-\psi x}$$

or

$$U' = -\psi U \tag{8}$$

The governing differential equation in the buckled zone ($0 \le \theta \le \phi$) for curved track is:

$$\frac{EI_{zz}}{R^4}\frac{d^4w}{d\theta^4} + \frac{(\overline{P} - \tau_o)}{R^2}\frac{d^2w}{d\theta^2} = -F[w(\theta)] + \frac{\overline{P}}{R} - \frac{\overline{P}}{R^2}\frac{d^2w_o}{d\theta^2} \tag{9}$$

As in the tangent case, the solution to this equation can be expressed in terms of an infinite trigonometric series:

$$w(\theta) = \sum_{m=1,3,5,\ldots}^{\infty} A_m \cos\left(\frac{m\pi\theta}{2\phi}\right) \tag{10}$$

$$\frac{\bar{P}}{R^2}\frac{d^2 w_o}{d\theta^2} = \sum_{m=1,3,5,\ldots}^{\infty} b_m \cos\left(\frac{m\pi\theta}{2\phi}\right) \tag{11}$$

$$F[w(x)] = \sum_{m=1,3,5,\ldots}^{\infty} a_m \cos\left(\frac{m\pi\theta}{2\phi}\right) \tag{12}$$

$$\frac{\bar{P}}{R} = \sum_{m=1,3,5,\ldots}^{\infty} \frac{\bar{P}}{R} c_m \cos\left(\frac{m\pi\theta}{2\phi}\right) \tag{13}$$

where,

$$A_m = \frac{-\left(a_m - \frac{\bar{P}}{R}c_m + \frac{\bar{P}}{R^2}b_m\right)}{\frac{EI_{zz}}{R^4}\left(\frac{m\pi}{2\theta}\right)^4 - \left(\frac{\bar{P}-\tau_o}{R^2}\right)\left(\frac{m\pi}{2\theta}\right)^2} \tag{14}$$

The foregoing equations satisfy zero deflection and curvature requirements at the ends of the buckled zone. An equation similar to that of 5.1 satisfying the zero slope condition relates the compressive force $\bar{P}$ to the assumed buckling length, L.

The differential equation of longitudinal equilibrium that applies to the adjoining zone ($\theta > \phi$) for the curved track case, again assuming proportional longitudinal resistance is:

$$\frac{AE}{R^2}\frac{d^2 U}{d\theta^2} = k_f U \tag{15}$$

Recall that $L = R\phi$ and $x = R\theta$. Thus the general solution to this equation is:

$$U(\theta) = C_3 e^{R\psi\theta} + C_4 e^{-R\psi\theta}$$

where

$$\psi^2 = \frac{k_f}{AE} \tag{16}$$

The function F in Equations (1) and (9) represents the lateral resistance. As shown in Section 3, three different idealizations are considered. In all these idealizations, F can be expressed as:

$$F = F_P F(w) \tag{17}$$

where F_P is the peak value which can be a function of x and $F(w)$ is the functional dependency on the lateral displacement w.

For the case where vehicle loading (dynamic case) is present, the peak resistance is a function of the longitudinal distance along the track:

$$F_{P(dynamic)}=\begin{cases}[F_P-\mu_f Q] & \text{for uplift}\\ [F_P+\mu_f R_v(x)] & \text{otherwise}\end{cases} \tag{18}$$

where F_P is the peak value of static lateral resistance, μ_f is the tie-ballast coefficient of "friction", Q is the self weight of the track, and $R_v(x)$ is the ballast vertical reaction to the vehicle wheel loads on the track. The vertical reaction can be calculated from classical beam on elastic foundation theory as shown later. Uplift occurs when the sum of the vertical deflection and the self weight of the track is less than zero, or mathematically, when $[Q+R_v(x)]<0$.

The Fourier coefficient that accounts for the effect of lateral resistance on the track, a_m, is derived from the following integral:

For tangent track:

$$a_m = \frac{2}{L}\int_0^L F[w(x)]\cos\left(\frac{m\pi x}{2L}\right)dx \tag{19}$$

For curved track:

$$a_m = \frac{2}{\phi}\int_0^{\phi} F[w(\theta)]\cos\left(\frac{m\pi\theta}{2\phi}\right)d\theta \tag{20}$$

For complex representation of $F(w)$, the integrals are evaluated using Filon's integration scheme. If the lateral resistance function F[w(x)], is a constant value, F_o, then this integral can be evaluated in closed form:

$$a_m = \frac{4F_o}{m\pi}\sin\left(\frac{m\pi}{2}\right) \tag{21}$$

The Fourier coefficient that accounts for the effect of initial imperfection in the track, b_m, is derived from the following integral:

For tangent track:

$$b_m = \frac{2}{L}\int_o^{L'} \frac{d^2 w_o}{dx^2}\cos\left(\frac{m\pi x}{2L}\right)dx \tag{22}$$

where,

$$L' = \begin{Bmatrix} L & \text{if } L \le L_o \\ L_o & \text{if } L > L_o \end{Bmatrix}$$

and

L_o = misalignment half-wavelength

For curved track:

$$b_m = \frac{2}{\phi}\int_o^{\phi'} \frac{d^2 w_o}{d\theta^2}\cos\left(\frac{m\pi\theta}{2\phi}\right)d\theta \tag{23}$$

where,

$$\phi' = \begin{Bmatrix} \phi & \text{if } \phi \le \phi_o \\ \phi_o & \text{if } \phi > \phi_o \end{Bmatrix}$$

The initial imperfection shape is assumed as a fourth degree polynomial:

$$w_o(x) = \delta_o\left[1 - 2\left(\frac{x}{L_o}\right)^2 + \left(\frac{x}{L_o}\right)^4\right] \tag{24}$$

where δ_o is the "offset" or the misalignment amplitude and $2L_o$ is the length over which the misalignment occurs. For the imperfection shape shown above, evaluation of equation (22) results in the following:

For $L \le L_o$

$$b_m = -\frac{16\delta_o}{m\pi L_o^2}\left\{1 - 3\left(\frac{L}{L_o}\right)^2\left[1 - 2\left(\frac{2}{m\pi}\right)^2\right]\right\}\sin\left(\frac{m\pi}{2}\right) \tag{25}$$

For $L>L_o$

$$b_m = -\frac{16\delta_o}{m\pi L_o^2}\left\{-6\left(\frac{L}{L_o}\right)\left(\frac{2}{m\pi}\right)\cos\left(\frac{m\pi L_o}{2L}\right)+2\left[-1+3\left(\frac{2L}{m\pi L_o}\right)^2\right]\sin\left(\frac{m\pi L_o}{2L}\right)\right\} \tag{26}$$

For $\phi \le \phi_o$

$$\frac{b_m}{R^2} = -\frac{16\delta_o}{m\pi L_o^2}\left\{1-3\left(\frac{L}{L_o}\right)^2\left[1-2\left(\frac{2}{m\pi}\right)^2\right]\right\}\sin\left(\frac{m\pi}{2}\right) \tag{27}$$

For $\phi > \phi_o$

$$\frac{b_m}{R^2} = -\frac{16\delta_o}{m\pi L_o^2}\left\{-6\left(\frac{L}{L_o}\right)\left(\frac{2}{m\pi}\right)\cos\left(\frac{m\pi L_o}{2L}\right)+2\left[-1+3\left(\frac{2L}{m\pi L_o}\right)^2\right]\sin\left(\frac{m\pi L_o}{2L}\right)\right\} \tag{28}$$

Note that $\phi = \frac{L}{R}$ and $\phi_o = \frac{L_o}{R}$.

Also,

$$c_m = \frac{2}{\phi}\int_o^{\phi}\cos\left(\frac{m\pi\theta}{2\phi}\right)d\theta = \frac{4}{m\pi}\sin\left(\frac{m\pi}{2}\right) \tag{29}$$

Temperature Calculations

The temperature equation is derived by using continuity requirements on the longitudinal displacement between the buckled and adjoining zones. It can be shown that:

$$U(L) = -\frac{\bar{P}L}{AE} - Z + \alpha TL \tag{30}$$

$$U'(L) = -\frac{\bar{P}}{AE} + \alpha T \tag{31}$$

where L is the buckled length and Z is defined below. Using equation (8), we obtain:

$$T = \frac{\bar{P}}{AE\alpha} + \frac{Z\psi}{\alpha(1+\psi L)} \tag{32}$$

where,

$$Z = \int_0^L \left(\frac{w'^2}{2} + w' w_o' \right) dx \tag{33}$$

The equation for Z can be rewritten, after an integration by parts:

$$Z = \int_0^L \left(\frac{w'^2}{2} - w w_o'' \right) dx \tag{34}$$

The expression for Z can be expressed as an infinite series by applying Fourier analysis:

$$Z = \frac{L}{4} \sum_{m=1,3,5,\ldots}^{\infty} \left[A_m^2 \left(\frac{m\pi}{2L} \right)^2 - 2A_m b_m \right] \tag{35}$$

In a similar fashion to the tangent analysis, the temperature equation for curved track is:

$$T = \frac{\bar{P}}{AE\alpha} + \frac{ZR\psi}{\alpha(1+\psi L)} \tag{36}$$

where the equation for Z can be written as (after integration by parts and application of a Fourier series):

$$ZR = \sum_{m=1,3,5,\ldots}^{\infty} \left[\frac{2L}{m\pi R^2} A_m \sin\left(\frac{m\pi}{2} \right) + \left(\frac{m\pi}{2} \right)^2 \frac{A_m^2}{4L} - \frac{A_m b_m L}{2R^2} \right] \tag{37}$$

In the limit as R approaches infinity or as the track curvature becomes tangent, the expression for ZR approaches the expression for Z in the tangent case since b_m for the tangent case is identical to b_m/R^2 for curved. Thus, the two temperature equations also reduce to the same expression in the limiting process.

Vertical Deflection and Reaction Calculation

Quasistatic load idealization is assumed to be adequate in determining loss of resistance in the "uplift" region, which occurs due to the vertical track deformation under wheel loads. The vertical deflection can be determined using the Winkler model. The differential equation for the vertical deflection v is:

$$EI_{yy} v'''' + K_v v = \sum \delta_i (x - x_i) V_i + Q \tag{38}$$

where

EI_{yy} = combined flexural rigidity for the two rails in the vertical plane.

K_v = track foundation stiffness (assumed constant).

V_i = vertical wheel loads.

δ_i = dirac delta functions.

Q = track weight/unit length.

In this equation, the effects of vertical imperfections and the compressive load in the rails are excluded for the sake of simplicity.

After solving equation (38) under the boundary conditions $v = v' \rightarrow 0$ at infinity, one can compute the distributed foundation (tie ballast) reaction $R_v(x)$ given by:

$$R_v = K_v \cdot v(x) \tag{39}$$

2.4 Energy Required for Buckling

As stated earlier the upper buckling temperature represents stability in the infinitesimal sense requiring no external energy for snap-through explosive buckling. At temperatures lower than this, (but higher than the lower buckling temperature), the track can buckle out upon the application of a finite external energy. Thus the energy needed to cause buckling can be used as a measure of the degree of stability. This measure will be useful in the development of CWR safety limits.

Referring to Figure 2-3, the prebuckling state is represented by position (1) while the postbuckling unstable branch is represented by state (2). It is assumed that if the track can be brought into state (2), it will automatically move to state (3).

The following quantities are defined.

V_1 = strain energy in the rails at stable equilibrium position (1).

V_2 = strain energy in the rails at unstable equilibrium position (2).

W = work done against resistances by moving track from position (1) to position (2).

Ω = energy required to move track from position (1) to position (2).

By an energy balance,

$$\Omega = (V_2 - V_1) + W \tag{40}$$

The strain energy components are given by the following integrals:

$$V_1 = \frac{1}{2}\int_0^{\infty} \frac{P^2_{\infty}}{AE} dx \tag{41}$$

where

$P_{\infty} = -AE\alpha T.$

Here, for simplicity, we neglect the energy due to bending in the prebuckling state:

$$V_2 = \frac{1}{2}\int_o^{\infty} \frac{P^2}{AE} dx + \frac{EI_{zz}}{2}\int_o^{\infty}\left(\frac{d^2w}{dx^2}\right)^2 dx \tag{42}$$

In the curved track case, the longitudinal force distribution becomes:

$$P = \begin{Bmatrix} \overline{P} & \text{for } 0 \le \theta \le \phi \\ AE\left(\frac{1}{R}\frac{du}{d\theta} - \alpha T\right) & \text{for } \theta > \phi \end{Bmatrix} \tag{43}$$

The work done against the lateral and longitudinal resistances are given by the following integrals:

$$W_1 = \int_0^{\infty}\int_0^{w(x)} F[w(x)]dw\,dx \tag{44}$$

$$W_2 = \int_0^{\infty}\int_0^{u(x)} f[u(x)]du\,dx \tag{45}$$

Thus, the total work done against ballast resistance (lateral and longitudinal) is

$$W = W_1 + W_2 \tag{46}$$

The difference in strain energy is calculated from the following equation:

$$V_2 - V_1 = \frac{1}{2}\int_0^{\infty} \frac{P^2 - P^2_{\infty}}{AE} dx + \frac{EI_{zz}}{2}\int_0^{\infty}\left(\frac{d^2w}{dx^2}\right)^2 dx \tag{47}$$

This equation shows that the total strain energy is the sum of two components: one due to compressive axial force and the other due to beam bending. The evaluation of these integrals is performed with the aid of the Fourier analysis. Under the assumption of proportional longitudinal resistance, the difference in strain energy can be expressed in a "closed form":

$$V_2 - V_1 = \frac{AE}{2}\left\{\frac{\bar{P}}{AE}\left[\frac{\bar{P}}{AE}\left(L+\frac{1}{2\psi}\right)+\frac{\alpha T}{\psi}\right]-(\alpha T)^2\left(L+\frac{3}{2\psi}\right)\right\}+\frac{EI_{zz}}{64L^3}\sum_{m=1,3,5,\ldots}^{\infty}(m\pi)^4 A_m^2 \quad (48)$$

The work done against lateral resistance can be evaluated from equation (44) once the lateral resistance is expressed in terms of a mathematical function.

The work done against a linear longitudinal resistance is given by

$$W_2 = \frac{k_f}{4\psi^3}\left(\frac{\bar{P}}{AE}-\alpha T\right)^2 \quad (49)$$

Numerical examples of energy required for track buckling, derived from the computer program, are presented in Appendix A.

2.5 Radial Breathing

Radial breathing is a phenomenon in high degree weak curves which move radially outwards with temperature rise and inwards with fall of temperature. However, local buckling can still occur if the relief in the compressive load is exceeded by its build-up due to temperature increase.

To estimate the buckling potential with some prebuckling radial movement, the curved track is first treated as a complete ring under uniform external pressure and compressive load. The external pressure is due to the tie reaction which is assumed to be linearly proportional to the radial displacement. Hence the initial linear portion of the resistance characteristic is important in the evaluation of the radial breathing (Figure 2-6).

The uniform ring idealization is conservative in that it ignores the "damping effect" of the neighboring tangent track segments. Figure 2-7 shows the buckled region with a uniform prebuckling displacement.

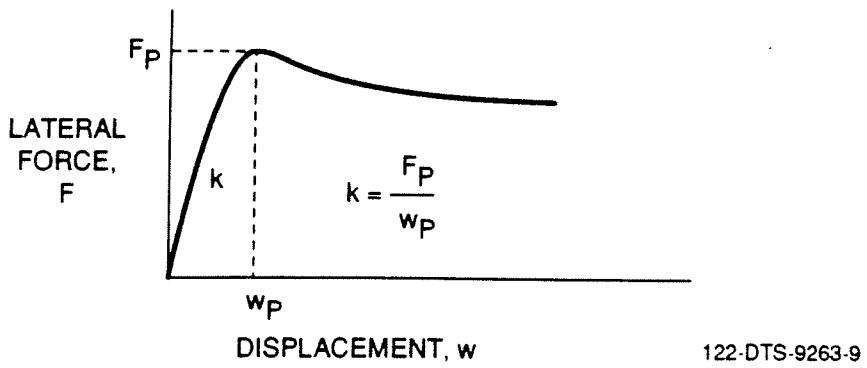

Figure 2-6. Definition of Initial Linear Stiffness of Track Resistance

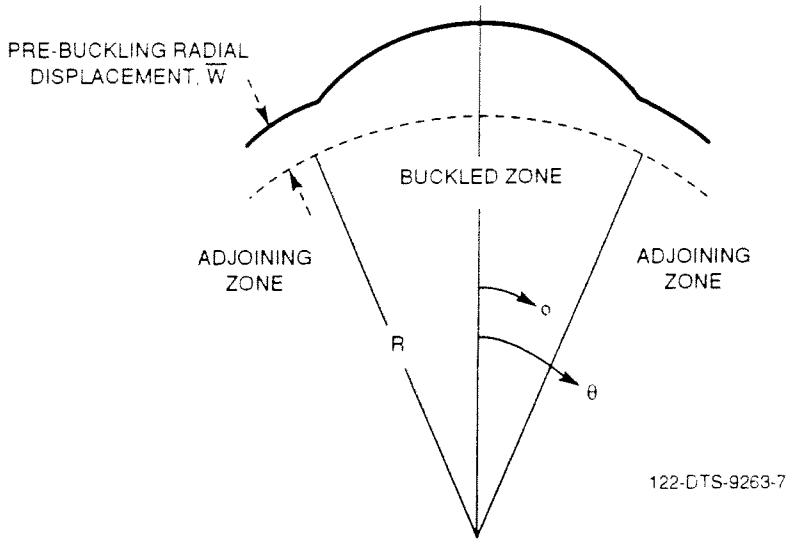

Figure 2-7. Buckling After Radial Breathing

The calculation of radial displacement $\overline{w}$ prior to local buckling is easily accomplished from the consideration of radial equilibrium of an element of track (6)

$$\frac{P}{R} = k\overline{w} \tag{50}$$

where

P = compressive load in the two rails

k = initial lateral stiffness

$$\approx F_P/w_P \tag{51}$$

Hence,

$$\overline{w} = P / Rk = \frac{P}{R}\frac{w_P}{F_P} \tag{52}$$

Since

$$P = -AE\left(\frac{\overline{w}}{R} - \alpha T\right) \tag{53}$$

$$\frac{\overline{w}}{R} = AE\alpha T \Big/ \left(AE + kR^2\right) \tag{54}$$

Following the analysis presented in subsection 2.3 it can be shown that the correction needed to incorporate the radial breathing influence on the upper and lower buckling temperatures is:

$$T = \frac{T_o}{1 - \dfrac{1}{1 + \dfrac{F_P}{w_P}\dfrac{R^2}{AE}}} \tag{55}$$

where

T_o = temperature calculated by previous analysis which neglects the radial breathing.

3. CWR TRACK BUCKLING PARAMETERS AND SENSITIVITY STUDY

The following subsections of this report describe the parameters considered in the buckling analyses and their effects on safety limits. Each of the major parameters may have "subvariables," which will be described. Through parametric studies, the effects of the individual parameters on buckling strength will be evaluated. The parametric studies are conducted using the computer codes developed by VNTSC and Foster-Miller, which incorporate the buckling theory described in Section 2. In most of the parametric sensitivity studies presented in this report, each parameter of interest is, in turn, isolated and varied through a reasonable practical range while the remaining parameters are kept at their nominal values. For later reference, the parameter ranges and nominal values used in these studies are listed in Table 3-1.

Table 3-1. Ranges and Nominal Values of Buckling Parameters

Parameter	Variable	Range	Nominal Value
Rail properties	Rail size	100#RE - 140#RE	136#RE
Curvature	Degree of curvature	Tangent - 15 deg	5 deg
Lateral resistance	Lateral resistance peak (F_P)	50 to 150 lb/in.	100 lb/in.
Tie/ballast friction	Tie/ballast friction coefficient (μ_f)	0.5 to 2.0	1.2
Torsional resistance	Torsional stiffness ($\bar{\tau}_o$)	0 to 2,000 in.-kips/rad	500 in.-kips/rad
Longitudinal resistance	Longitudinal stiffness (k_ℓ)	25 to 500 psi	200 psi
Track foundation vertical stiffness	Track foundation vertical stiffness (k_v)	2,000 to 10,000 psi	6,000 psi
Misalignments	Misalignment amplitude (δ_o)	0.5 to 1.75 in.	1.5 in.
	Misalignment wavelength ($2L_o$)	L_o = 100 to 500 in.	L_o = 180.4 in.
Vehicle parameters	Axle load	15,575 to 65,750 lb	65,000 lb
	Truck center spacing (TCS)	350 to 700 in.	506 in.

3.1 Effects of Rail Properties

The effects of the rail properties on buckling are presented in this section. The pertinent rail properties include: rail cross-sectional area; cross-sectional moments of inertia for bending in both the vertical (I_{yy}) and horizontal (I_{zz}) planes; and the track self-weight, which includes the weight of rails, ties and fasteners. These parameters are conveniently listed according to the rail size (in terms of pounds/yard) in Table 3-2. The rail size is the major variable used to study the effects of rail properties on buckling strength.

The results for the effects of rail size on buckling are shown in Figure 3-1 for rail sizes ranging from 100#RE to 140#RE. To isolate the effects of rail size, all other parameters assume their default values, as listed in Table 3-1. The results show that the upper and lower critical temperatures both decrease with increasing rail size, with the upper temperature showing the largest decrease. Although the rail bending moment of inertia increases with increasing size, the rail cross-sectional area also increases. The increase in area increases the thermal force, which offsets the corresponding increase in bending stiffness, thus reducing the overall buckling strength.

It must be stated that although small rail sections improve buckling strength, they may not be preferred in revenue service due to increased bending stress from wheel loads, thereby reducing fatigue life.

3.2 Effects of Curvature

The effects of track curvature are investigated using curves ranging from 0 deg (tangent) to 15 deg. To illustrate the influence of the lateral resistance on curved track buckling, the buckling temperatures are calculated for three cases representing tracks of varying peak lateral resistance: F_P = 75, 100 and 150 lb/in. These three cases represent weak (recently maintained), marginal, and strong (well consolidated) tracks, respectively.

Table 3-2. Typical Rail Properties

Rail (lb/yd)	Area (in.2)	Self Weight (lb/in.)	I_{yy} (in.4)	I_{zz} (in.4)
100	9.95	18.14	49.0	9.4
115	11.25	18.87	65.6	10.8
132	12.95	19.84	88.2	14.6
136	13.35	20.06	94.9	14.7
140	13.80	20.31	96.8	14.8

Note: Properties shown are for a single rail, except for self weight, which includes 2 rails, ties and fasteners.

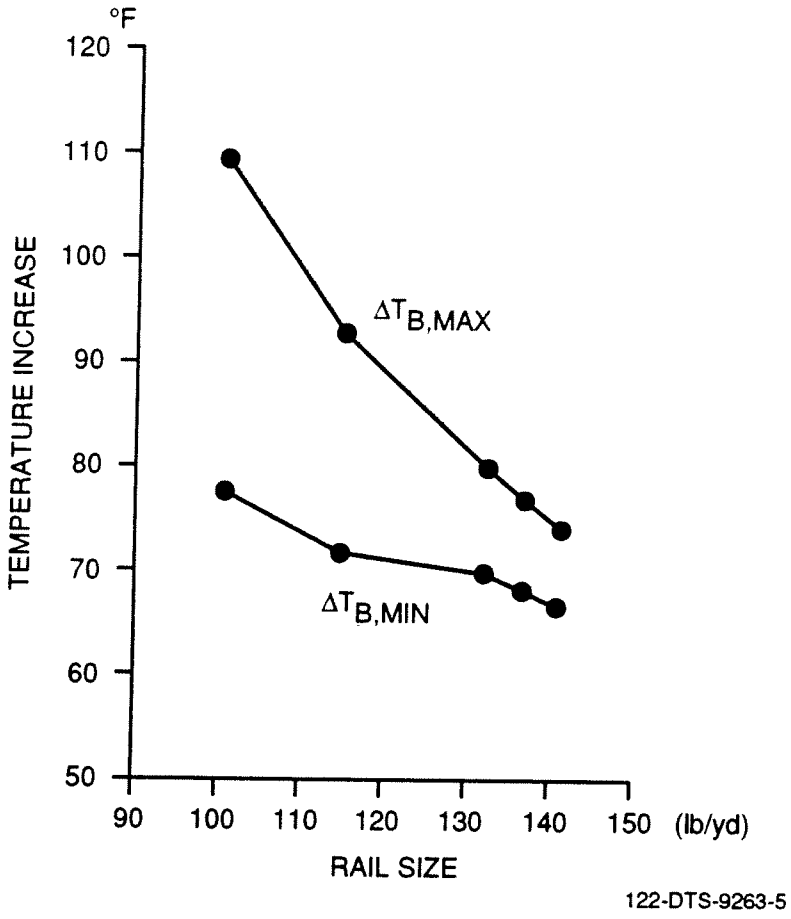

Figure 3-1. Influence of Rail Size

The results of this study are shown in Figures 3-2, 3-3 and 3-4. In each case, the results show that increasing curvature reduces both the upper and lower buckling temperatures. For high curvature tracks, or tracks with a weak lateral resistance, the buckling temperatures are drastically reduced in comparison to tangent track. It is most important to note the fact that for weak (recently maintained) tracks with $F_P = 75$ lb/in., progressive buckling can occur in curves of about 7 deg and higher. The buckling temperature increase for such tracks falls below 55°F. Such tracks are vulnerable to buckle in summer, even with a rail neutral temperature of 80°F.

Radial Breathing Effects

The above analysis takes into account radial breathing effects for high degree curves. Contrary to the prevalent thinking, radial breathing does not significantly alleviate the increased buckling potential of curved track. Figure 3-5 shows the increased buckling strength due to radial breathing of high degree curves. To obtain significant benefit of rail force reduction from radial breathing, the lateral resistance would have to be extremely low, as shown on the figure. However, a low lateral resistance is undesirable, as it does not provide sufficient resistance to lateral forces from the vehicle, and the resulting track shift due to combined vehicle and thermal loads will be excessive for safe vehicle negotiation.

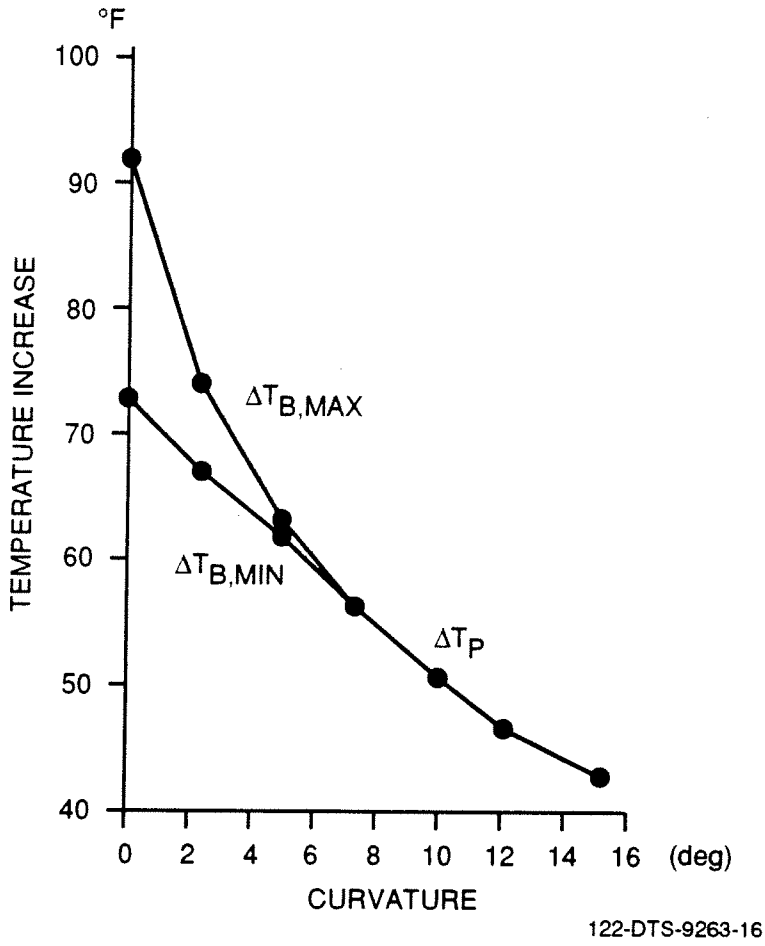

Figure 3-2. Influence of Curvature (F_P = 75 lb/in.)

3.3 Effects of Lateral Resistance

The tendency of the track to buckle laterally due to thermal loads is resisted by the ballast lateral forces exerted on the ties. Extensive experimental studies have been performed by VNTSC to characterize this lateral resistance. The preferred method of experimentally obtaining lateral resistance data is to perform a Single Tie Push Test (STPT), in which a concentrated lateral load is applied to an unanchored tie. During the push test, the force required to mobilize the tie and the resulting tie displacement are measured. Results from previous work (Appendix B) indicate that the initial force characteristic is approximately linear to a peak value (F_P) at a small displacement of the order of 0.25 in. or less, which is followed by a "spring softening" effect to a limiting resistance value (F_L), occurring at a limiting lateral deflection (w_L). This characteristic is schematically shown in Figure 3-6. Several idealizations of the lateral resistance characteristic have been investigated for computer simulation. Three of these idealized characteristics (constant, softening or drooping, and full nonlinear) are diagrammed in Figure 3-7, and are summarized below.

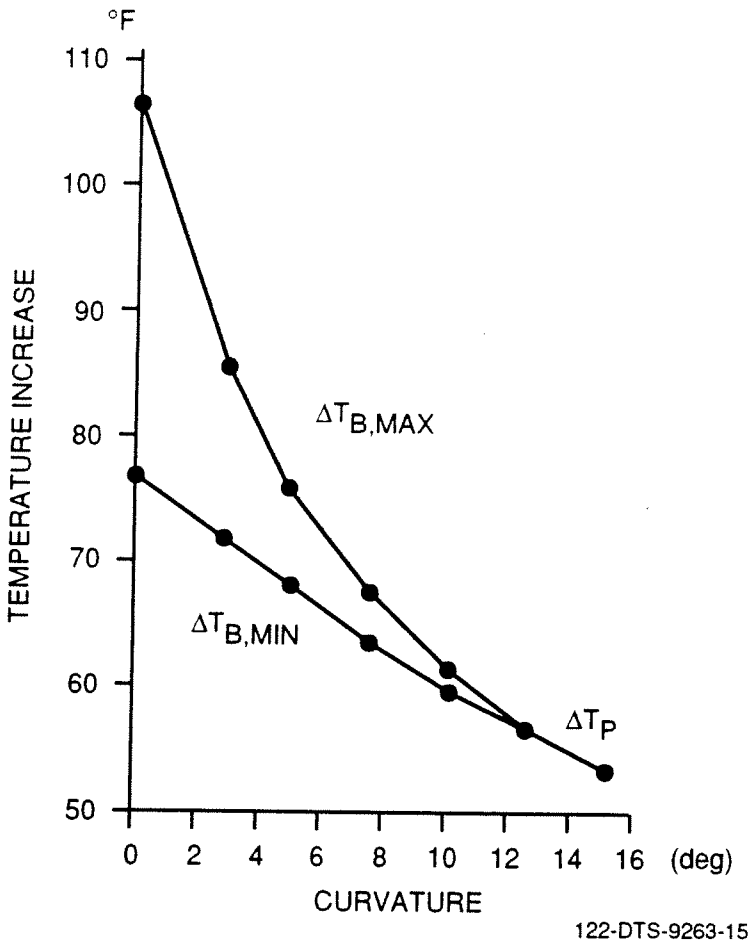

Figure 3-3. Influence of Curvature (F_P = 100 lb/in.)

Constant Lateral Resistance

This characteristic assumes a constant resistance equal to the peak resistance value,

$F = F_P$

as is shown in Figure 3-7a. This is a very crude idealization, except in the case of very weak track, and does not reflect any of the nonlinear characteristics of typical tracks.

Softening or Drooping Lateral Resistance

This idealization, shown in Figure 3-7b assumes an exponential decay from an initial peak value, F_P, to a limiting value, F_L as given by

$F = F_P [k + (1-k) \exp(-\mu_2 w)]$

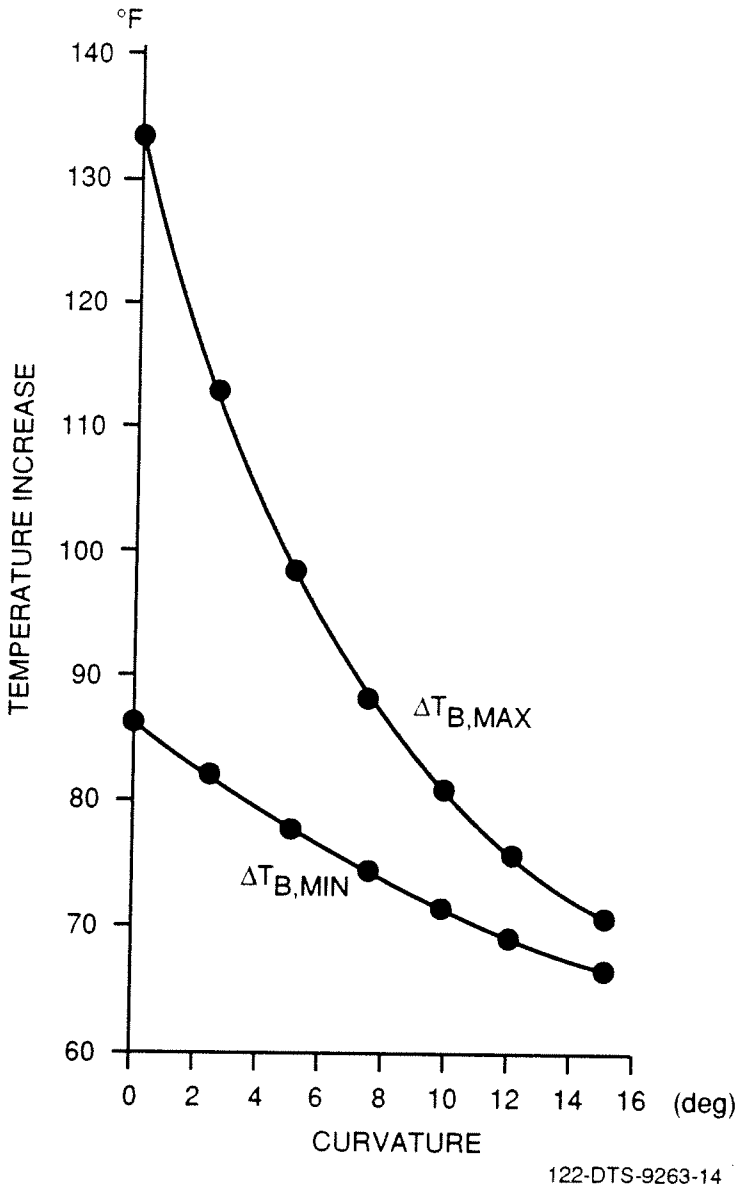

Figure 3-4. Influence of Curvature (F_P = 150 lb/in.)

where

$k = F_L/F_P$
$\mu_2 = 4/w_L$
w_L = deflection at which limiting resistance is reached

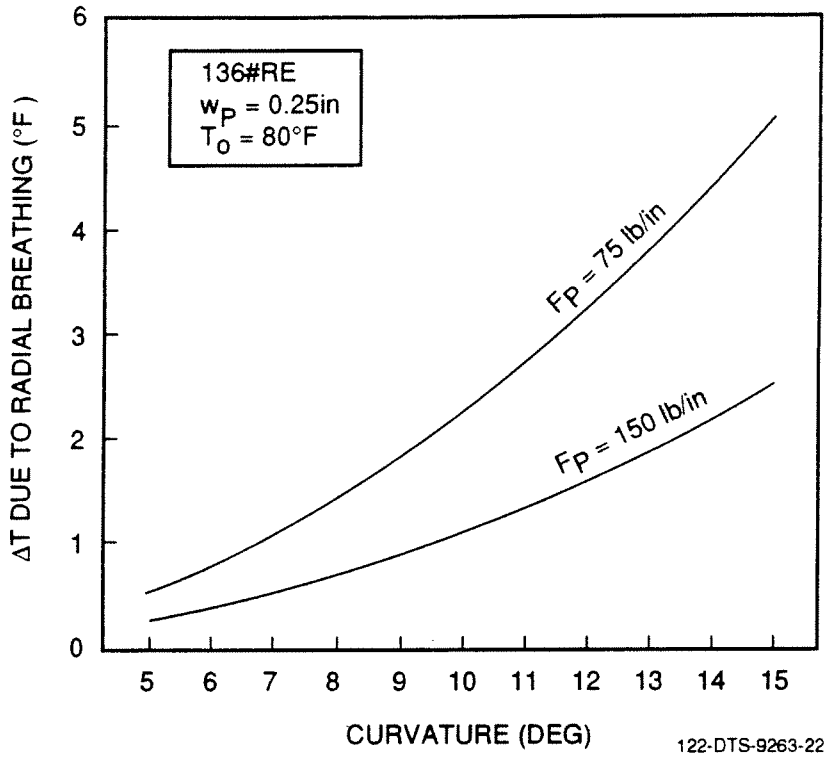

Figure 3-5. Buckling Strength Increase Due to Radial Breathing

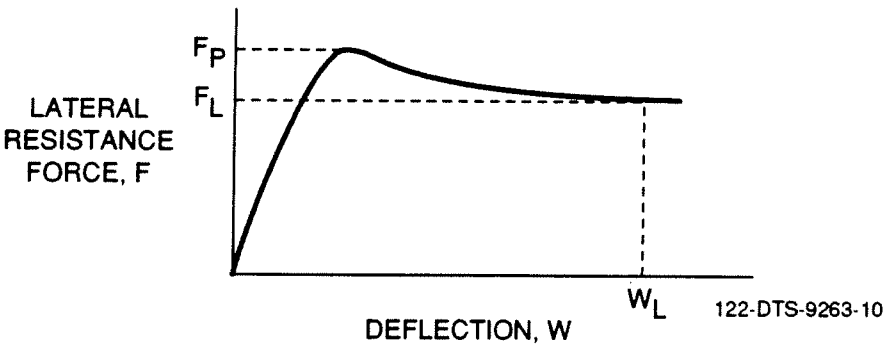

Figure 3-6. Typical Lateral Response Characteristic

Full Nonlinear Lateral Resistance

The full nonlinear lateral resistance function is shown in Figure 3-7c and can be mathematically idealized by the expression:

$$F = F_P [1 - \exp(-\mu_1 w)] \{k + (1-k) \exp[-\mu_2 (w - 4/\mu_1)]\}$$

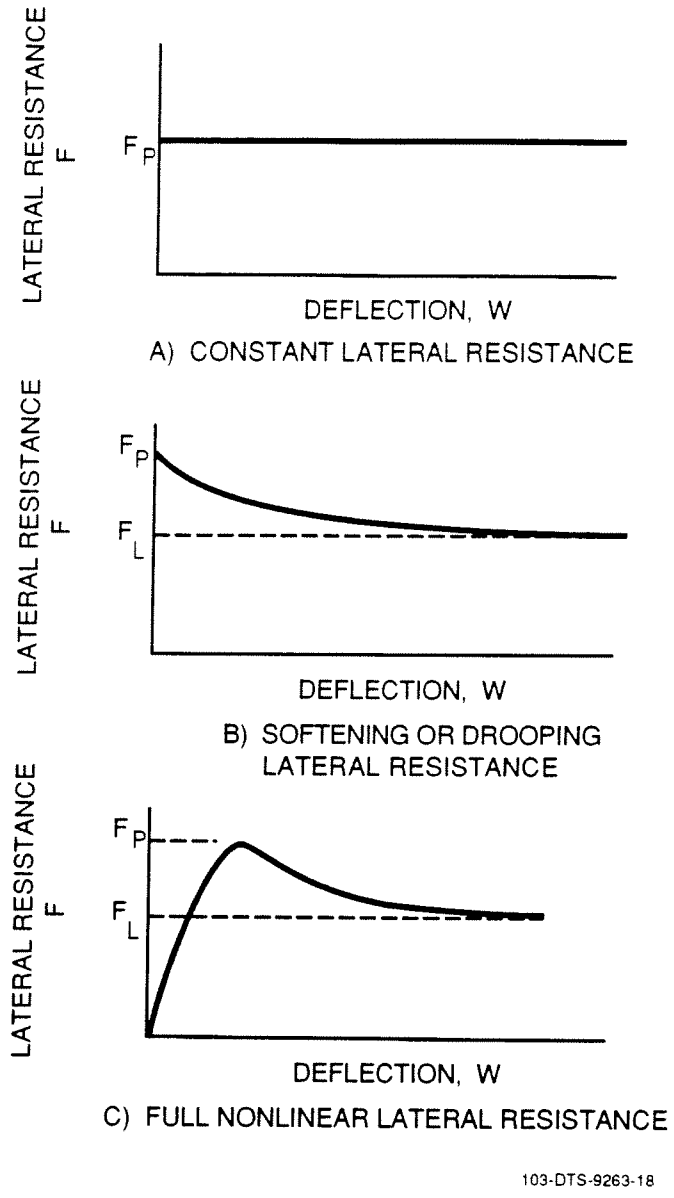

Figure 3-7. Lateral Resistance Idealizations

where

μ_1 = initial stiffness parameter

Comparisons among the three resistance functions indicate that the constant peak resistance ($F = F_P$) greatly overestimates the upper and lower critical temperatures, as is shown in Figure 3-8. In contrast, the results for the softening and full nonlinear functions are virtually identical.

Alternatively, using a constant lateral resistance equal to the limiting resistance value (F_L) underestimates the critical temperatures. As shown in Figure 3-9, the buckling response for the constant limiting resistance value is actually a progressive case, with no discrete upper and lower buckling temperatures. The softening case (as well as the nearly identical full softening case) lies between the two constant resistance cases.

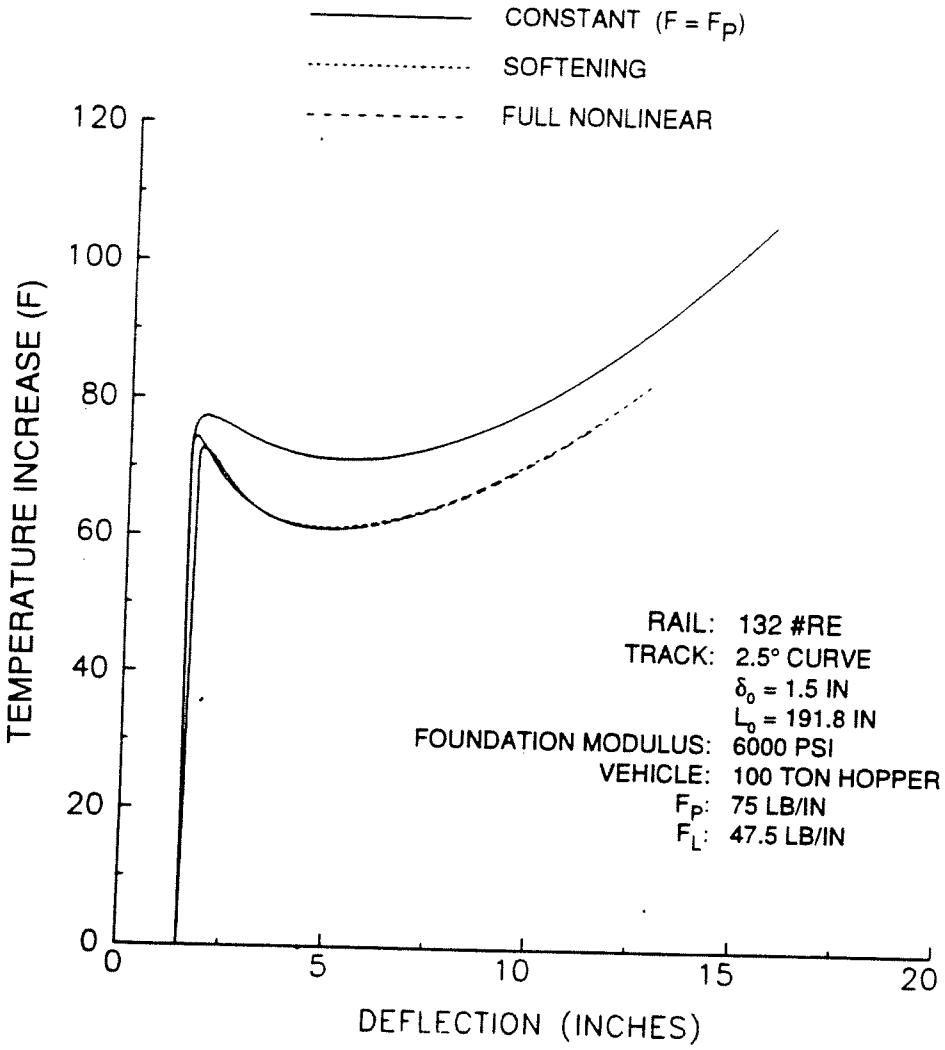

Figure 3-8. Comparison of Response for Constant, Softening and Full Nonlinear Idealizations

The shortcomings of the constant resistance function make it undesirable for analysis of buckling response. The differences between the softening and full nonlinear functions are generally negligible. Although the full nonlinear function is a more complete description of typical lateral response characteristics, it is also complex, requiring unduly large numbers of iterations for convergence in the computer program. The softening lateral resistance produces results reasonably close to that of the full nonlinear model. Thus, for calculation of buckling response, the softening lateral resistance characteristic is the preferred approach.

The softening resistance function is defined by two variables: the ratio of the limiting and peak resistances (k); and the deflection at which the limiting resistance is reached (w_L). These parameters depend on the type of ballast and level of ballast consolidation. To simplify and reduce the number of parameters required for definition of the softening resistance, a series of tests were conducted by VNTSC to correlate F_L and w_L to F_P, which is a parameter that can be directly measured using single tie push tests. On the basis of this experimental work, approximate linear relationships were developed between F_P and F_L, and between F_P and w_L. These correlations are listed in Table 3-3 for granite and slag ballast. Thus, the peak lateral resistance, F_P, is the primary parameter that is used to study the effects of lateral resistance on buckling strength.

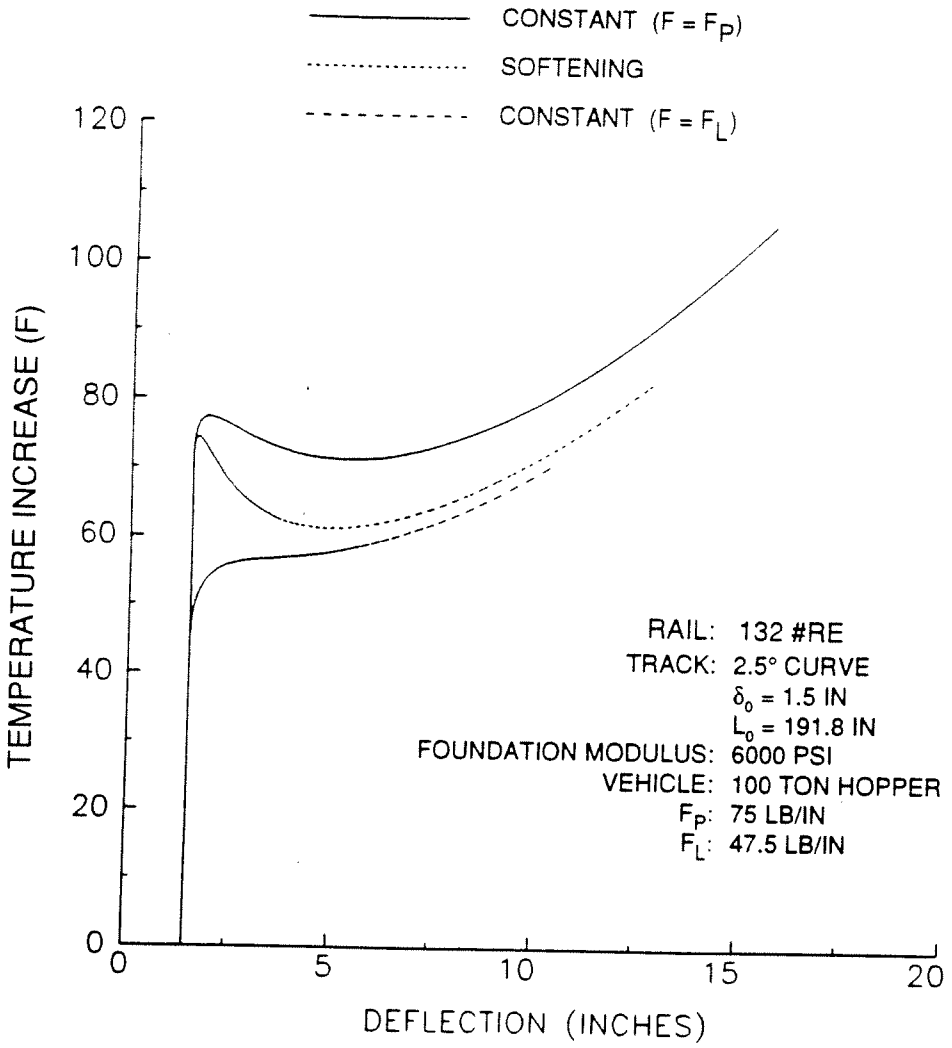

Figure 3-9. Comparison of Response for Alternate Constant Idealizations

Table 3-3. Correlations for "Softening" Lateral Resistance

Ballast Type	F_P/F_L Correlation	F_P/w_L Correlation
Granite	$F_L = 0.3\ F_P + 25$	$w_L = 0.025\ F_P + 2.6$
Slag	$F_L = 0.06\ F_P + 30$	$w_L = 0.009\ F_P + 3.5$
Note: Units for F_P and F_L are lb/in. Units for w_L are inches.		

Effects of F_P on Buckling

To determine the effects of lateral resistance on buckling, the parameter F_P is varied over a practical range representing very weak or recently maintained track (F_P = 50 lb/in.) up to very strong, well consolidated track (F_P = 150 lb/in.). The buckling results are shown in Figure 3-10. The results show that for very weak track, progressive buckling can occur for temperature increases of 50°F or less. Such tracks are vulnerable to buckle in summer, even with a rail neutral temperature of 80°F. As F_P

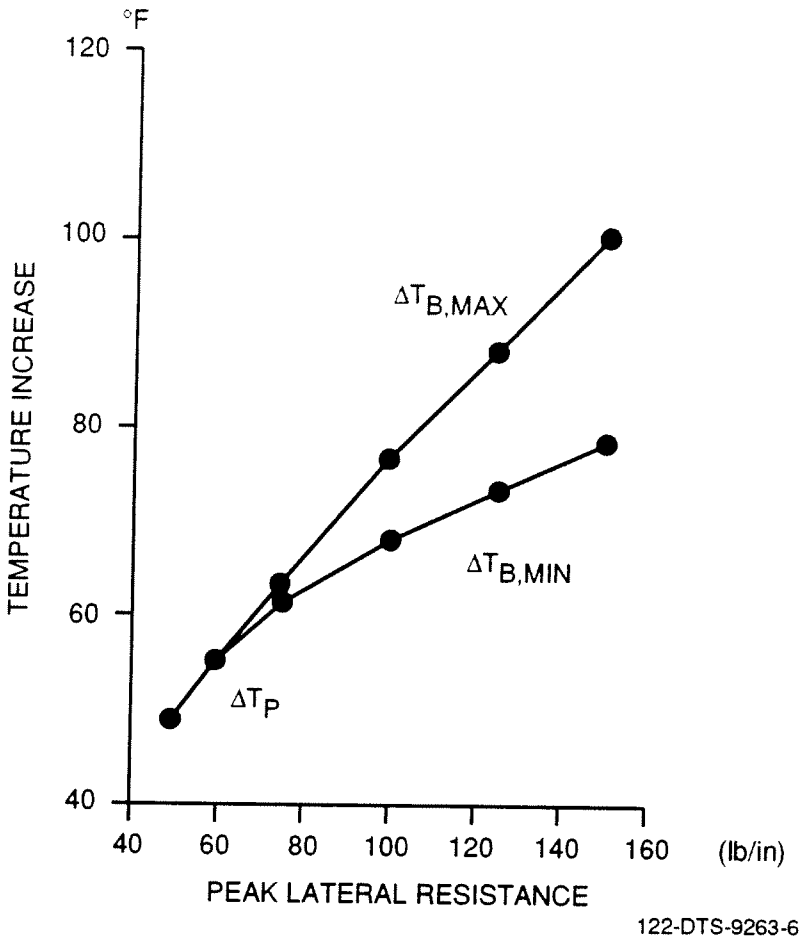

Figure 3-10. Influence of Track Peak Lateral Resistance

increases, both the upper and lower buckling temperatures increase. For very strong track ($F_P > 130$ lb/in.), the buckling temperature increase is greater than 70°F.

The results presented above are for a nominal 5 deg curved track. Naturally, as the degree of curvature increases, the buckling strength is drastically reduced, particularly for weak track, as discussed in subsection 3.2.

Clearly, it is important to maintain a high lateral resistance to avoid buckling, especially for curved track. The practical implication of this work is that the lateral resistance (i.e., level of ballast consolidation) can be used by the railroad to control track buckling safety. A well consolidated track will have a high lateral resistance peak and a greater resistance to track buckling. This topic will be discussed in greater detail in Appendix B.

3.4 Effects of Tie/Ballast Friction

The tie bottom surface roughness is an important parameter as it determines the component of the base resistance. All other conditions remaining unchanged (i.e., rail size, tie weight, ballast type),

the lateral resistance, hence the buckling strength should increase with increasing tie bottom roughness. However, in the case of wood ties, the roughness cannot be easily controlled but fortunately increases with the age of tie as the ballast tends to "lock" itself in the irregular bottom tie surface. The concrete ties are relatively smooth, and even when the tie bottom is artificially roughened at the time of manufacture, it tends to become smooth in course of service life due to the grinding action between the tie and the ballast stones.

The purpose of this parametric study here is to show that rougher and coarser ties perform better from buckling strength point of view. The roughness factor is artificially expressed as a friction coefficient which is defined as the ratio of the measured base resistance to tie self weight. This coefficient shall not be confused with the Coulomb friction between two surfaces, whose value never exceeds unity.

The lateral resistance can be expressed as the sum of the base, side and end shoulder components of the tie:

$$F = F_b + F_s + F_e$$

Defining the coefficient μ_f in terms of weight of tie (includes weight of rail and fasteners):

$$F_b = \mu_f Q$$

we see that μ_f can be considered as an index of tie bottom roughness. If the vehicle contributes an additional load of R_V (lb/in.) on the tie, the dynamic resistance can be calculated from Equation (18).

The coefficient μ_f in Equation (18) is strictly a function of total tie reaction. The average value of μ_f typically varies in the range from 0.5 to 2. Table 3-4 shows assumed values of the three resistance components for wood tie track with a typical weight Q = 20 lb/in.

The effects of the tie-ballast "friction" coefficient are shown in Figure 3-11. As expected, the increasing surface roughness of the tie bottom (increasing μ_f) increases both the buckling temperatures. Over the range studied here, the increase of the buckling temperatures is less than 10°F.

Table 3-4. Three Components of Resistance and Their Assumed Variations with μ_f

μ_f	F_b(lb/in.)	F_s(lb/in.)	F_e(lb/in.)
2.0	40	40	20
1.0	20	40	20
0.5	10	40	20

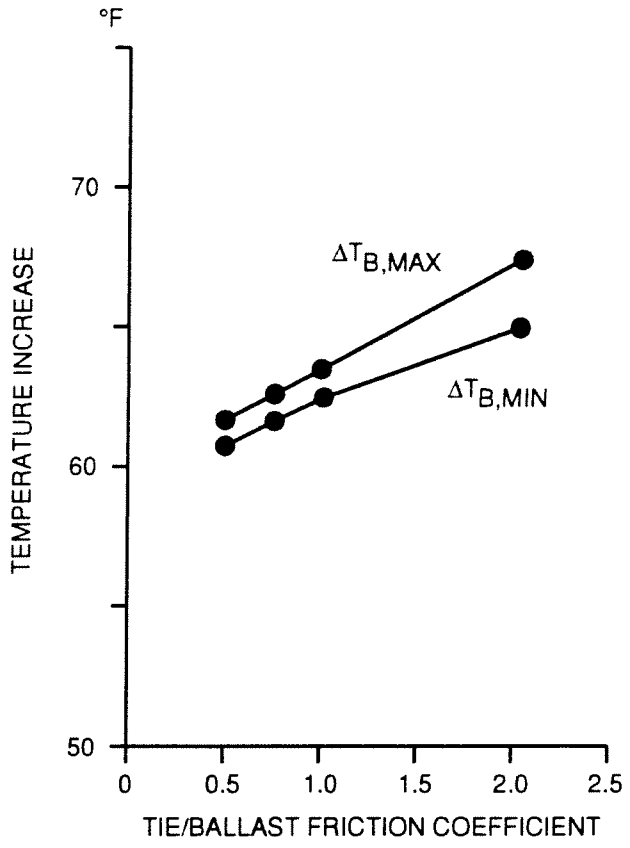

Figure 3-11. Influence of Tie/Ballast "Friction" Coefficient

3.5 Effects of Torsional Resistance

As noted in Section 2, torsional resistance is exerted on the rails by the fasteners, and the resistance characteristics vary with tie and fastener types. Typical results of torsional resistance measurements from tests recently conducted by VNTSC (Appendix C) are shown in Figure 3-12 for various tie and fastener types. These resistance characteristics can be idealized as:

$$\bar{\tau} = \bar{\tau}_o \theta$$

where:

$\bar{\tau}$ = applied torque per fastener
$\bar{\tau}_o$ = torsional stiffness per fastener
θ = rotation angle

Table 3-5 gives typical ranges of stiffness values obtained from test data presented in Appendix C. Note that τ_o in Equation (1) is obtained by multiplying $\bar{\tau}_o$ by 2 and then dividing by the tie spacing.

The effects of fastener torsional resistance on buckling are examined using the linear torsional stiffness ranging from 0 to 2,000 in.-kips/rad. The buckling results are shown in Figure 3-13. Both

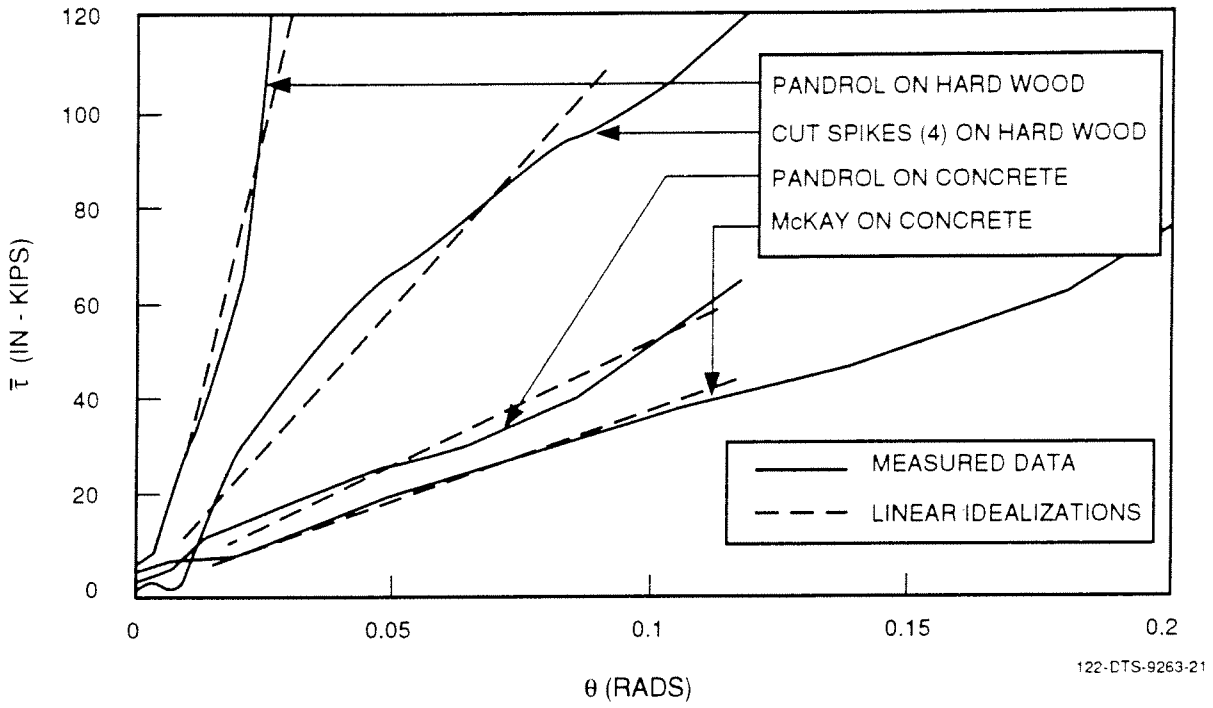

Figure 3-12. Linearization of Torsional Resistance

Table 3-5. Torsional Stiffness Values

Type of Tie	Fastener	$\bar{\tau}_o$ (in.-kips/rad)
Hardwood	Pandrol	3,700 - 7,400
Hardwood	Cut Spikes (4)	800 - 1,400
Concrete	Pandrol	120 - 520
Concrete	McKay	300 - 440

buckling temperatures increase with increasing torsional stiffness. The lower buckling temperature is more sensitive to the resistance changes, resulting in a significant increase. For typical wood ties a lower buckling temperature increase of 10 to 12 deg can be achieved by increasing torsional resistance. The impact on the upper critical temperature is not as significant. The rapid increase in the lower buckling temperature with respect to the torsional stiffness is due to the large buckled wavelengths involved at this temperature. At high stiffness values the two buckling temperatures coalesce. Although this represents a progressive buckle, it occurs at a much higher temperature than the upper buckling temperature corresponding to lower stiffness values. As such, it does not represent any decrease in buckling strength.

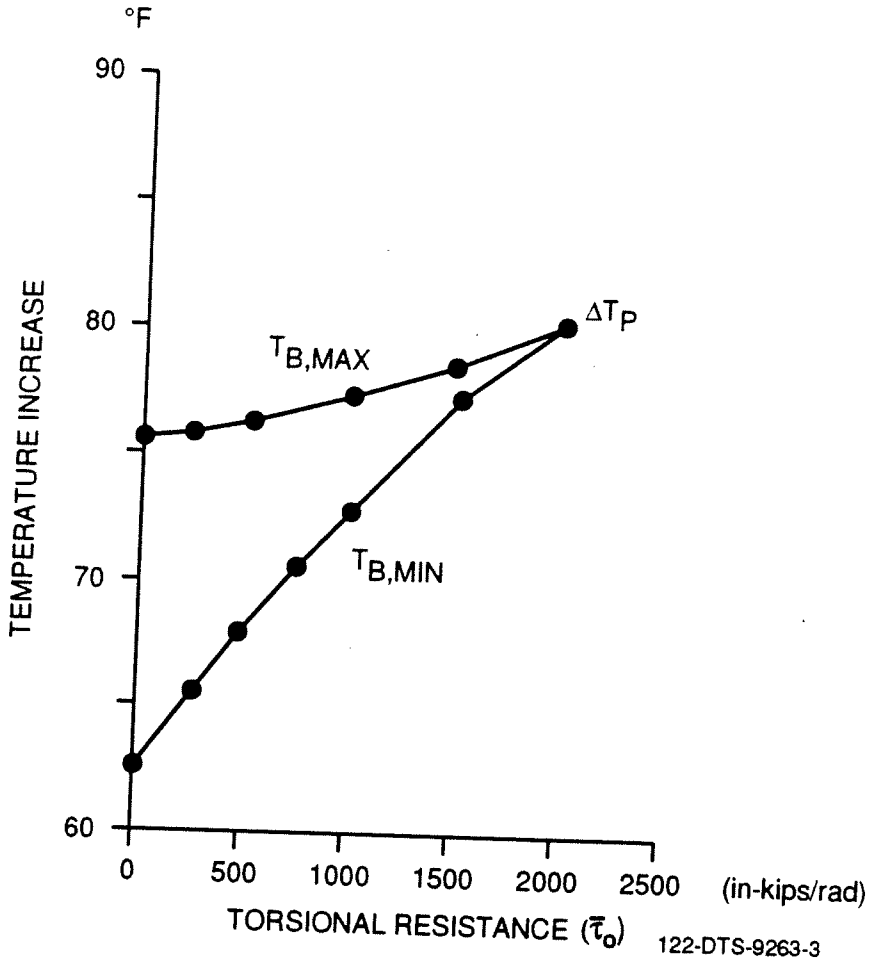

Figure 3-13. Influence of Torsional Resistance

It must be stated that the torsional stiffness numbers cited here for the three fasteners were obtained using a limited number of tests conducted at the Transportation Test Center (TTC) in Colorado. The stiffness numbers were used to illustrate the usefulness of the parameter. It is not the purpose of this analysis to recommend one fastener over another.

3.6 Effects of Longitudinal Resistance

Track longitudinal resistance is the resistance offered by ties and ballast to the rails as they tend to move in the longitudinal direction in the event of buckling, thermal force gradients, or in response to braking and accelerating train action. At unanchored or loosely anchored ties, the longitudinal resistance is very low. At properly anchored ties, the resistance offered by the ballast is much higher. Typical data from VNTSC tests (Appendix D) conducted at TTC are shown in Figure 3-14. Due to the small longitudinal displacement that occurs during buckling (usually less than 0.25 in.), a linear initial characteristic is typically assumed, as given by:

$f = k_f u$

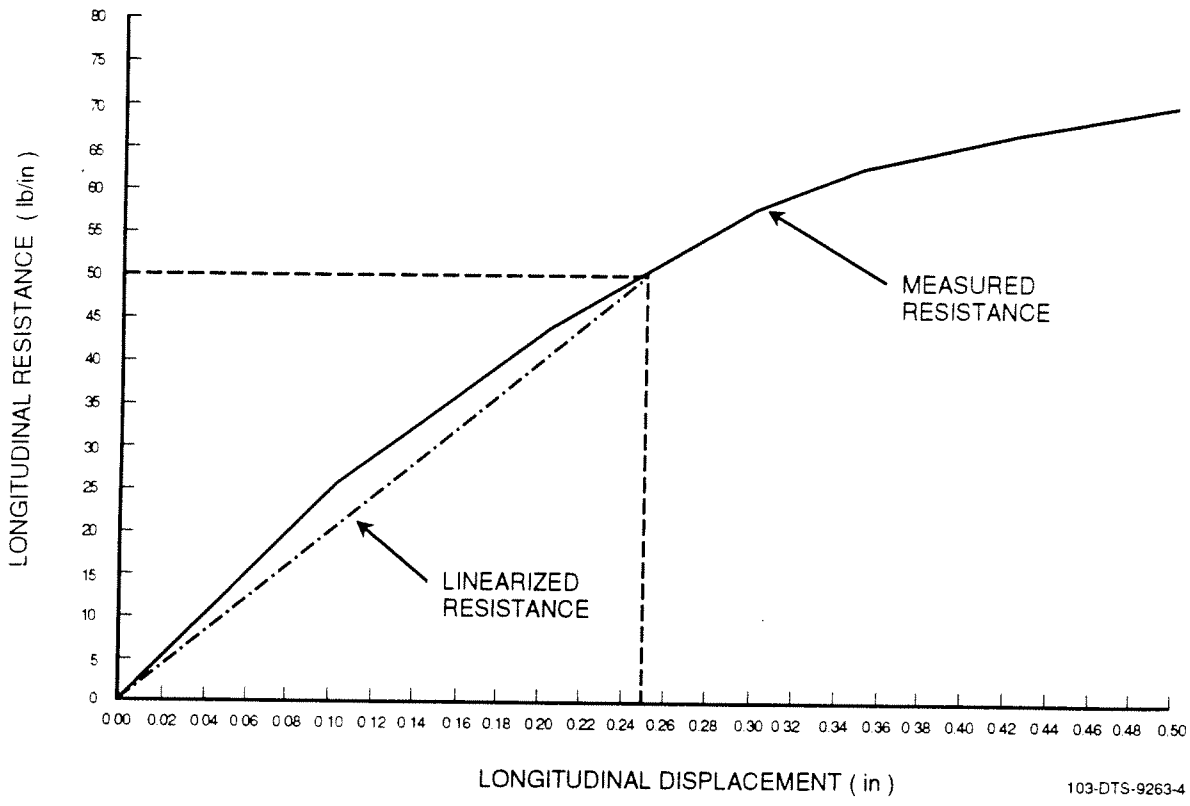

Figure 3-14. Typical Longitudinal Resistance Characteristic

where:

k_f = longitudinal stiffness

u = longitudinal displacement

This idealization is also shown in Figure 3-14. Typical measured values of k_f from tests conducted by VNTSC for various tie and ballast conditions are listed in Table 3-6.

The effects of longitudinal resistance are examined using variations in the longitudinal stiffness. A typical range of stiffness values (25 to 500 psi) is assumed. The buckling results are shown in Figure 3-15. The lower critical temperature is more sensitive to the changes in longitudinal stiffness, and increases with increasing resistance. In contrast, the upper critical temperature is essentially independent of the changing stiffness, and shows only a very slight increase across the range of stiffness values. It must be noted that longitudinal stiffness is also important in controlling neutral temperature variations and as such plays an important role in buckling safety.

3.7 Effects of Track Foundation Vertical Stiffness

As noted in Section 2, the presence of vehicle loads causes an uplift region in the rails, which is dependent upon the track foundation stiffness. The effects of foundation stiffness are examined using

Table 3-6. Typical Measured Longitudinal Stiffness Values

Tie Condition	Ballast Condition	k_f (psi)
ETA	Consolidated	324
EOTA	Consolidated	254
ETA	Tamped	213
EOTA	Consolidated 1/2 crib	126
E3TA	Tamped	178

ETA = Every tie anchored.
EOTA = Every other tie anchored.
E3TA = Every third tie anchored.

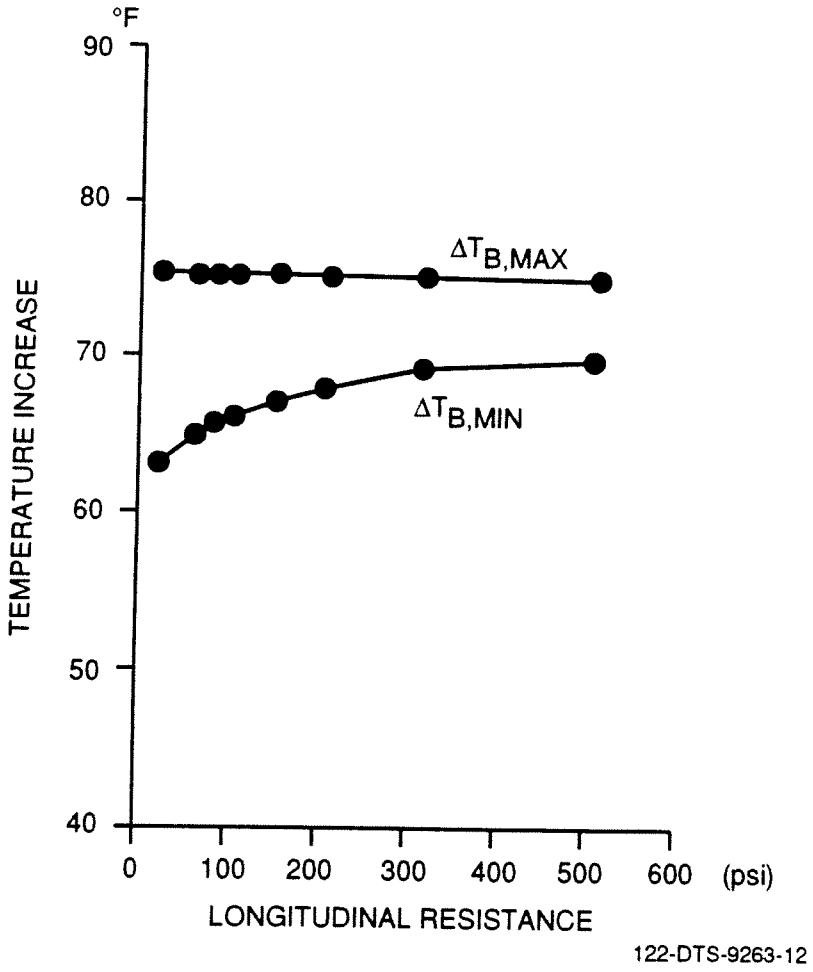

Figure 3-15. Influence of Longitudinal Resistance

a typical range of 2 to 10 ksi. All other parameters are set at the default values. The buckling temperature results are shown in Figure 3-16. Here the critical temperatures do not follow the same trends with increasing stiffness. The upper critical temperature is more sensitive to stiffness changes, and decreases slightly before showing a substantial increase for stiffness values greater than 4 ksi. The lower critical temperature first decreases, but then increases slightly. These trends are due to the complex relationship between the vehicle-induced uplift wave and buckling lengths.

3.8 Effects of Initial Misalignments

Misalignment parameters include the track misalignment amplitude (δ_0) and misalignment wavelength ($2L_0$). Several functional forms are available for idealization of the misalignment shape, including:

(a) Sinusoidal misalignment shape $w_0(x) = \delta_0 \cos\left(\frac{m\pi x}{2L_0}\right)$

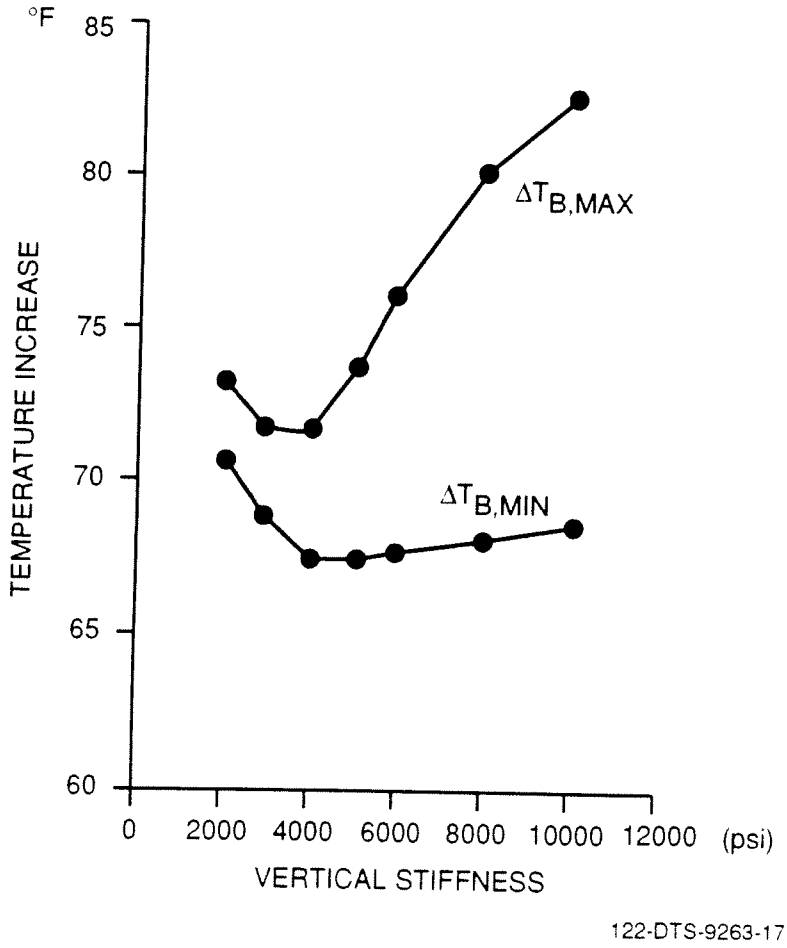

Figure 3-16. Influence of Track Foundation Vertical Stiffness

(b) Parabolic misalignment shape $w_0(x) = \delta_0\left[1-\left(\frac{x}{L_0}\right)^2\right]$

(c) Fourth order polynomial misalignment shape $w_0(x) = \delta_0\left[1-2\left(\frac{x}{L_0}\right)^2+\left(\frac{x}{L_0}\right)^4\right]$

Of these shape functions, the fourth order shape is preferred, as it is more consistent with the Shape I buckling mode assumption with zero end deflection and slopes.

Effects of Misalignment Amplitude

The misalignment effects are examined first by using typical misalignment amplitudes ranging from 0.5 to 1.75 in. The corresponding misalignment wavelengths are calculated using a special program, and are shown in Table 3-7. All other parameters assume their default values. The buckling results are shown in Figure 3-17. Both temperature quantities decrease as the misalignment amplitude increases, with the upper critical temperature being more sensitive to these changes. The changes in the lower critical temperature are comparatively small.

Effects of Misalignment Wavelength

The misalignment effects are studied using a constant misalignment amplitude of 1.5 in., but with changing misalignment wavelength. Typical misalignment half wavelengths ranging from 100 to 500 in. are assumed. The results are shown in Figure 3-18. The lower critical temperature is relatively insensitive to the effects of wavelength. However, the upper critical temperature decreases sharply as the wavelength is reduced. Similarly to the effects of curvature, a progressive buckling condition is reached at a half wavelength of approximately 100 in., when the ratio of misalignment amplitude to misalignment wavelength is largest.

The foregoing results show that control of misalignments is very effective in increasing the CWR track buckling strength. Sharp kinks with small wavelengths should be particularly minimized in the revenue conditions.

Table 3-7. Parameters for Effects of Misalignment Amplitude

δ_0 (in.)	L_0 (in.)
0.50	134.8
0.75	149.9
1.50	180.4
1.75	188.3

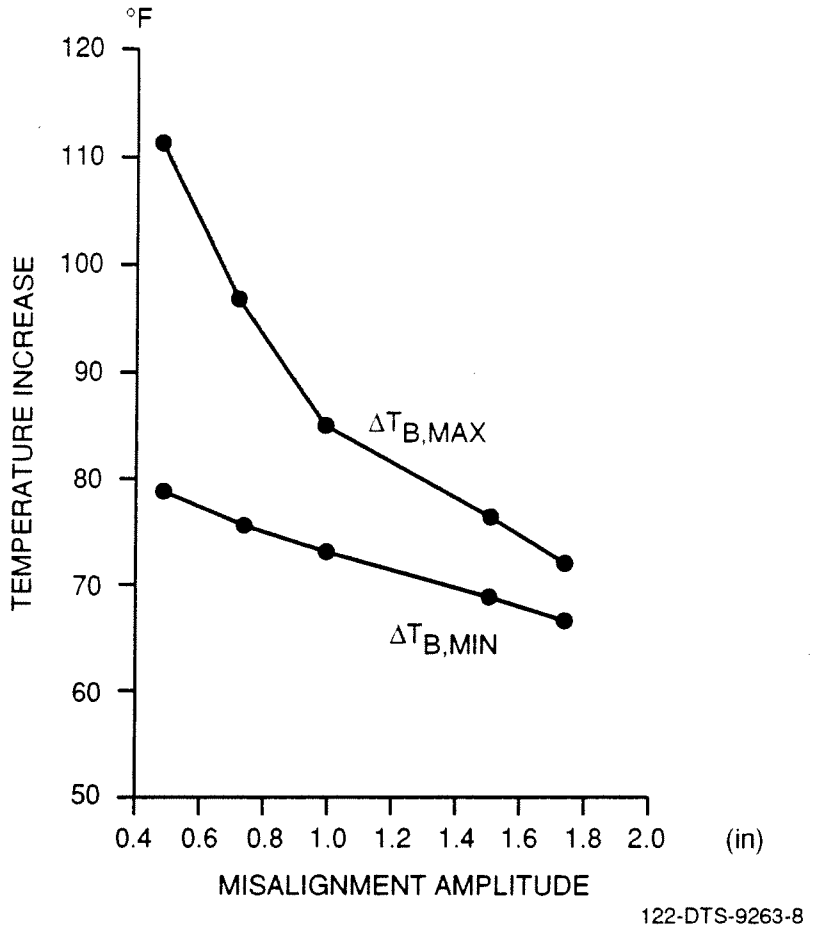

Figure 3-17. Influence of Misalignment Amplitude

3.9 Effects of Vehicle Parameters

As discussed in Section 2, the effect of vehicle loads is to cause rail uplift and a reduction of buckling strength in comparison with the static buckling case, due to the loss of lateral resistance in the uplift region. The primary vehicle parameters are the axle loads and the truck center spacing (TCS), which vary with vehicle size and type.

Effects of Axle Loads

To examine the effects of these vehicle parameters on buckling, the effects of axle load are first studied using a typical hopper car. The axle load is varied to reflect changes in the car's cargo weight, ranging from the empty weight load of 15,575 lb to the maximum gross weight load of 65,750 lb. The axle spacing and truck center spacing for this car are 70 and 506 in., respectively. All other parameters are set at the default values. The buckling results are shown in Figure 3-19. The lower critical temperature is relatively insensitive to the effects of axle load, and is essentially constant. However, the upper critical temperature decreases with the increasing axle load. This is a very important feature of the dynamic buckling analysis. The rapid decrease in the upper critical temperature reduces the margin of safety and the energy barrier for buckling.

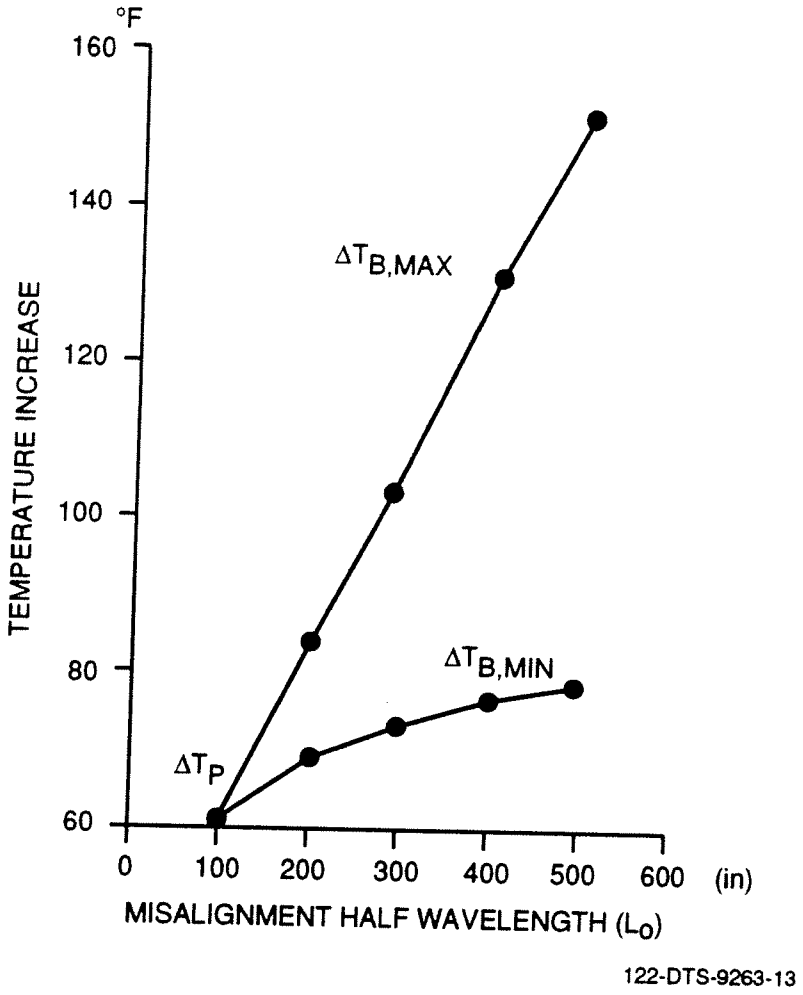

Figure 3-18. Influence of Misalignment Wavelength

Effect of TCS

The effects of vehicle truck center spacing (TCS) are also examined. The truck center spacing is varied from 350 to 700 in. to reflect changes in car size. Each of these cars has four axles with an axle spacing of 70 in. and an axle load of 65,000. All other parameters assume their default values. The buckling results are shown in Figure 3-20. For the small values of TCS, the two critical temperatures are approximately equal and higher than about 73°F. The upper and lower buckling temperatures diverge at a TCS of about 470 in. The upper buckling temperature then increases while the lower buckling temperature continues to level off at 66°F. For large TCS values, the upper and lower temperatures approach the values predicted by static buckling theory (approximately 90°F and 68°F, respectively) as one would expect. It can be seen that a critical truck center spacing is about 470 in., approximately corresponding to that of hopper cars. This is considered to be critical because this has the lowest temperature at which progressive buckling can occur with no energy barrier that exists for the longer truck center spacing. Although the longer truck center spacing gives slightly smaller $T_{B,MIN}$, this energy barrier provides a higher safety margin against possible explosive buckling.

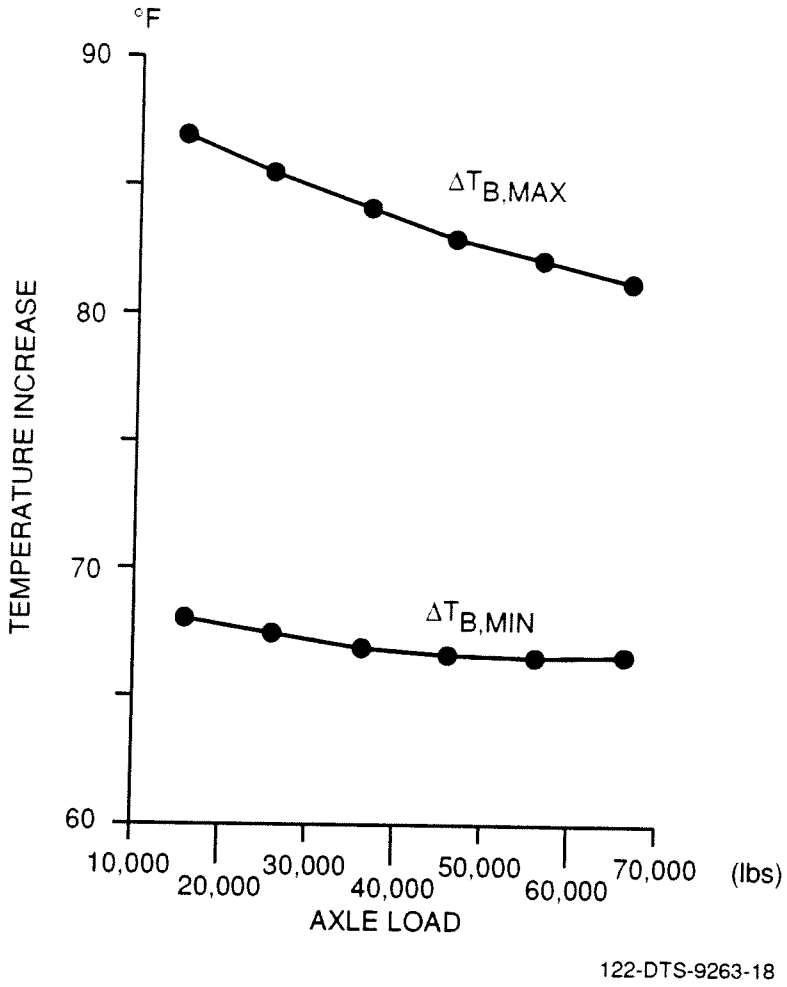

Figure 3-19. Influence of Axle Load

From the foregoing results, it can be stated that heavy axle loads reduce the track buckling safety, unless the track lateral resistance is increased. The critical truck center spacing of about 470 in. suggests that it is adequate to study the "worst" case of a hopper car in the estimation of dynamic buckling strength.

3.10 Summary of Parametric Effects

Based on the results presented in the preceding sections, track buckling strength is high when the conditions prescribed in Table 3-8 are met.

The results of the parametric studies have shown that several parameters have a significant impact on the upper and lower buckling temperatures. However, not all of these parameters can be easily controlled by the railroads in revenue service. Further, some of these parameters (such as rail size or track curvature) while being controllable, may also be influenced by other design or operating considerations, and thus optimization from a buckling safety standpoint is involved.

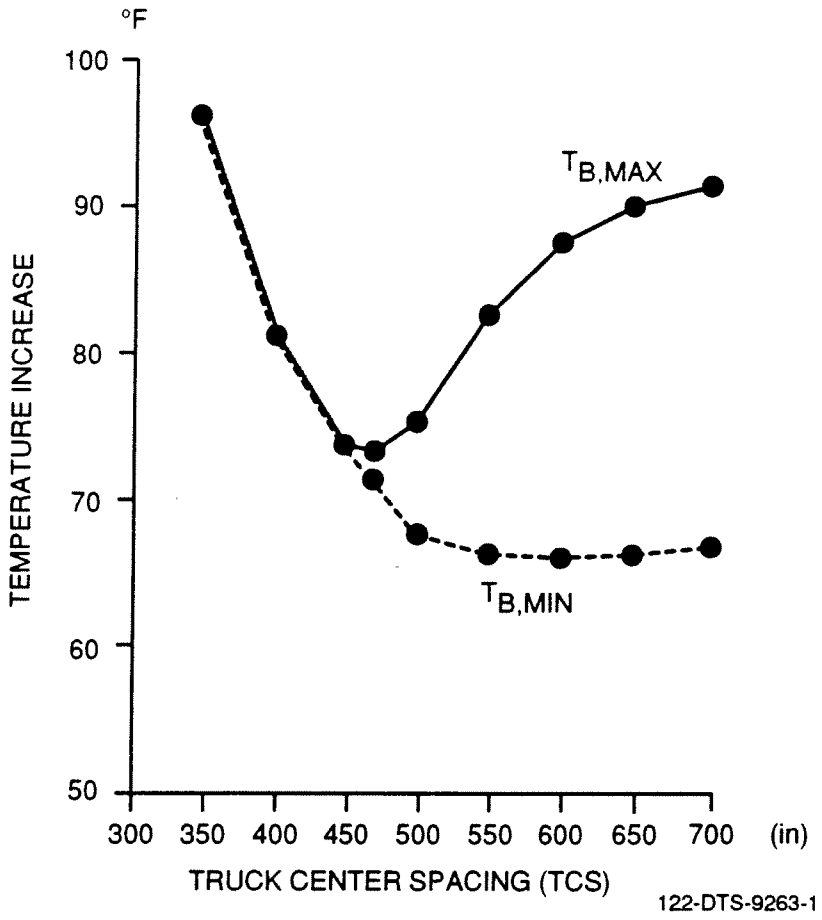

Figure 3-20. Influence of Truck Center Spacing

Table 3-8. Desired Parameters for High Buckling Strength

Parameter	Desired Value	Comments
Rail size	Small	Rail size is determined from fatigue and wheel load considerations. Use the smallest size possible from these considerations.
Curvature	Low (or tangent)	Avoid high degree curves where possible in new installations. High neutral temperature and good lateral resistance are required.
Peak lateral resistance	High	High resistance is required. Use good ballast. Consolidate by traffic or ballast consolidators after tamping. Generous shoulders and full cribs are recommended.
Rail/tie friction coefficient	High	Ballast consolidation tends to increase the coefficient. For concrete ties it is especially important to ensure rough bottom surfaces.
Torsional resistance	High	Certain fasteners have higher values compared to cut spikes on wood ties and the lower buckling temperature can be increased with such fasteners.
Longitudinal resistance	High	The benefit of this parameter is more in controlling the rail neutral temperature. Every tie can be anchored to increase the value of the parameter in preference to every other tie.
Track foundation stiffness	High	Stiffer track is better from buckling point of view. The stiffness is controlled also by sub-ballast, subgrade and soil conditions underneath.
Misalignment amplitude	Small	Good alignment is very important. Inspection with track geometry cars will be very helpful. Make sure ballast is reconsolidated after any realignment operation.
Misalignment wavelength	Large	
Axle load	Small	Increased freight loads tend to reduce the upper buckling temperatures. They may also need larger rail sections which can further reduce buckling strength.
Truck center spacing	Large	The hopper car represents the worst case from this parameter point of view.

4. SAFETY CONCEPTS AND APPLICATION

The computer model has been validated by dynamic buckling tests [2,3,4] conducted on tangent, 5 and 7.5 deg curves. Significant parameters such as the lateral resistance and misalignment amplitude were varied in these tests and the sensitivity of buckling temperatures with respect to these parameters was correlated with the theoretical expectations presented in the previous section. Certain basic features of the safety concepts were also evaluated in these test programs.

The computer model can be used to generate data on which the safety criteria can be based. In view of the large number of parameters involved, such data would be unwieldy. For practical purposes, the parameters can be classified into two groups. The primary group includes:

- Rail size.
- Lateral resistance.
- Misalignment.
- Curvature.
- Rail neutral temperature.

All other parameters out of the list presented in Section 2 may be considered as the secondary group. The primary parameters have significant influence on the upper and lower buckling temperatures, and they are also more *controllable* than the secondary group in the revenue service conditions. For the development of safety specifications, the secondary group parameters are set at their nominal values. These values are arbitrary to some extent. If the secondary parameter values are significantly different from the assumed nominal values, it is suggested that the computer program be used for an exact evaluation of the buckling temperatures. It must be noted that the torsional stiffness of fasteners could have been included as a primary parameter, particularly for concrete tracks. For the wood tie tracks considered here, a fixed value appropriate for standard cut spike construction has been assumed.

It must be noted that the longitudinal track resistance which depends on the type of fastener and the anchoring pattern is also an important parameter as it controls the rail neutral temperature in service life and also has some influence on the lower buckling temperature. For the development of safety limits, the longitudinal stiffness is assigned a fixed value. The safety limits are expressed in terms of allowable temperature increase. The subject of longitudinal resistance influence on the rail destressing operations and the resulting neutral temperature under different anchoring patterns will be studied in a future work.

Even within the primary parameters, the lateral resistance and misalignments cannot be exactly stipulated in the revenue service conditions. It is assumed that the railroad track supervisors will gain

some knowledge of the peak lateral resistance through the use of the Single Tie Push Test (STPT) or other devices, or they will be able to estimate it on the basis of track consolidation (MGT level) (Appendix B). The peak resistance has already been correlated with the limiting resistance to enable the inclusion of the complete characteristic of the resistance curve in the analysis.

The track lateral misalignments are defined in terms of the amplitude and the wavelength. The amplitude can be based on the FRA allowables for the class of track. The wavelength is still a difficult parameter, which, if not known, can be estimated on the basis of an analytic method built into the computer program.

4.1 Basis of Safety Concepts

A few candidate safety concepts have been proposed in the previous works (7). The fundamental approach in all these is to derive an allowable increase in the rail temperature (T_{ALL}) over the force-free neutral temperature (T_N) for buckling safety. The allowable increase is related to the upper and the lower buckling temperatures, and a chosen dynamic margin of safety (DMS). The margin of safety is defined here as the difference between the temperature at which the CWR track will buckle under vehicle and thermal loads and the maximum rail temperature in service operations. The buckling temperatures are derived using the computer program as functions of the peak lateral resistance and the amplitude misalignment for given track curvature and rail size. Thus, for a given rail size and amplitude of misalignment, the allowable rail temperature can be presented as a function of the peak lateral resistance for varying curvatures in a single chart. Alternatively, since the allowable rail temperature is dictated by the geographic location and not controllable in the revenue service, the foregoing information can be recast in the form of the minimum required lateral resistance (MRL) for a given allowable rail temperature (typically in the range of 140 to 160°F), as a function of track curvature for fixed rail size and amplitude of misalignment. Such a plot is more convenient for use by the industry, as shown later.

4.2 Criterion for Allowable Rail Temperature

As stated earlier, the allowable rail temperature is to be derived from the upper and the lower critical temperatures and a prescribed dynamic margin of safety (DMS). A DMS of 10 to 20°F is found to be adequate for buckling safety based on test results [3]. In earlier works [7], a DMS of 20°F had been recommended in view of uncertainties in the input parameters. A DMS of 10°F is now considered to be sufficient due to the improved theoretical formulations in the computer program and a better understanding of the input parameter descriptions.

The track buckling strength in terms of theoretical buckling response curves can be classified in three groups (Figure 4-1).

Case I (Strong Resistance)

In this case, the difference between the upper and the lower buckling temperatures is greater than 10°F. The safety stipulation for this case is that the allowable rail temperature be restricted to the lower buckling temperature

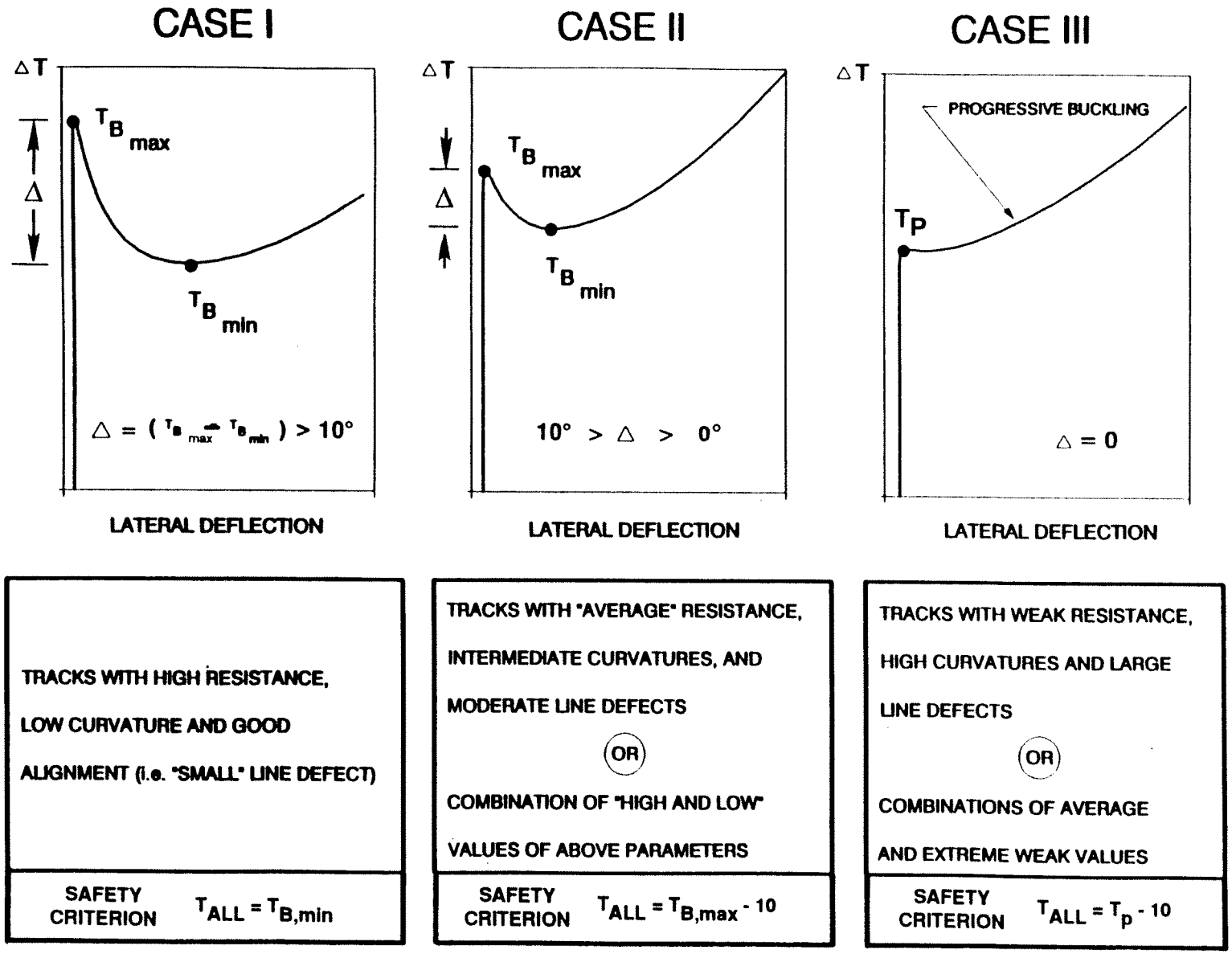

Figure 4-1. Allowable Temperature Definition

$T_{ALL} = T_{B,MIN}$

The rationale for this is based on the buckling energy considerations presented in [7] which revealed that the energy quickly decreases with the increase in the rail temperature over the lower critical temperature. Hence, although previous investigations explored higher allowable temperature, the resulting increase in the allowable temperature is found to be marginal for the majority of cases, particularly involving high degree curves. The higher risk associated with such increase in the allowable temperature over the baseline value ($T_{B,MIN}$) is not warranted. Therefore, for Case I, $T_{B,MIN}$ will provide a reliable allowable temperature with a margin of safety no less than 10°F. Note that even at $T_{B,MIN}$ the track can buckle out, if sufficient external energy is supplied.

Case II (Average to Marginal Resistance)

Here the difference between the two buckling temperatures is less than 10°F, typically occurring for tracks with average resistance and intermediate curvatures. In view of the fact that the track will certainly buckle at the upper critical temperature, and a margin of safety of 10°F is needed, the allowable rail temperature is

$T_{ALL} = T_{B,MAX} - 10°$

Case III (Poor Resistance)

In this case, the upper and the lower critical temperatures coalesce at the knee, T_P. This situation occurs in high curvature tracks with low lateral resistance. The response beyond T_P is progressive. At T_P, the track tends to move laterally at a fairly rapid rate with a small increase in temperature. Therefore, T_P is considered to be a buckling temperature for such tracks. For a margin of safety of 10°F, the allowable temperature is

$T_{ALL} = T_P - 10°$

4.3 Typical Results

Using the foregoing criteria, typical results for allowable rail temperatures can be plotted as in Figure 4-2 for a range of track curvatures. Additional plots for a range of neutral temperature can be prepared as in Figure 4-3.

The results in Figure 4-2 can be used to generate the minimum required lateral (MRL) resistance for a given neutral temperature. For example, if we assume that the 5 deg curve is destressed at a neutral temperature of 70°F, and the expected maximum rail temperature is 140°F in summer, the MRL is 2,250 lb/tie; for 7.5 deg curve under the same conditions, the MRL is 2,700 lb/tie. If these curved tracks have reduced neutral temperature (due to seasonal, variational and other effects), the MRL will be higher. The tracks will buckle out if the MRL is not provided. Slow orders and other precautionary measures should be taken till the tracks get consolidated by traffic to the minimum required levels [8].

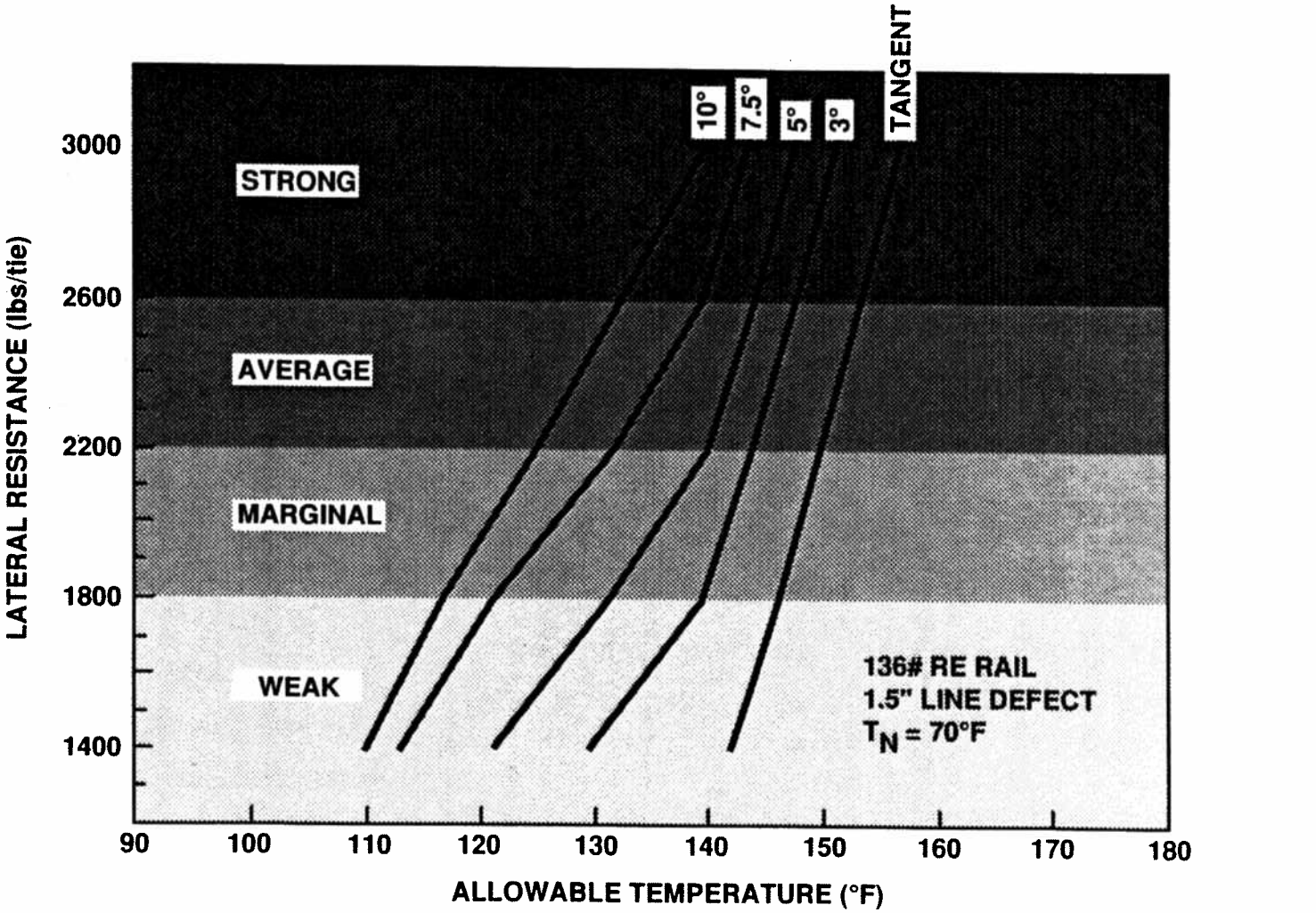

Figure 4-2. Typical Safety Limit Plot

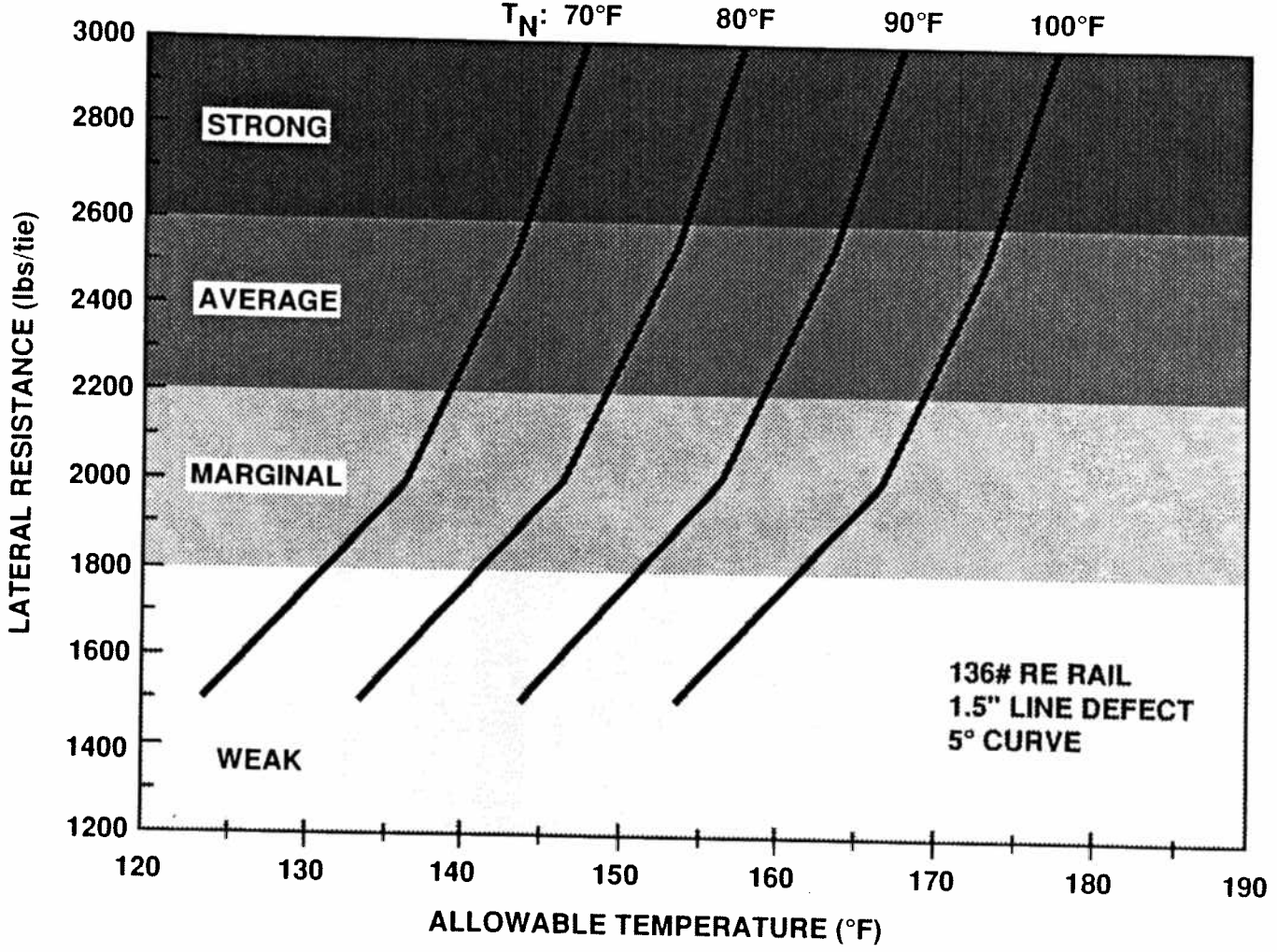

Figure 4-3. Safety Limit Plots for Different Neutral Temperatures

4.4 Experimental Validation

Dynamic buckling tests were carried out during 1983-84 and 1986-87 in the United States at the Transportation Test Center, in Pueblo, CO on tangent and curved CWR tracks. Detailed summaries of these tests are given in [2-4].

The principal objectives of these tests were:

- Experimental validation of dynamic buckling theory and identification of significant parameters influencing CWR track buckling response under thermal and vehicle-induced loads.

- Determination of required margin of safety for safe operations and verification of proposed safety concepts and limits.

Test Methodology

The test methodology generally consisted of providing rail heating by electric current using substations or diesel locomotives. The test track lengths varied, but were of the order of 1,000 ft to minimize end effects and obtain uniform rail force distribution in the central segment of the test zone. Lateral misalignments were set intentionally in the test track and all other existing misalignments were mapped using a track geometry car or stringlining techniques. The tracks were destressed and instrumented with longitudinal rail force and vehicle wheel load gauges as well as displacement transducers to measure longitudinal, lateral and vertical movements of the rails. Thermocouples were used to measure rail temperature. Data loggers and strip chart recorders were employed to record data at frequent intervals. Track resistance was measured by both panel pull tests and single tie push tests. The maximum number of cars in the test consist was 70, but varied depending on the tests.

4.4.1 Dynamic Buckling Theory Verification Tests

Comparison of Buckling Strength Under Hopper and Locomotive

To compare the relative influence of the central bending wave under a loaded 100-ton hopper and locomotive, equal levels of misalignment were set under each of the vehicles. Vertical and lateral displacements were measured as the rails were heated. Figure 4-4 shows a comparison of lateral displacements under each vehicle as a function of temperature. The misalignment growth under the hopper car is much more severe, indicating the influence of the longer uplift wave present under the 100-ton hopper car, and that uplift wave is a contributing factor in the misalignment growth mechanism, hence a critical component of the dynamic buckling analysis. Subsequent dynamic tests further confirm this uplift wave influence.

In another test, the measured response of the track with a large misalignment under a stationary hopper car favorably compared with the theoretical prediction (Figure 4-5). This test facilitated determination of lower buckling temperature and the progressive buckling characteristics.

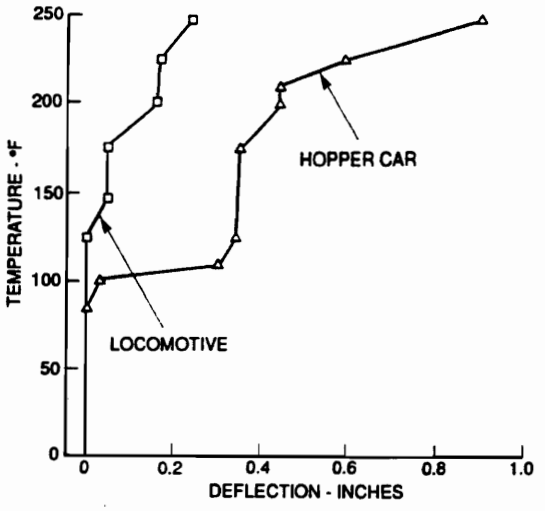

Figure 4-4. Response of Track Under Vehicles

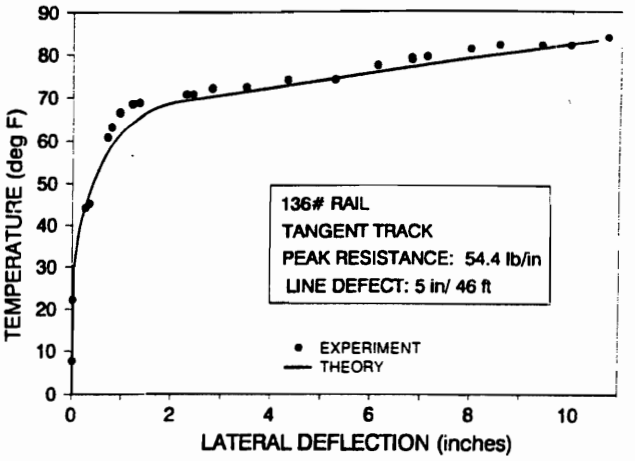

Figure 4-5. Progressive Buckling Test (Tangent)

Comparison of Static and Dynamic Strengths of CWR

A weak 5-deg curved track was tested dynamically by a locomotive and hopper car at slow speeds. Up to 40°F and five train passes, no growth of initial misalignment resulted. Train passes made above 40°F increased the misalignment; at 62°F, the curve buckled to a deflection of 9 in. as shown in Figure 4-6. The buckling response was in good agreement with the dynamic theory, but more importantly, these tests gave the first indication of a 10 to 20°F dynamic factor of safety requirement.

Effect by Uplift Wave

In several tests, the growth of imperfections under the passage of different cars was monitored using strip chart recorders. Figure 4-7 is a typical output from the charts. The significant influence

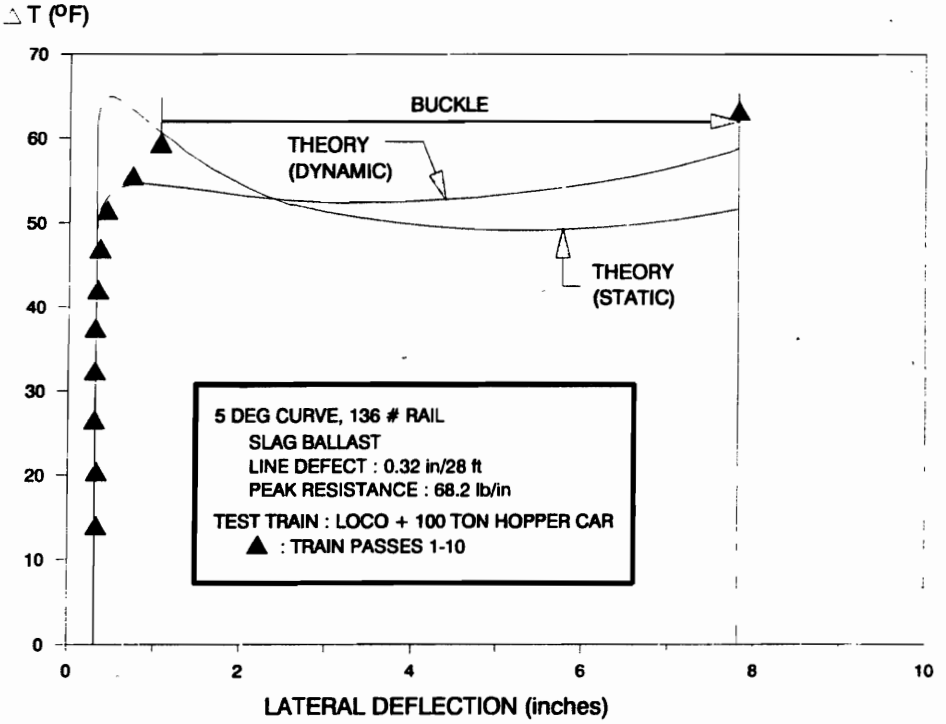

Figure 4-6. Dynamic Buckling of Curved Track

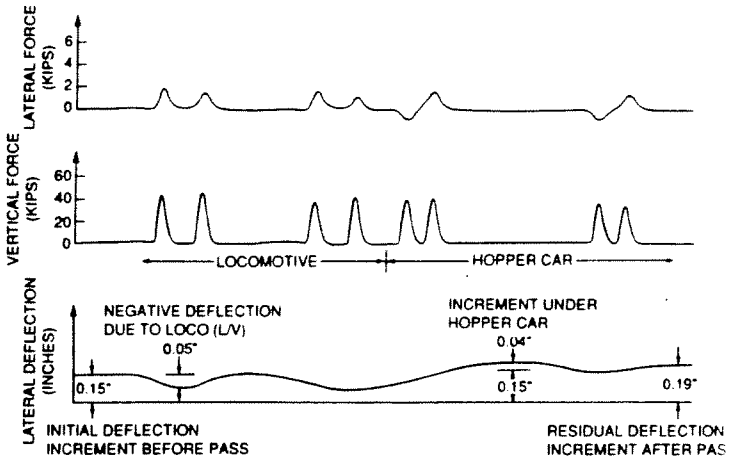

Figure 4-7. Strip Chart Record for Pass No. 8 on 5-deg Curve Test

of the central bending wave of the hopper car can be seen. In contrast, the locomotive did not increase the deflection, which is in agreement with the theoretical predictions.

4.4.2 Safety Concept Validation

Safety concepts and limits were partially verified on a tangent, 5- and 7.5-deg curved tracks as follows:

- Tangent Track Tests (Tangent I and Tangent II): In Tangent I, lateral resistance (peak) of 69.1 lb/in. and in Tangent II 80 lb/in. were simulated and train passes were made at incremental rail heating. Results are shown in Table 4-1. The conditions represent Case I type tracks as referred to previously. No significant movement occurred at the safe allowable limits. Although higher temperatures were attained in the test, the vehicles were not operated at full speed. Further, the distribution of compressive load was found to be nonuniform along the track due to the

Table 4-1. Data from Safety Tests

Test Track	Lateral Resistance F_P (lb/in.)	Misalignment Amplitude δ_0 (in.)	Misalignment Length $2L_0$ (in.)	$\Delta T_{ALL} = \Delta T_{B,MIN}$ (°F)	$\Delta T_{B,MAX}$ (°F)	ΔT_{test} (°F)
Tanget I	69	0.88	336	81	117	92
Tangent II	80	0.81	319	83	129	100
Curve I	84	0.55	305	74	103	72
Curve II	100	0.70	310	75	110	80

longitudinal movement of end sections of heated rail. This accounts for the apparent buckling strength increase.

- 5-Deg Curve Tests (Curve I and Curve II): Results for Curve I and Curve II representing different peak resistance values are shown in Table 4-1. Again, the results are satisfactory from the allowable safe limits viewpoint.

- 7.5-Deg Curve: The objective in this test was not only to validate the safe limit, but also to determine the ultimate buckling strength under a moving consist. The allowable limit of 52°F was reached without causing significant growth of misalignment due to vehicle passage. Analytic and experimental results are shown in Figure 4-8. At 62°F above the stress-free temperature, the progressive growth of this misalignment was experienced under the passage of each car. This resulted in a total deflection of 4 to 5 in. under the eighth car in the final run of the 24-car consist, just prior to the derailment of the test train. The test shows that the track can withstand the allowable temperatures, and that buckling occurred below $T_{B.MAX}$ and above $T_{B.MIN}$.

The results of the weak 5-deg curve referred to in subsection 4.4.1 and the 7.5-deg curve are also shown on typical safety limit plots in Figure 4-9. The test points are situated sufficiently distant on the right from the safety curves to assure at least a 10°F margin of safety for safe operations.

4.5 Deflection Based Criterion

As stated earlier an alternative safety criterion was proposed, but found to be impractical. This criterion was based on allowable deflection. Referring to Case III (Figure 4-1) situation, it was proposed that an allowable deflection criterion would yield a higher allowable temperature over Tp. The reason behind this is that high degree curves can tolerate sizable lateral deflections without

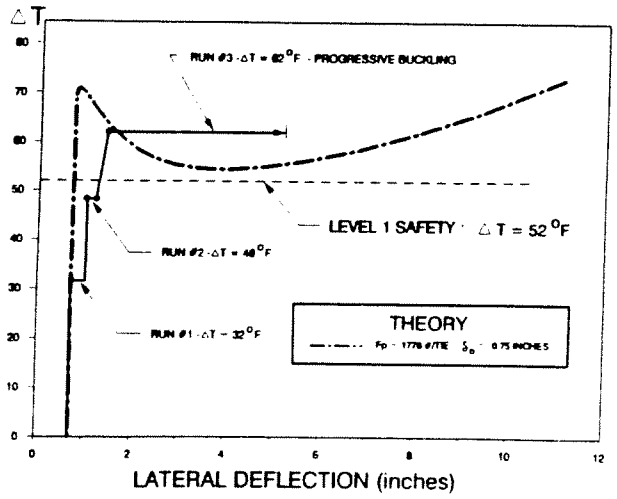

Figure 4-8. Dynamic Buckling Test Analysis versus Experiment (7.5 deg Curve)

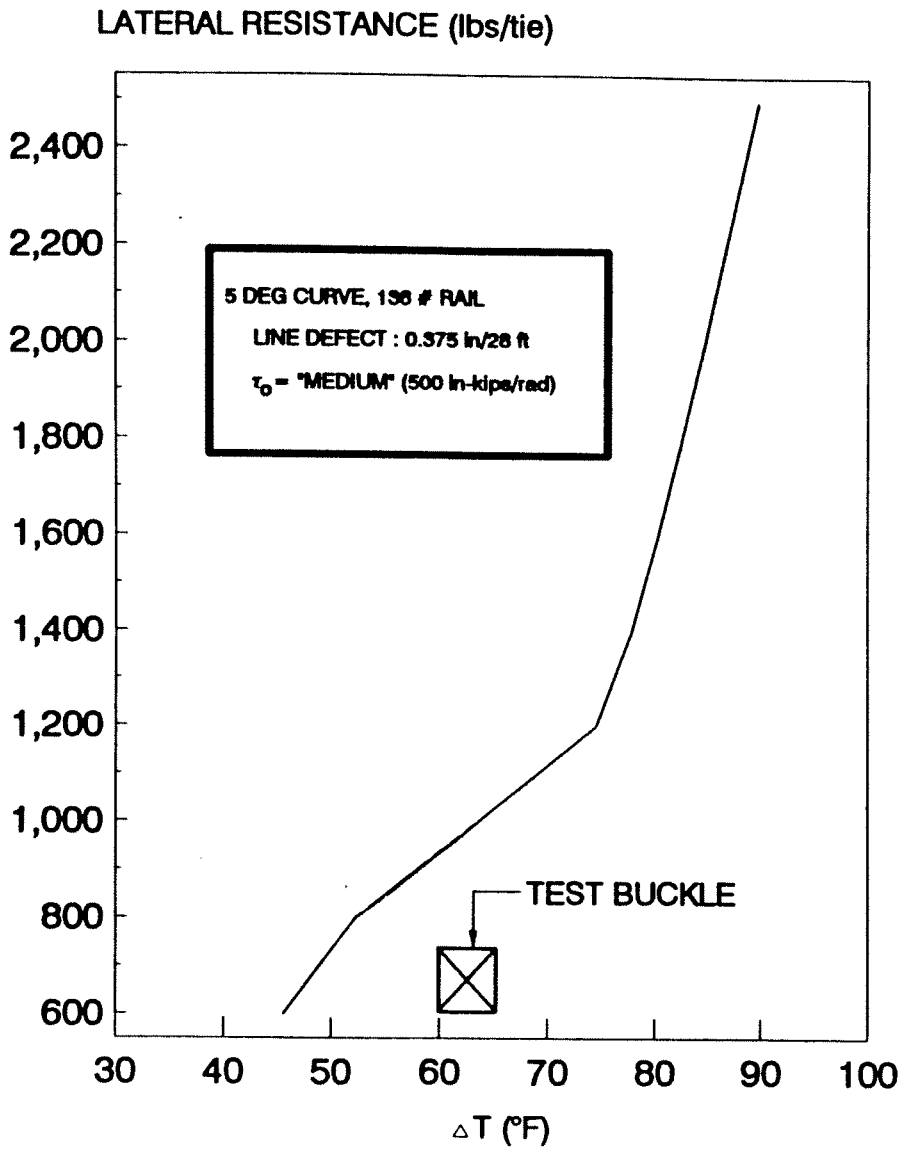

(a) 5° CURVE

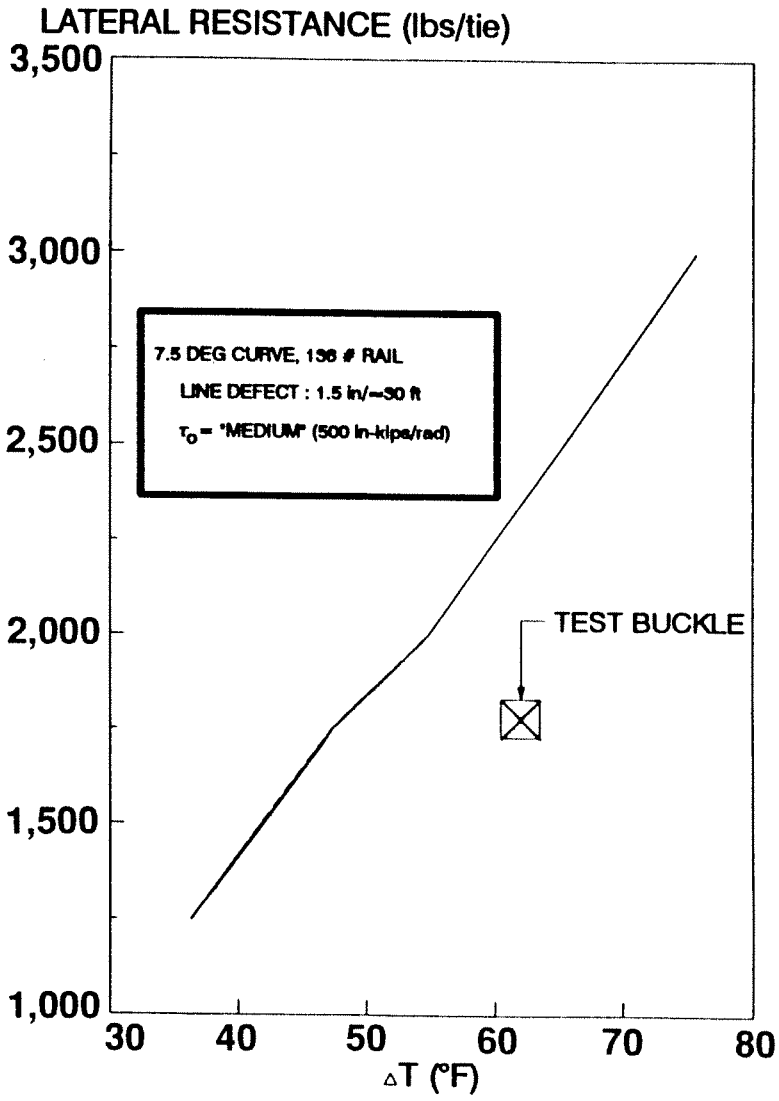

(b) 7.5° CURVE

Figure 4-9. Test Data Plotted on Safety Limit Charts

causing problems for train negotiation. The main problem with the deflection criterion is that the ballast does not act like a spring at track deflections larger than a few millimeters. The resultant deflection tends to be cumulative with the passage of multiple wheels eventually reaching a critical limit. Furthermore, the track deflections tend to destroy the shoulder and other components of the ballast resistance. The lack of control on the ballast resistance due to the track deflections does not make the deflection criterion a viable tool for buckling safety implementation.

5. CONCLUSIONS AND RECOMMENDATIONS

Based on the work presented in the previous sections, the following conclusions and recommendations are drawn:

1. The PC based software using the dynamic buckling theory developed by VNTSC and Foster-Miller has incorporated a wide range of parameters which influence track stability. Using this software, predictions of CWR track buckling response and calculations of the energy required to buckle the tracks can be made with reasonable accuracy.

2. Above the lower critical temperature (at which the energy required to buckle is finite), the buckling energy of CWR track decreases rapidly with increasing temperature, and is zero at the upper critical temperature. Similarly, the finite energy required to buckle the track at the lower critical temperature decreases rapidly with increasing track curvature or increasing misalignment amplitude.

3. Curvature in general is one of the most important parameters which influence buckling strength. Buckling strength decreases rapidly with increasing curvature. For track conditions with a lateral resistance peak of 100 lb/in. (2,000 lb/tie) the buckling response tends to be progressive at curvatures greater than 10 deg.

4. The lateral resistance is also one of the most important parameters influencing buckling. In particular, the lateral resistance peak, F_p, strongly influences the upper critical temperature, whereas the limiting resistance, F_L, significantly influences the lower critical temperature. The peak constant idealization overestimates both the upper and lower critical temperatures. The softening model gives results close to the full nonlinear model, but is less complex and requires fewer iterations for convergence of the solution.

5. The torsional resistance characteristics can generally be linearized within the range of practical interest. The torsional resistance significantly influences the lower critical temperature; for typical wood ties, an increase of 10 to 12°F can be achieved by increasing torsional resistance. The impact on the upper critical temperature is not as significant.

6. The longitudinal resistance characteristics are not linear, but due to the typically small deflections, the resistance can be linearized in the range of interest. The longitudinal resistance has minimal influence on the upper critical temperature. However, the lower critical temperature shows a possible increase of approximately 10°F over the range of longitudinal resistance of 0 to 500 psi.

7. The results show that the upper and lower critical temperatures both decrease with increasing rail size, with the upper temperature showing the largest decrease. Although the rail bending moment of inertia increases with increasing size, the rail cross-sectional area also increases. The increase in area increases the thermal force, which overcomes the corresponding increase in bending stiffness, thus reducing the overall buckling strength.

8. Misalignments significantly influence the upper critical temperature, and to a lesser extent, the lower critical temperature as well. Increasing misalignment amplitude or decreasing misalignment wavelength acts to reduce the upper critical temperature. A large misalignment amplitude with a small wavelength can result in progressive buckling.

9. Increasing track foundation vertical stiffness generally increases the upper critical temperature. The effects on the lower critical temperature are relatively insignificant, especially when the foundation modulus is greater than approximately 4,000 psi.

10. Vehicle loads significantly affect the upper critical temperature, which decreases with increasing axle loads. The lower critical temperature is not significantly affected by these load variations. Similarly, truck center spacing most strongly influences the upper critical temperature, with the lower critical temperature being relatively unaffected.

11. The allowable rail buckling temperature for safety can be expressed as a function of the lateral resistance peak and misalignment amplitude for a given track curvature and rail size. The allowable temperature can then be related to the upper and lower critical temperatures, and a prescribed dynamic margin of safety. A dynamic margin of safety of 10°F is considered to be adequate in buckling safety specifications.

Recommendations

1. The computer code developed by VNTSC and Foster-Miller should be made into a more user friendly expert system for use by the industry. The railroads can use the program to evaluate their specific track and environmental conditions.

2. Implementation of safety limits is also an important consideration for CWR track. The available hardware to measure the lateral resistance (Single Tie Push Test Device, Appendix B), and the neutral temperature (Rail Uplift Device, Appendix E) need further refinement for speedy practical applications. The safety limits can be "uncoupled" in the form of a minimum lateral resistance (MLR) and a minimum neutral temperature (MNT). Using this basis, a Go or No-Go inspection method should also be developed along with the safety limits.

3. The lateral and longitudinal resistance data used in the study are pertinent to the wood tie track. For concrete tie track, the resistance characteristics could be different and need to be evaluated through testing for incorporation in the computer model.

4. The influence of heavy axle loads on CWR track buckling seems to be significant according to the computer model. Experimental validation of this influence will be of practical interest to the industry which is contemplating increasing freight loads on the cars.

5. The track lateral shift under large L/V at high speeds has not been included in the computer code. This mechanism can contribute to the formation and growth of initial misalignments. The present code assumes an initial misalignment amplitude and investigates the stability under thermal and vehicle vertical loads. Inclusion of L/V in the overall safety limits should be considered for high speed track (greater than 125 mph).

6. REFERENCES

1. Kish, A., G. Samavedam, and D. Jeong, *Influence of Vehicle Induced Loads on the Lateral Stability of CWR Track*, FRA/ORD-85-3 (March 1985).

2. Samavedam, G., A. Kish, and D. Jeong, *Experimental Investigations of Dynamic Buckling of CWR Tracks*, DOT/FRA/ORD-86/07 (November 1986).

3. Samavedam, G. and A. Kish, *Analyses of Phase III Dynamic Buckling Tests*, DOT/FRA/ORD-89/08 (1990).

4. Kish, A. and G. Samavedam, *Dynamic Buckling Test Analyses of a High Degree CWR Track*, DOT/FRA/ORD-90/13 (1990).

5. Kerr, A.D., *Analysis of Thermal Track Buckling in the Lateral Plane*, DOT/FRA/ORD-76/285, NTIS PB267938 (September 1976).

6. Samavedam, G., *Buckling and Post Buckling Analyses of CWR in the Lateral Plane*, Technical Note TN-TS-34, British Railways Board, R&D Division (January 1979).

7. Kish, A. and G. Samavedam, "Dynamic Buckling of CWR Tracks: Theory, Tests and Safety Concepts," *Proceedings of TRB on Track Lateral Stability* (May 1990).

8. Samavedam, G. and A. Kish, "Buckling Safety Assurance from Rail Force and Lateral Resistance Measurements," *Proceedings of TRB on Track Lateral Stability* (May 1990).

9. Kish, A., S. Kalay, A. Hazell, J. Schoengart and G. Samavedam, "Rail Longitudinal Force Measurement Evaluation Studies Using the Track Loading Vehicle," *AREA Bulletin 741* (October 1993).

APPENDIX A

BUCKLING ENERGY CONSIDERATIONS

As stated in the text, the external energy required to buckle the CWR track at a given rail temperature can be used as a measure of the degree of stability. The energy may originate from several sources including the dynamic lateral loads producing work in displacing the track laterally.

The energy computed in the program is that required to buckle the track explosively from the initial stable branch AB (Figure 2-3) into the post-buckled stable branch SC shown in this figure. Clearly, at the point B where $T = T_{B,MAX}$ the required energy to buckle the track is zero. At the lower critical temperature (point A), $T_{B,MIN}$, the track requires a finite amount of energy for buckling. The variation of the buckling energy as a function of rail temperature, along AB, can be determined from the computer code. For the progressive buckling case (Figure 2-4), there is only one equilibrium branch, beyond T_P, hence, the energy concept has no relevance.

The safety limits on the allowable rail temperature are designed to provide some energy barrier to prevent explosive buckling. Two examples, one for a tangent and the other for a 5 degree curved track, quantifying the energy, are presented in Figures A-1 and A-2. Table A-1 gives the list of assumed parameters for these examples.

These examples clearly show the rapid decrease in the required buckling energy from $T_{B,MIN}$ to $T_{B,MAX}$ in both tangent and curved cases. The significant decrease in the degree of stability (measured in terms of the reduced buckling energy) of the curved track in comparison with the tangent track can also be seen. The energy computations support the basis of the safety criteria illustrated in Figure 4-1. The margin of safety, Δ, in this figure can be a qualitative measure of the energy barrier at $T_{B,MIN}$. Case I in the figure has a higher energy barrier compared to Case II due to its higher Δ. The allowable temperature, T_{ALL}, for Case I is $T_{B,MIN}$, whereas for Case II it is stipulated at a reduced value due to the lower energy barrier of the latter.

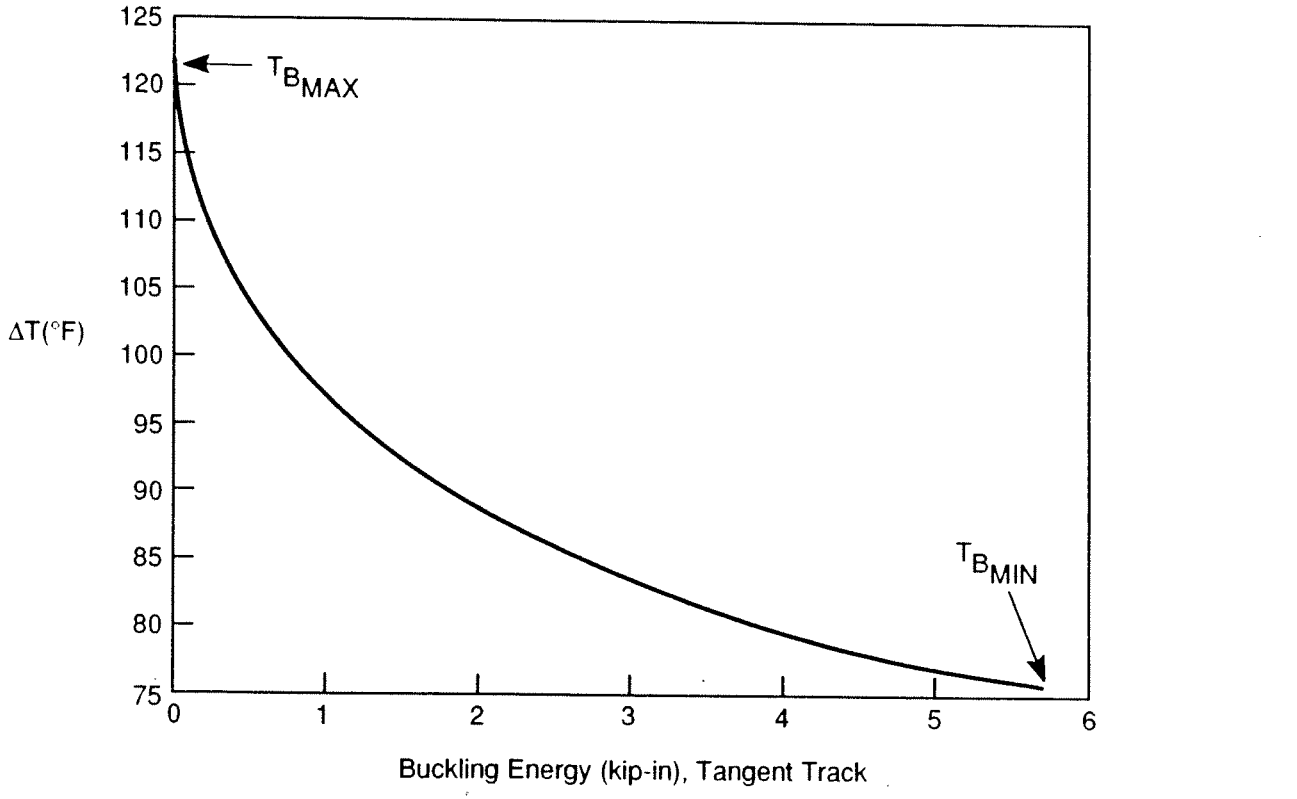

Figure A-1. Buckling Energy, Tangent Track

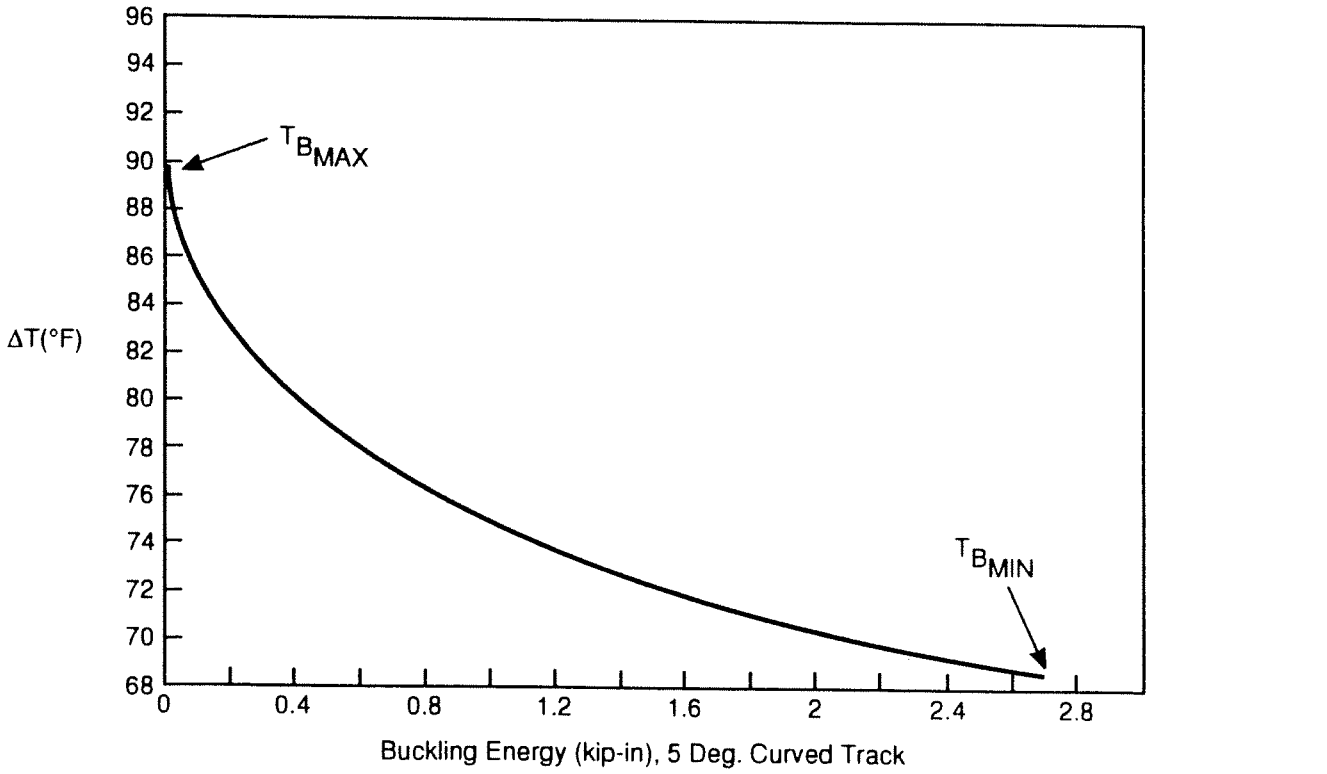

Figure A-2. Buckling Energy, 5 deg Curved Track

Table A-1. Assumed Parameters

Rail Size (lb/yard)	132
Ballast Type	Granite
Peak Lateral Resistance (lb/in.)	125
Tie-Ballast Friction Coefficient	1.2
Torsional Resistance	0
Longitudinal Stiffness (lb/in./in.)	200
Foundation Modulus (lb/in./in.) (Vertical stiffness)	6,000
Misalignment Amplitude (in.)	1.5
Misalignment Wavelength (in.) ($2L_o$)	360
Vehicle	Hopper Car

APPENDIX B

LATERAL RESISTANCE EVALUATION AND CORRELATIONS

Track lateral resistance has been measured by a number of research workers in the United States and abroad. The recommended measurement scheme mobilizes only a single tie; some of the previous techniques require lateral movement of a cut panel or the "entire" track section by a concentrated lateral load. In the case where only a single tie is mobilized, the resistance is directly represented by the load-deflection response of the tie; whereas in the case of the panel, the load-deflection response is a combined effect of rail flexural rigidity, rail longitudinal force and nonuniform resistance offered by several ties. The panel deflection response is not directly usable as an input parameter in the buckling analysis. In past buckling investigations, single tie push tests (STPT) were not favored for the lateral resistance measurement because of the "scatter" or variations in the individual tie resistance values. The panel method seemed to provide a "realistic average" for the track resistance, whereas the single tie test seemed to produce a value much higher than the panel average. Therefore, in some previous investigations, the peak STPT values have been divided by an empirical factor in the range 1.3 to 1.5 to arrive at the equivalent panel values. It can be shown that the STPT results are indeed representative of the actual *nonlinear* track resistance, and it is not appropriate to divide the peak values by a factor to arrive at the equivalent panel resistance. The panel response under applied lateral loads can be predicted with reasonable accuracy by treating the rails as a beam on a nonlinear elastic foundation, the nonlinear spacing stiffness being determined by the STPT.

The advantages of the STPT over the panel test are:

- STPTs yield a more fundamental characteristic of the ballast resistance.
- The test is easy to set up and perform.
- The hardware is man-portable and can be used by track crew with minimal training.
- If a discrete panel is used, rail cutting is very destructive and data interpretation is difficult.
- For the continuous panel, the data is substantially skewed by rail longitudinal forces influencing the deflection response.

The disadvantage of the STPT is the variation of the results from tie to tie. However, an arithmetic average of the individual test results is adequate to determine the buckling and safe allowable temperatures from the safety limit charts currently under consideration. It has been shown that for a 50 ft section of CWR track, three randomly selected ties would be adequate to yield a resistance value that can predict the buckling temperatures within 10°F. Individual tie resistance variation is therefore not a significant factor in track resistance characterization.

B.1 Test Hardware

Although STPTs were performed many years ago in the United States and abroad, they were restricted to very small tie displacements and did not cover the "softening" portion of the resistance characteristic. Further, the equipment used was bulky and not suitable for generation of a large database. A new lightweight portable device with a portable X-Y plotter was therefore developed.

The STPT device is shown in Figure B-1. It consists of a hydraulic control unit with a pump and a rig with a hydraulic cylinder. Having removed the spikes, rail anchors and tie plates, the rig assembly grabs the test tie which is now free to move laterally under the rails. The hydraulic piston mounted on the rig reacts with the force required to move the tie against one of the rails. Hydraulic pressure can be provided by the hand pump, or by an electric pump to speed up the operation. Most reported testing was performed by the latter method.

A pressure transducer or load cell in line with the piston and pressure gauge in the control unit (as a backup) indicate the load applied; a rotary potentiometer mounted on the tie measures the displacement with respect to the stationary second rail. The load-displacement relationship is plotted using an X-Y plotter.

B.2 Typical Results

VNTSC conducted a large number of track characterization tests using the STPT device at the Transportation Test Center's (TTC) test tracks in Pueblo, CO and on a number of railroads. Figure B-2 shows typical results for relatively strong, medium and weak tracks. In general, there are two salient points on the characteristics: the peak, F_P, occurring at displacements on the order of 0.25 in. and the limiting value, F_L, at about 5 in. or less. The softening behavior becomes pronounced from high F_P (>1,000 lb), whereas for low F_P (<1,000 lb), the resistance is practically constant with $FL \equiv F_P$.

Figure B-3 gives typical STPT data from tests conducted at TTC, Pueblo, CO. This data is averaged for a large number of tests in the test zones, each of which is several hundred feet long.

The data shows the resistance values up to 2 in. tie displacement for granite and slag at fractional and large consolidation levels. On the basis of such data, the influence of consolidation, type of ballast and the minimum number of STPT required to characterize the track resistance will be presented in the following sections.

B.3 Correlation Study

From the previous data, it is seen that ties need to be laterally displaced over a large distance (≈5 in.) to capture the limiting resistance values. This may be undesirable in revenue service track. Therefore, a correlation between the peak value, F_P, which can be easily determined at small displacements, and the limiting value F_L, has been developed here for use in the buckling model. The scatter in the peak values for a given track has been evaluated, and the sampling size, i.e., number of required STPT over a given track segment for the purpose of averaging the peaks has been determined.

Limiting versus Peak Resistance Values

Considerable test data has been generated to correlate the limiting resistance, F_L, with the peak value, F_P. This correlation depends principally on the type of ballast material. For granite ballast, the linear regression analysis of the data has given the following equation:

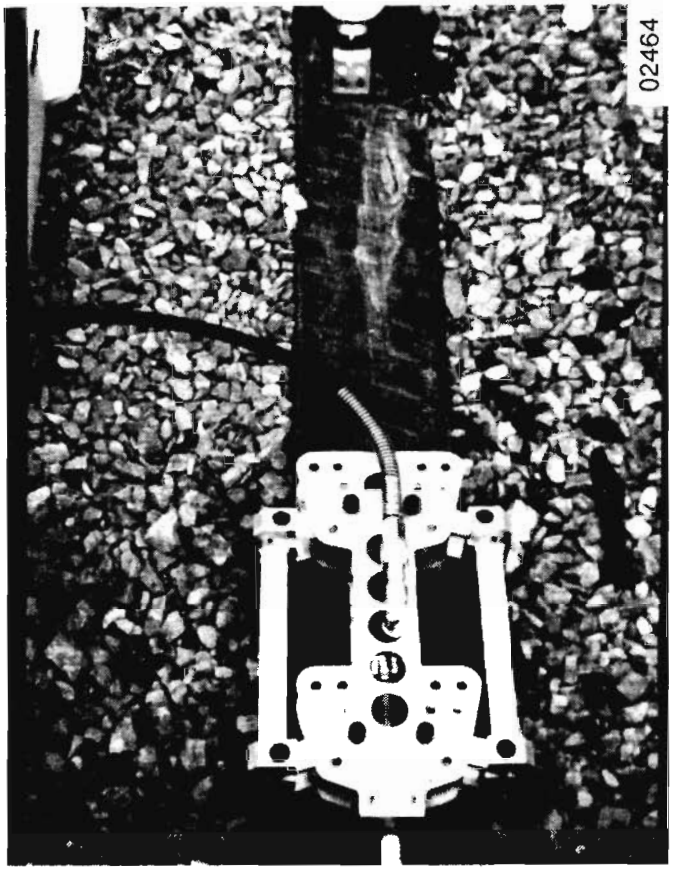

Figure B-1. STPT Device with Plotter

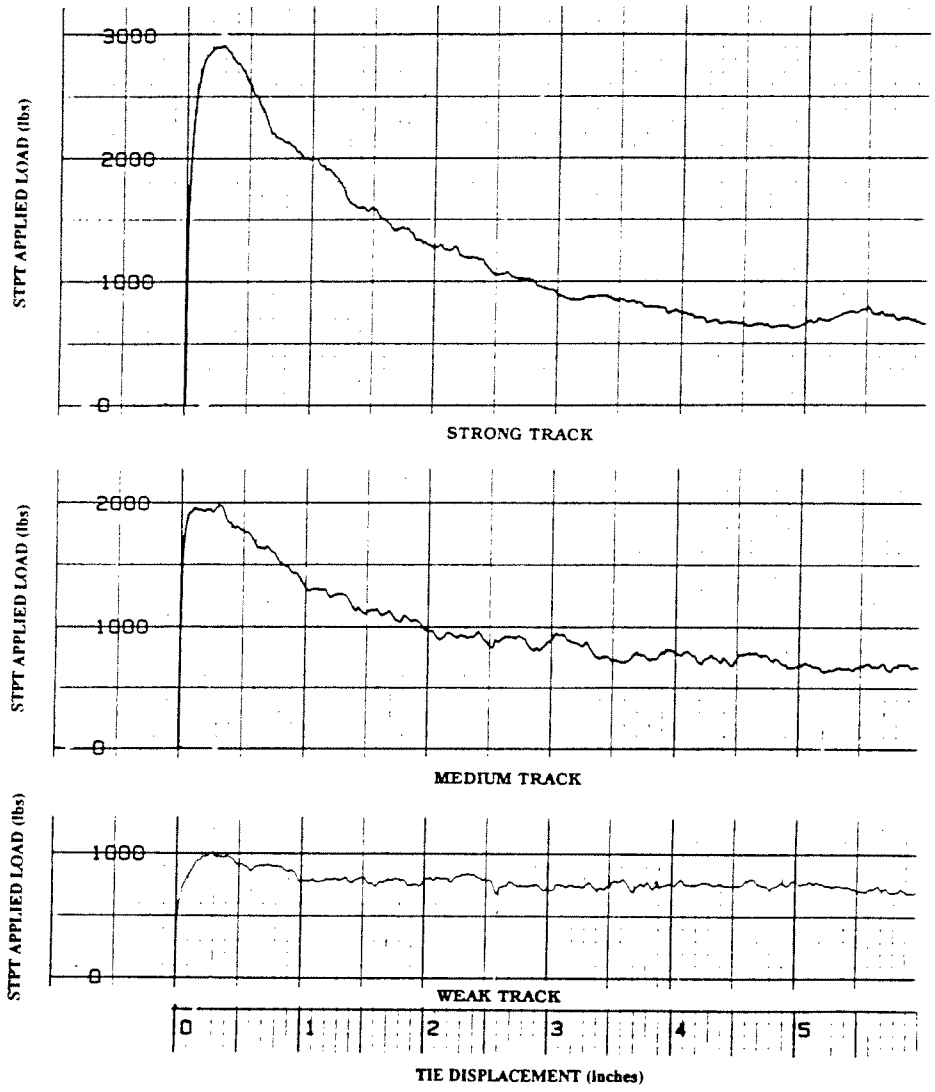

Figure B-2. Typical STPT for Track Response

$$F_L = (0.3\ F_P + 500)\ \text{lb for } F_P > 726\ \text{lb} \quad (1)$$

For $F_P \leq 726$ lb, the case of weak track, we can assume that $F_L = F_P$.

For slag ballast, the equation is found to be:

$$F_L = (0.06\ F_P + 600)\ \text{lb for } F_P > 638\ \text{lb} \quad (2)$$

For $F_P \leq 638$ lb, $F_L = F_P$ as before.

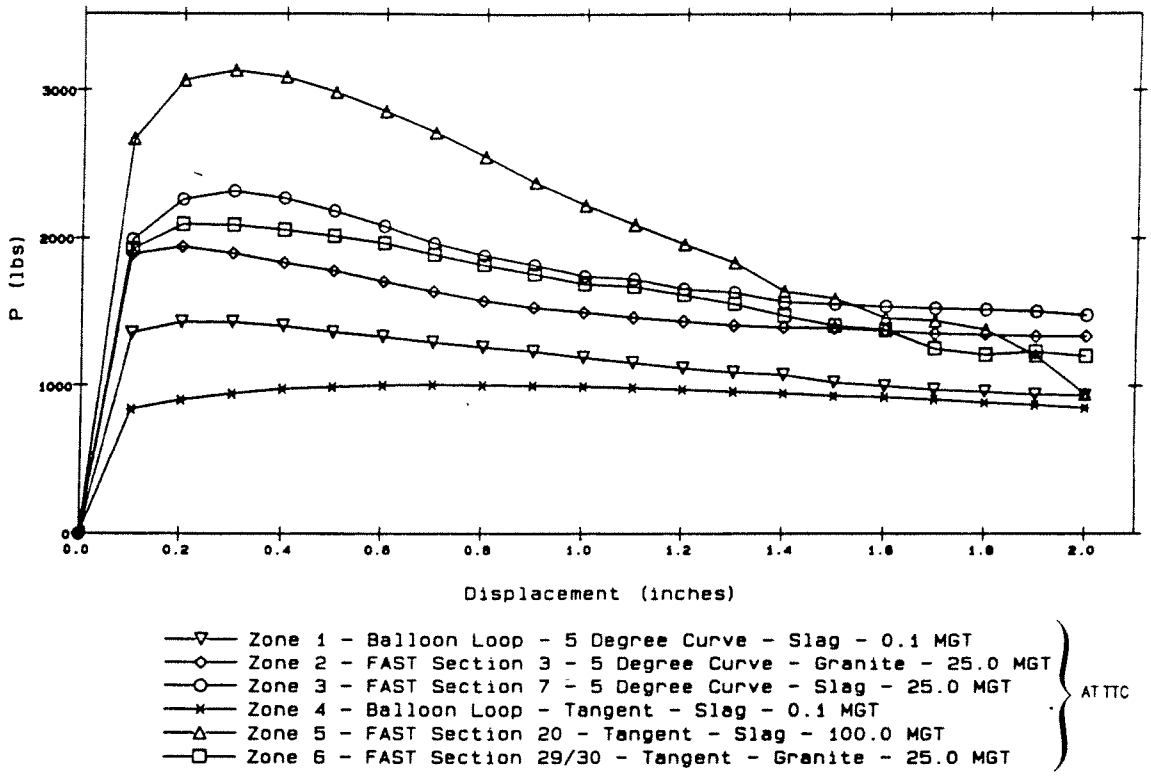

Figure B-3. Ballast Resistance Characterization Tests - Average STPT Behavior Summary

The ability of granite to provide higher limiting lateral resistance is seen from the equations plotted in Figure B-4. It must be noted that the foregoing empirical equations are based on the tests on slag and granite ballasted tracks at TTC, Pueblo, which had a shoulder width of about 12 to 14 in. The equations may not be strictly applicable to other track conditions. The equations are provided to show that it may not be necessary to push test ties over large lateral displacements to determine the full characteristic. Knowledge of the peak value alone may be adequate; this can be easily determined at small displacements without significantly damaging the track.

In the absence of data on limiting values, the foregoing equation may be used in the buckling analysis.

Effect of Track Consolidation

It is known that consolidation under traffic (measured by tonnage accumulation in MGT) increases lateral resistance to some limit. Beyond this limit, consolidation has little effect. What is commonly stated in the literature is that there is a unique relationship between MGT and the absolute value of track lateral resistance. The problem is that immediately after tamping or other maintenance operation, the track resistance drops to a low but unknown value. If the resistance after tamping is measured, the subsequent resistance due to consolidation can be estimated from the data presented here.

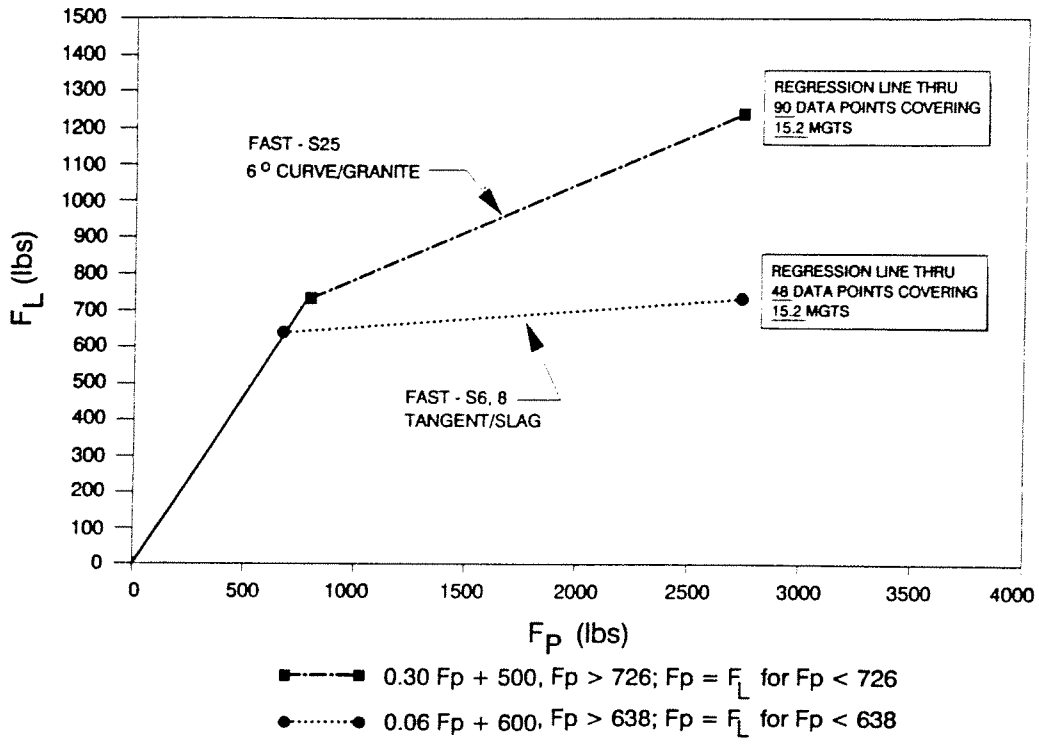

Figure B-4. Peak versus Limit Resistance Comparison

Tests to understand the influence of consolidation on the peak resistance values were conducted on three zones made up of slag, traprock and granite ballast, respectively, and subjected to the same traffic levels. The test results are shown in Figure B-5. Clearly, the resistances at zero MGT for the three zones were not equal, even though the same tamping procedure was employed for each of these zones. The starting values (1,800 lb for slag, 1,520 lb for granite and 1,200 lb for traprock) should be considered as site-specific and cannot be attributed to a particular ballast alone. Previous track operations at these locations, tie conditions and age, and resistance levels prior to tamping can play an important role on the reduced resistance levels after tamping.

Data on peak resistance values collected at several increments in MGT is shown in Figures B-5 and B-6. This data clearly indicates that the resistance values increase monotonically up to some level. Figure B-6 is of particular interest, as it shows the significant gain in peak lateral resistance for small increments in consolidation. Such data will be helpful in determining slow order duration for reduced train speeds soon after tamping or similar track operations.

Sampling Size

Due to inherent variations in the ballast and tie conditions, not all the STPTs in a given section will yield the same values. The longer the section is, the greater will be the scatter in the individual resistance values. Besides the section length, the scatter will also depend on the track maintenance standards of the railroad. Tests have also indicated that for a given track section, the scatter increases with the increasing consolidation level.

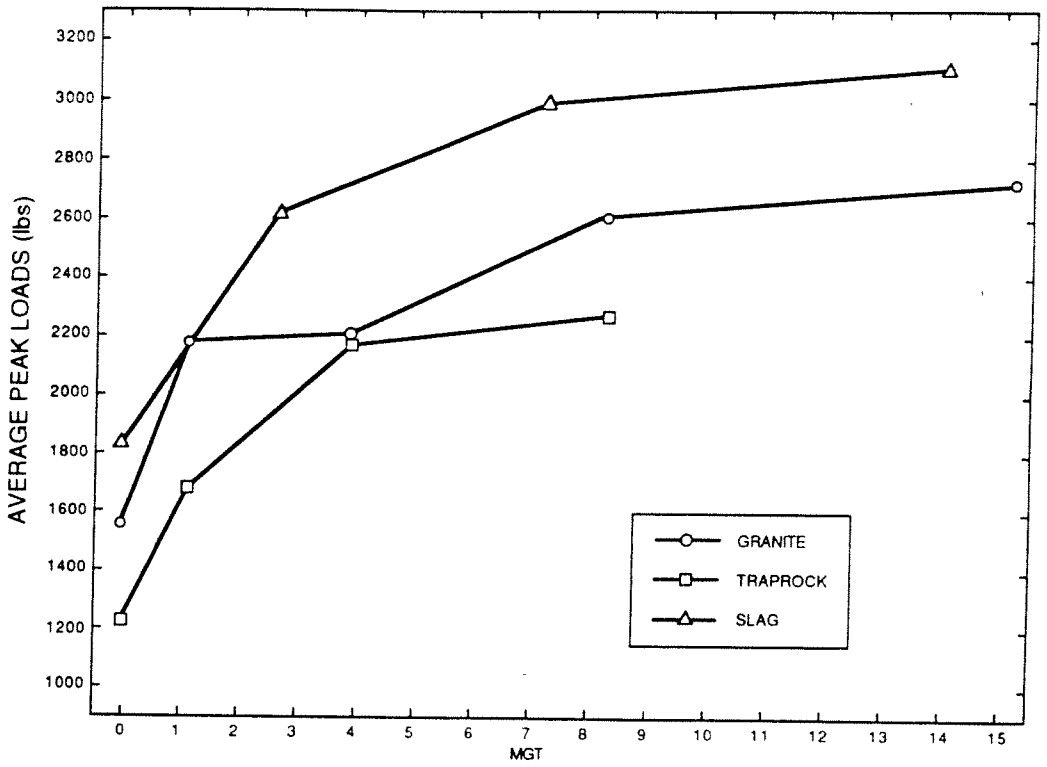

Figure B-5. Ballast Consolidation Influence (AAR/TTC, Pueblo, CO)

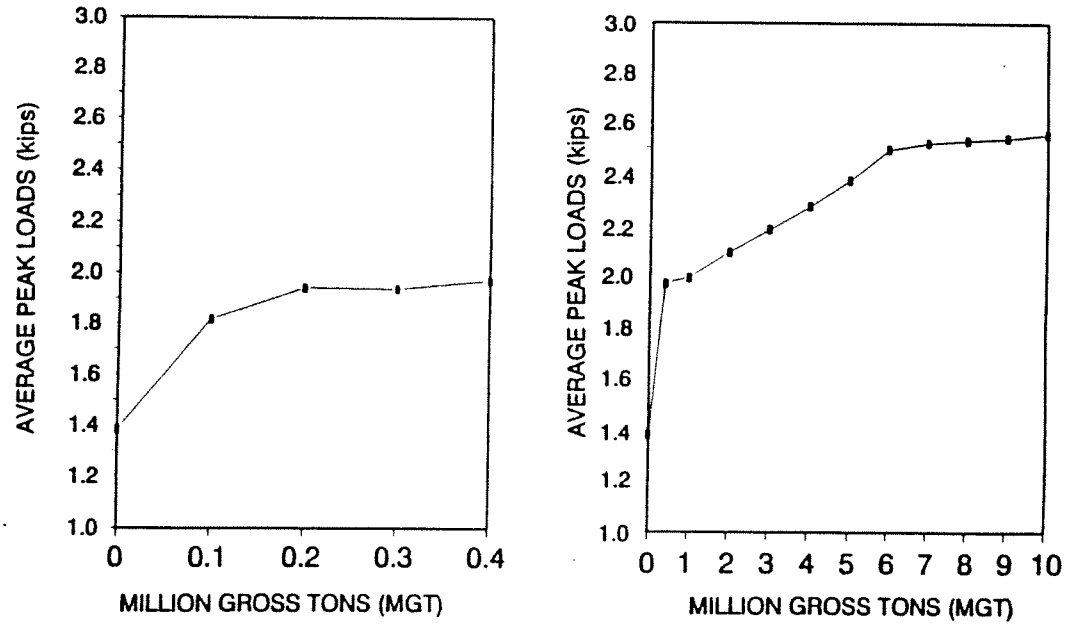

Figure B-6. Fast Ballast Resistance Characterization Tests - Consolidation Influence (Tangent Track - Granite Ballast)

Although the computer model can account for the individual tie variations, it is not practical or desirable to test a large number of ties for buckling safety predictions. The question therefore arises whether a minimum (optimum) number for single tie tests can be established for a given section length, the average of which can be considered as the resistance for the section under consideration. Such an average can then be used as an input parameter in the buckling model.

To address the foregoing question, a large number of tests were performed at TTC, Pueblo on different track sections, at different consolidation levels. Test sections about 50 ft in length were considered for the case studies. In each of the sections, every alternate tie was tested and the average of the 15 tested ties was considered to be the lateral resistance for the 50 ft long section.

If fewer than 15 ties in each of the 50 ft long sections were tested, the average of these results would clearly differ from the overall average, F_o. Suppose we select randomly three ties whose peak resistance values are F_1, F_2 and F_3. Defining the average of these as F_m, the error with respect to the overall average F_o is

$$\text{Percentage error} = (F_m - F_o)/F_o$$

Using a random number generator, the percentage error was determined in five trials (each trial yields one set of F_1, F_2 and F_3 from the random number generator) and the *maximum* error produced in these trails for each of the six 50 ft test sections is plotted in Figure B-7. This is repeated for all the zones previously referred to in Figure B-3.

From Figure B-7, it is seen that the maximum error is about 20 percent. This error generally translates into an error of about 10°F in the safe allowable temperature from the buckling model. (Clearly, by testing more than three ties in every 50 ft section, the error can be correspondingly reduced below 10°F.) Hence, we conclude that a sample of three randomly selected ties for every 50 ft section may be adequate in the field application of STPT. Clearly, a linear extrapolation of this result would imply testing six ties for 100 ft sections. However, by visual inspection and proper engineering judgement, the number of STPTs required per unit of length can further be reduced as the length of section increased.

Results for a sample size of five ties/50 ft section, not presented here, indicate a maximum error of 10 percent, which is more than adequate from a practical point of view.

Figure B-7 also indicates that tracks with low consolidation levels have a lower percentage error than highly consolidated tracks. This is fortunate because STPT results are more important for tracks with low consolidation levels.

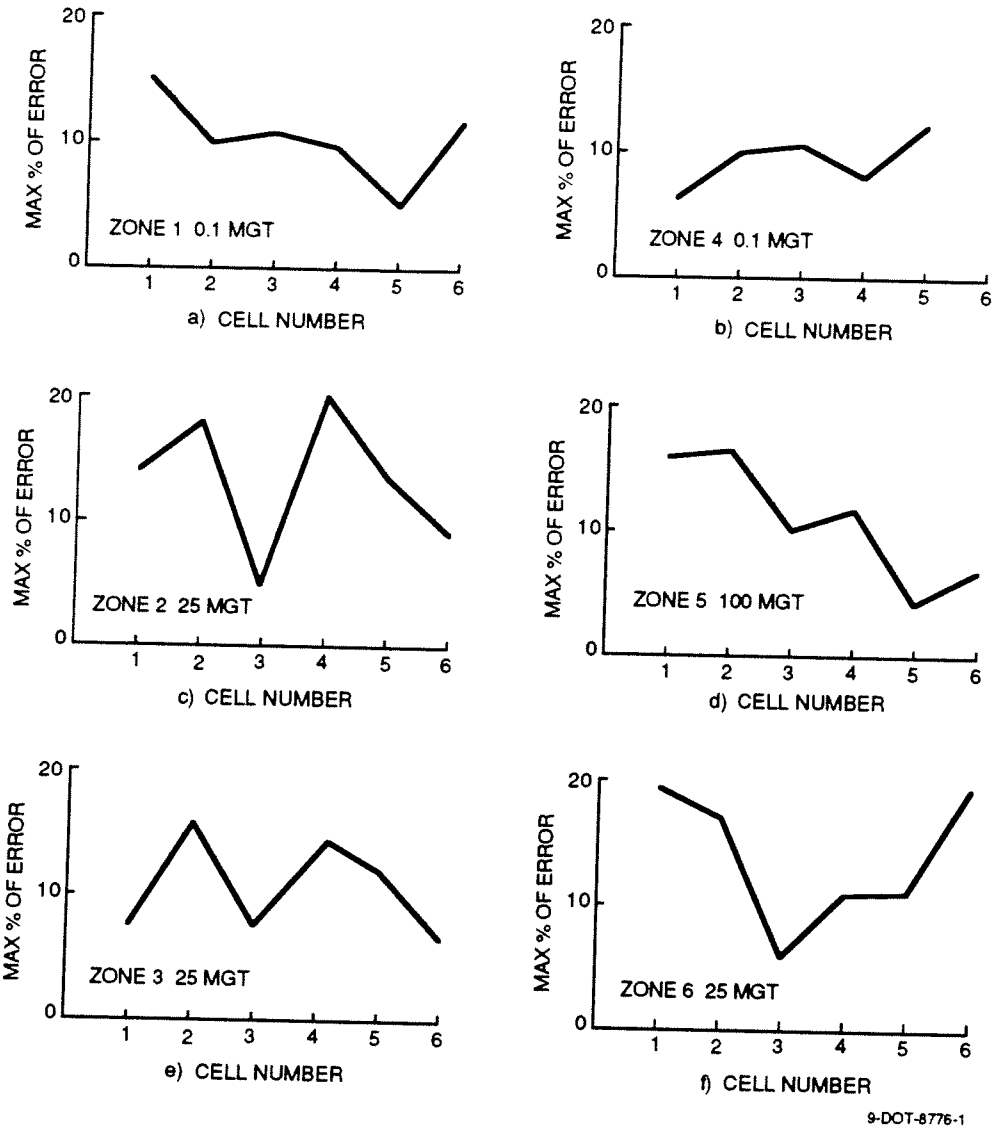

Figure B-7. Error Due to Finite Sampling of Test Ties

APPENDIX C

TORSIONAL STIFFNESS EVALUATION

The torsional resistance is offered in the fasteners when the rail tends to rotate with respect to the ties. In recent work by VNTSC two test series were used to evaluate the resistance responses of common fastening systems. Series I utilized laboratory test conditions to obtain the full response curve of the complete fastener system, while Series II focused on the in situ response of fastener systems under field conditions. Many rail fastener systems were tested including Pandrol clips, McKay Safeloks and cutspikes with an emphasis placed on wood ties with cutspike construction.

In the laboratory tests, the tie was held rigidly in a fixture, and equal and opposite loads were applied as shown schematically in Figure C-1. The lateral loads were applied via hydraulic cylinders at the rail base to prevent rotation about the longitudinal axis. The rail displacement was measured at the base by transducer. All tests were conducted to at least a 5 degree rotation or until the onset of tie material degradation or visible tie rotation. In cases of concrete tie fasteners, testing was further suspended if insulators broke.

In the field tests, wood ties with cutspike construction under existing service conditions were considered. The rails were cut into 40 in. sections. Two configurations of loading were used in the testing as shown in Figure C-2. Configuration B in Figure C-2 is preferred to Configuration A, as it produces pure torque without lateral load on the fasteners. The test section chosen was 136#RE jointed rail with rail anchors on every other tie permitting an assessment of anchor influence. A total of 16 rail segments were tested. The test configuration again followed the configuration given in Figure C-1 with the exception that STPT rigs were used on adjacent ties to impart the required moment load to the test rail.

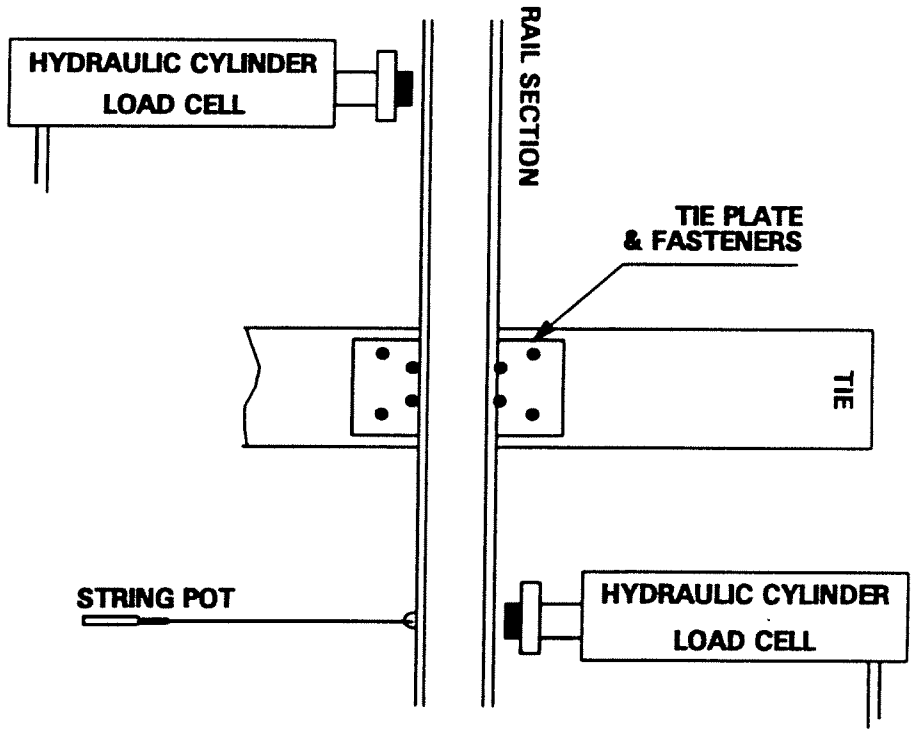

Figure C-1. Laboratory Setup

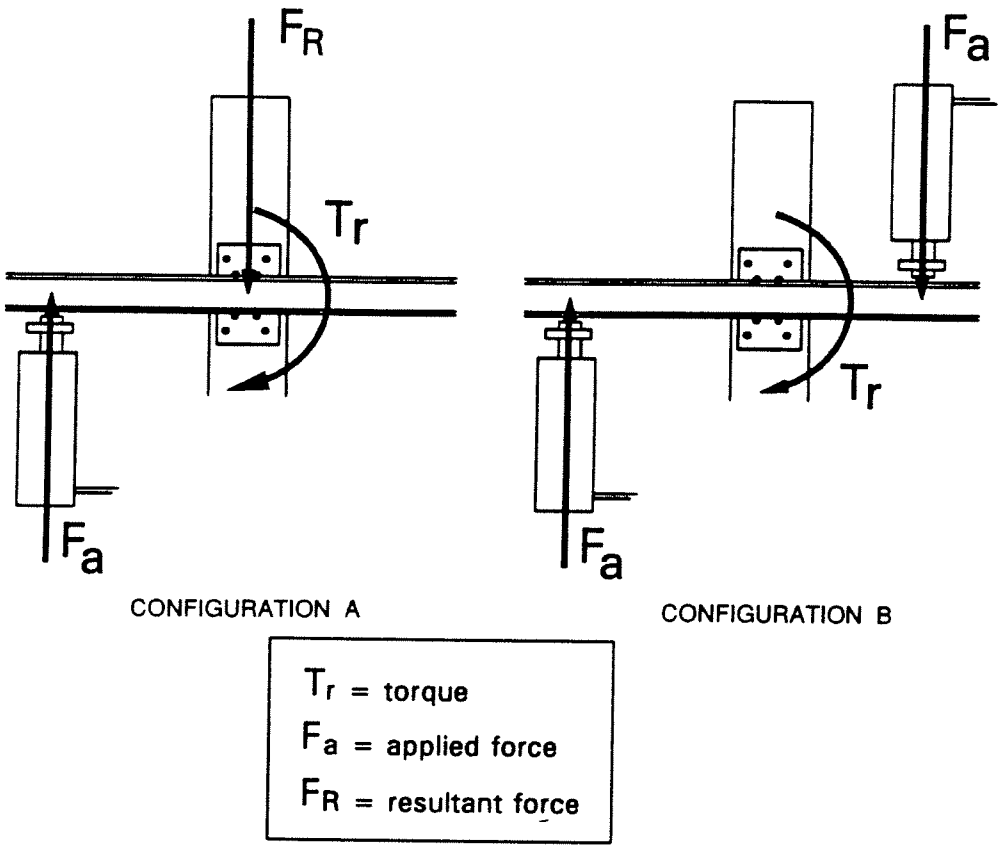

Figure C-2. Field Setups

C.1 Concrete Tie Test Results

McKay Safelok and Pandrol fastener systems were tested on concrete ties. Several test runs were performed to determine the effect of fully driven clips versus partially driven. No apparent difference in torisonal resistance response was observed. Further comparisons were made between polyurethane pads versus rubber pads; again no significant differences were observed in the response curves. Overall, both systems exhibited a soft torsional resistance response in comparison with wood tie systems as will be seen in the following section. The reason for the soft response is primarily due to the elasticity offered by the resilient pads and the softness of the insulators. This elastic attribute of the pads allowed the applied torque to be absorbed through insulator "crushing" rather than by the clips themselves, a fact that was observed through examination of the insulators upon completion of each test run. The response for pandrol clips was in the same range as those of the McKay Safelok, suggesting fastening types on concrete ties play little role in determining the torsional resistance; rather the existence of insulators/pads appears to be the controlling factor. The comparison of the Pandrol and McKay results can be seen in the Figure C-3.

C.2 Wood Tie Test Results

As referred to above, the wood tie fastening systems tested produced a much stiffer result than the concrete Pandrol and McKay systems, Figure C-4. The specific fasteners tested on wood ties were a typical cutspike construction and Pandrol fastener clips with both lock and screw spikes. Torsional

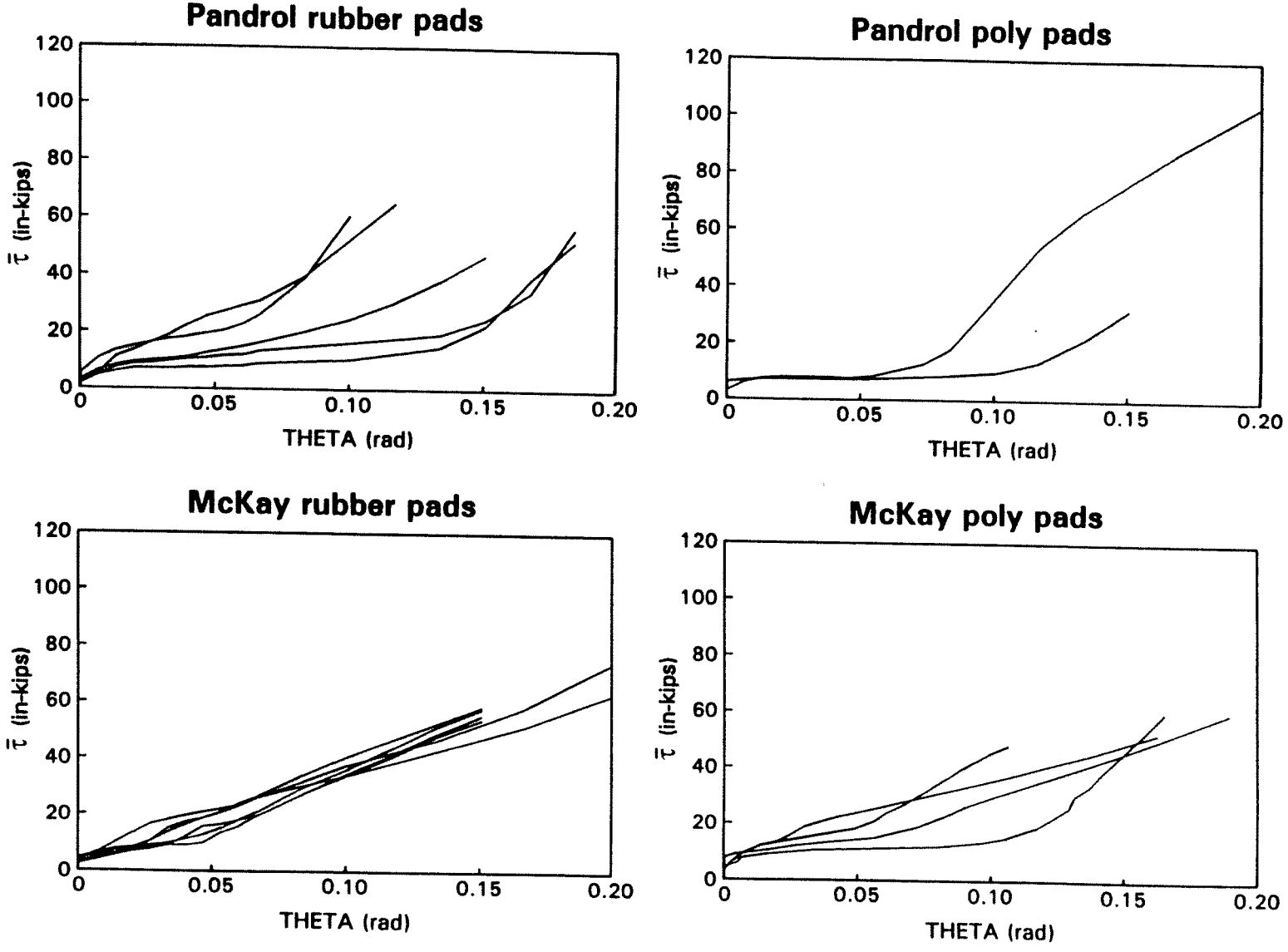

Figure C-3. Concrete Tie Fastener Test Data

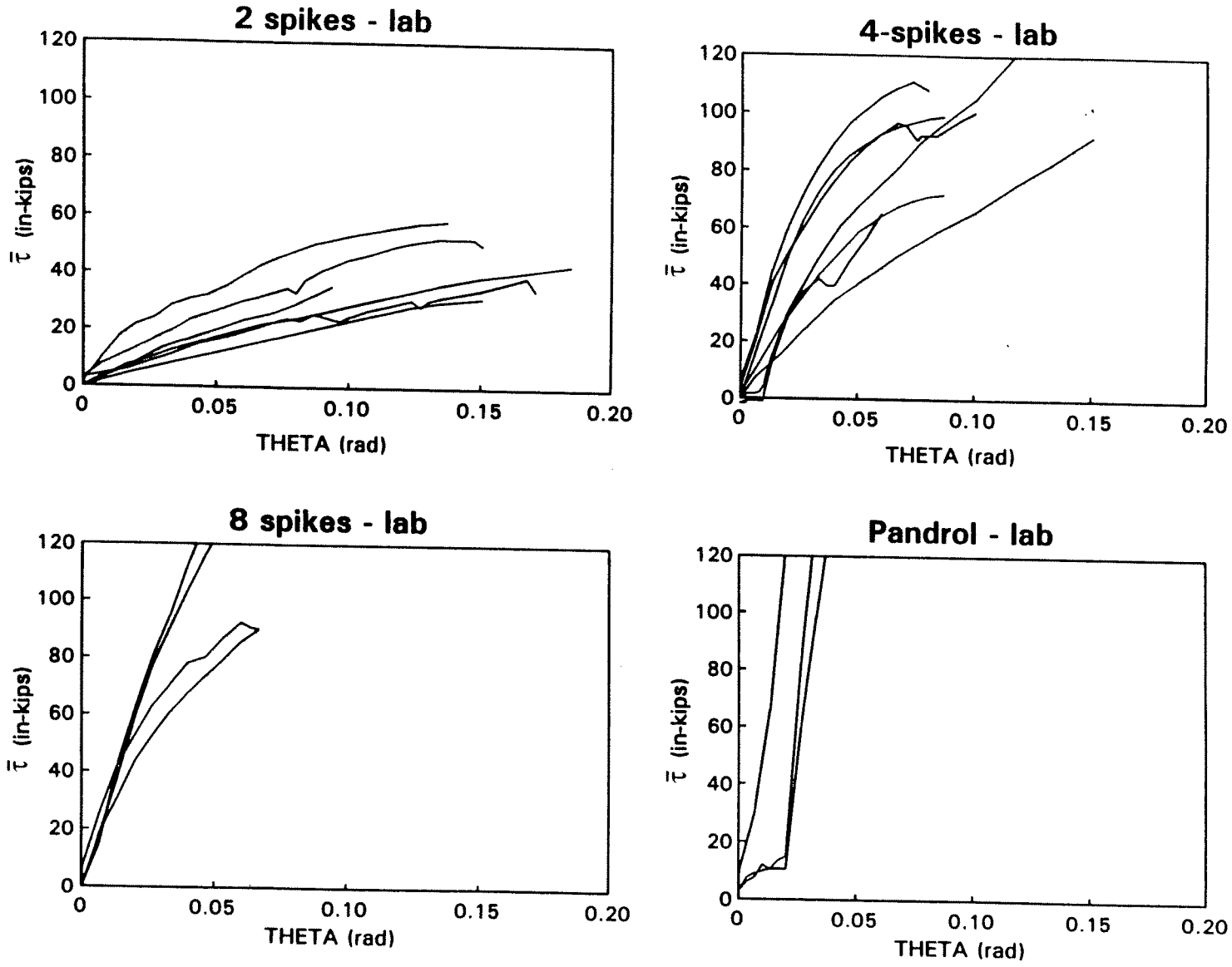

Figure C-4. Wood Tie Fastener Test Data

response was compared for a variety of wood tie types and condition. It was found that tie type/ condition had little or no influence on the response characteristic, whereas the fastener type itself was a significant parameter. As expected, Pandrols on wood ties were the stiffest, regardless of the use of lock versus screw spikes, followed by eight spikes per plate, four spikes per plate, and finally the softest wood tie characteristic was offered by two spikes per plate.

The ranges of torsional stiffness data for the various conditions are given in Figure C-5. For the most common spike pattern, four spikes per plate, an average torsional stiffness, $\bar{\tau}_0$, of 1203.5 kips-in./rad was computed with a standard deviation, σ, of 375.4. A comparison of the remaining fastener configurations is shown in Table C-1.

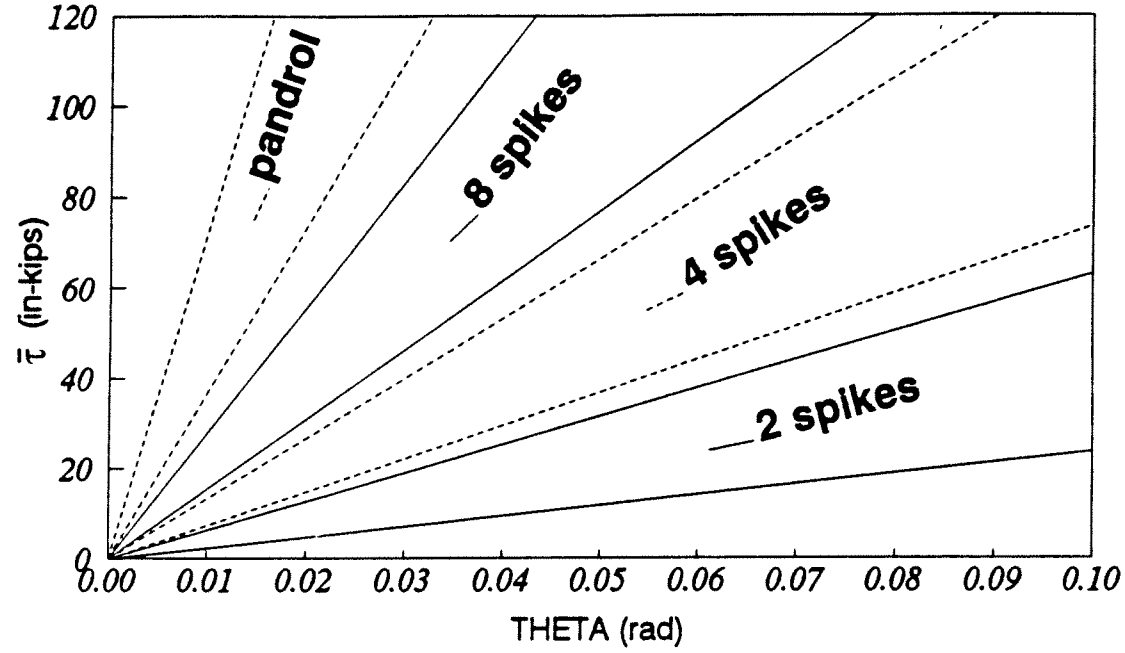

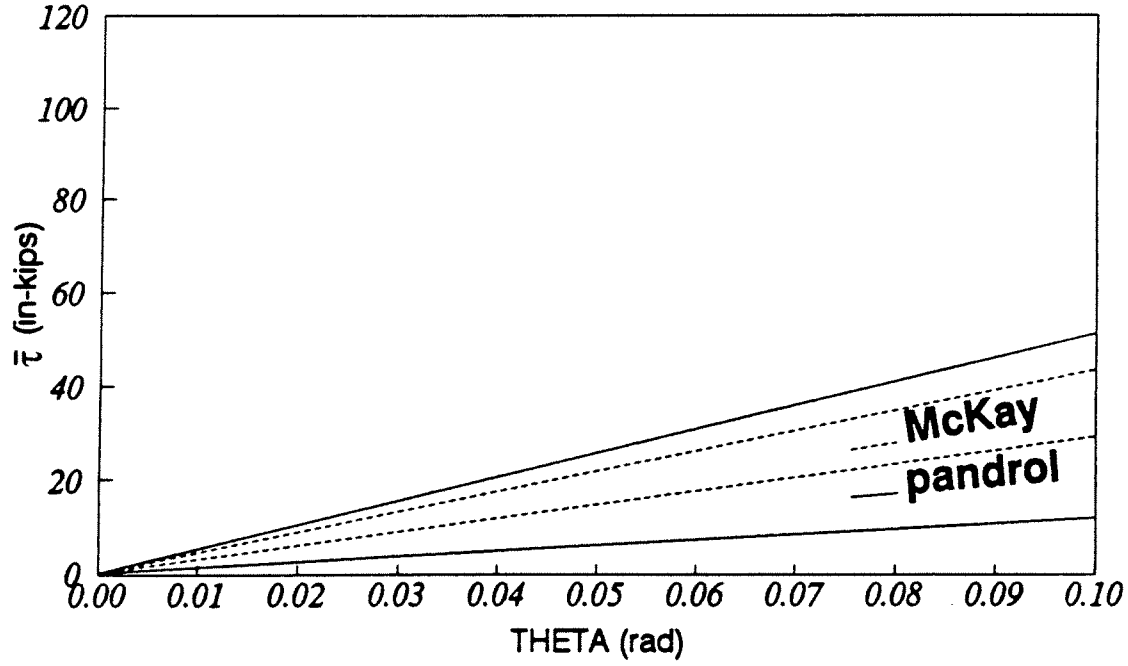

Figure C-5. Range of Linearized Stiffness

Table C-1. Torsional Stiffness Summary

	Fastener System	Average $\bar{\tau}_0$ (kips-in./rad)	σ	No. Tests
Wood ties	Pandrol	5026	1957	3
	8 spikes/plate	2165	589	6
	4 spikes/plate	1203	384	22
	2 spikes/plate	386	145	4
Concrete ties	Pandrol	281	159	7
	McKay Safeloks	343	83	10

σ = Standard Deviation

APPENDIX D

LONGITUDINAL RESISTANCE CHARACTERIZATION

Track longitudinal resistance is defined as the resistance offered by ties and/or ballast to the rails, as they tend to move in the longitudinal direction in the event of buckling, or due to braking and accelerating trains, or due to longitudinal thermal force gradients. At unanchored or loosely anchored ties, the longitudinal resistance is very low. At properly anchored ties, the resistance offered by the ballast is much higher.

The resistance varies with rail displacement as in Figure D-1. Because of the small longitudinal displacement that occurs during a buckling event, the initial stiffness of k_f is adequate in the buckling analyses.

D.1 Test Hardware

The track longitudinal resistance has been determined by isolating a four- or eight-tie panel from the rest of the track, and applying a longitudinal load to both rails by means of hydraulic cylinder (Figure D-2). Longitudinal load was applied to the tested panel until the panel displacement reached a maximum of 2 in. A total of nine tests were performed on panels at the Transportation Test Center (TTC) in Pueblo, CO. Some of these were four-tie panels others were eight-tie panels. Variables included rail anchoring method: Every Tie Anchored (ETA), Every Other Tie Anchored (EOTA), Every Third Tie Anchored (E3TA), and ballast condition (consolidated, tamped, and half crib).

D.2 Test Results

Data included applied longitudinal load, longitudinal displacement, and rail/tie displacement. The load and displacement data were also plotted directly onto an x-y plotter in some cases. A summary of test results is presented in Table D-1. Typical results for these tests are shown in Figure D-3.

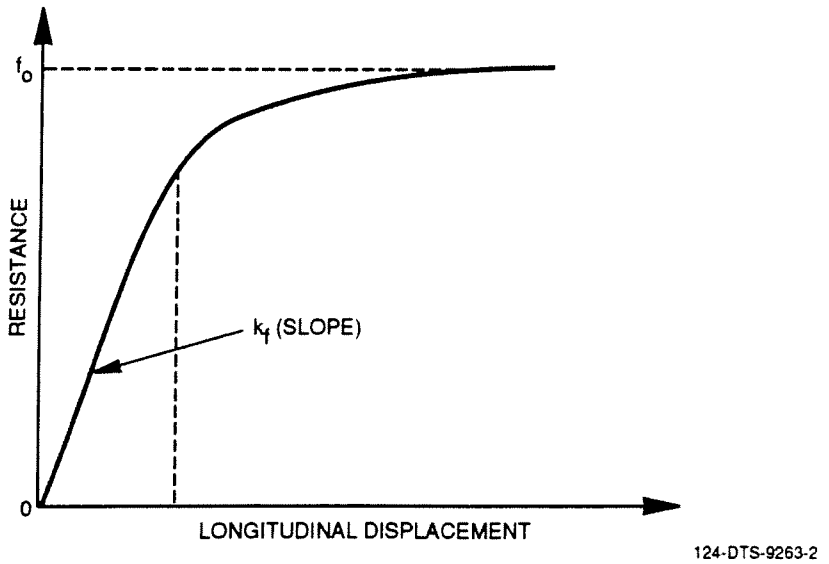

Figure D-1. Typical Longitudinal Resistance Characteristic

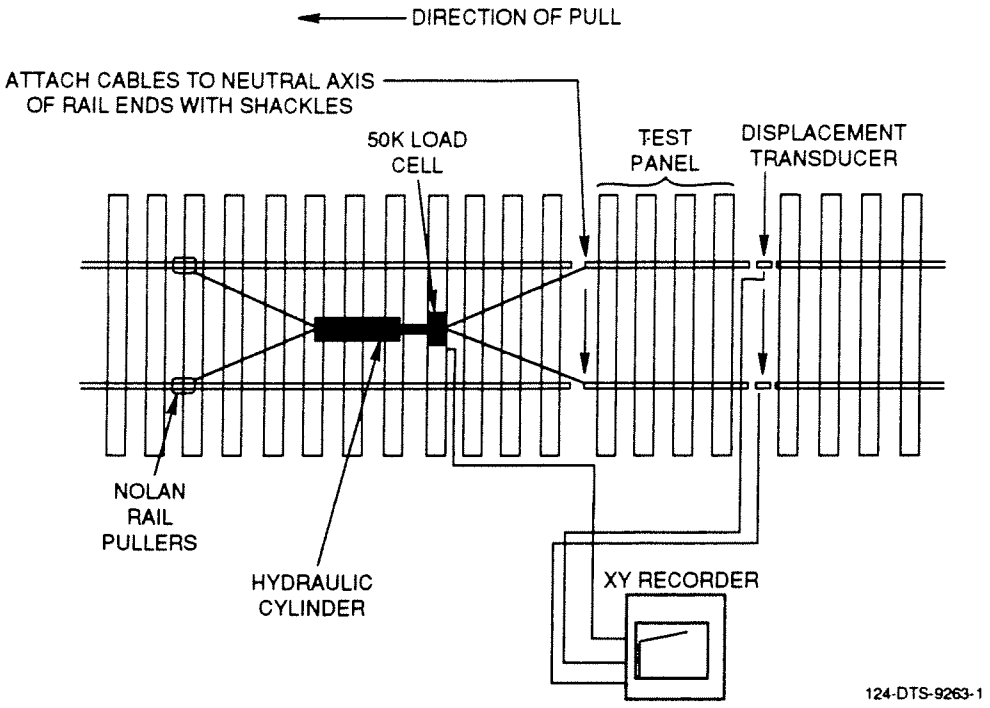

Figure D-2. Test Setup for Longitudinal Resistance Measurement

The test data show the significant influence of the ballast crib level and the anchoring pattern on the track longitudinal resistance as well as the influence of track consolidation. There is also the effect of the number of ties pulled in the test panel, although this difference tends to be under 10 percent at large longitudinal displacements.

The full crib increases the resistance over 50 percent compared to that of the half crib. Track consolidation can increase the resistance by about 30 percent. Anchoring every tie increases the resistance by about 20 percent in consolidated tracks. In tamped tracks, anchoring every third tie reduces the resistance by about 30 percent at small displacements (0.25 in.) compared to every other tie anchored condition.

Table D-1. Track Longitudinal Resistance Summary

Consolidated (kips/tie)				ETA (kips/tie)			EOTA (kips/tie)			ETA and Tamped (kips/tie)			8-Tie and Tamped (kips/tie)		
Defl. (in.)	ETA (1)	EOTA (2)	% Diff.	C (1)	T (5)	% Diff.	FC (2)	HC (4)	% Diff.	4-Tie (5)a	8-Tie (5)b	% Diff.	E3TA (6)	ETA (7)	% Diff.
0.25	1.62	1.27	21.6	1.62	0.85	47.5	1.27	0.63	50.0	0.85	1.28	33.6	0.89	1.28	30.5
0.50	2.08	1.64	21.2	2.08	1.33	36.1	1.64	0.71	56.7	1.33	1.51	11.9	1.17	1.51	22.5
0.75	2.29	1.81	21.0	2.29	1.52	33.6	1.81	0.74	59.1	1.52	1.67	9.0	1.31	1.67	21.6
1.00	2.28	1.91	16.2	2.28	1.56	31.6	1.91	0.74	61.3	1.56	1.72	9.3	1.39	1.72	19.2
Limit	2.31	1.91	17.3	2.31	1.61	30.3	1.91	0.74	61.3	1.61	1.77	9.0	1.48	1.77	16.4

Condition	Linear Stiffness, k_f (kips/in./in.)		Limiting Resistsance, f_0 (kips/in.)
	0.25	0.50	
ETA (consolidated)	0.324	0.208	0.116
EOTA (consolidated)	0.254	0.164	0.096
ETA (tamped)*	0.213	0.142	0.085
EOTA (consolidated 1/2 crib)	0.126	0.071	0.037
E3TA (tamped)	0.178	0.117	0.074

ETA: Every tie anchored
EOTA: Every other tie anchored
T: Tamped
C: Consolidated
FC: Full crib
HC: Half crib
*Average of 4-tie and 8-tie panel
( ) Test No.

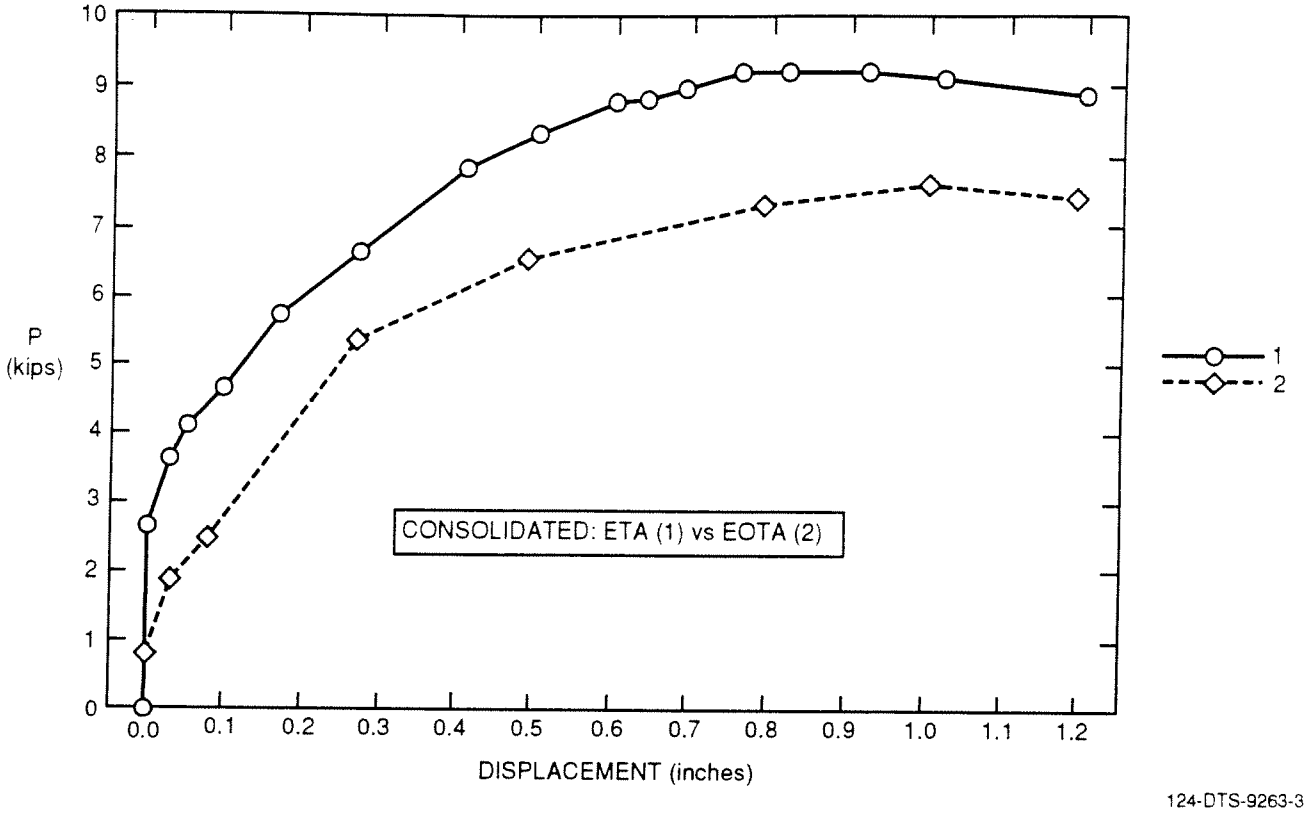

Figure D-3. Typical Longitudinal Resistance Test Results

APPENDIX E

RAIL NEUTRAL TEMPERATURE EVALUATION

The CWR neutral temperature is an important parameter controlling the buckling safety of CWR tracks. The neutral or force-free temperature of CWR can be different from the initial temperature at installation. If the rail force, P, is known at a given rail temperature, T, then *assuming the rails are fully constrained*, the neutral temperature, T_N, can be calculated from the equation:

$$P = AE\alpha(T - T_N)$$

Here, A = rail cross-sectional area; E = modulus; α = coefficient of thermal expansion. Of course, the rails are not fully constrained, but the equation can still be used to define a "variable" neutral temperature. Mechanisms contributing to neutral temperature variations include rail longitudinal movements, track lateral shift/radial breathing in curves, and track vertical settlement. Rail longitudinal movement results from train braking and acceleration forces, or from differential thermal forces (sun and shade). Track lateral shift can be caused by excessive truck hunting, lateral forces generated by curving, or negotiation of lateral misalignments. Rail force can cause radial breathing of curves in weak ballast conditions. Vertical differential settlement of rails can occur on new or recently surfaced track, or in areas of weak subgrade conditions.

These natural mechanisms demand that the CWR neutral temperature be determined from time to time. Track maintenance operations can also affect the neutral temperature. It is desirable to determine the rail neutral temperatures after the track undergoes any such operations. This is particularly important in spring and summer to assure safe, permissible values for buckling safety. Field data collected by VNTSC using strain gauges affixed to rail on a number of revenue service tracks and tracks at TTC showed that the neutral temperature could drop by 20 to 40°F from the installation value, thus significantly increasing the buckling risk on a hot day.

E.1 Measurement of Rail Force

Rail force measurement by Berry gauge, strain gauge and the British Rail Vibrating wire are well-known but are not convenient for practical use in the field. They cannot provide the absolute rail force and need an initial reference level, usually obtained by cutting the rail. The vibrating wire technique needs a hole cut in the rail web. A number of other techniques are under development, and generally suffer from problems of reliability, sensitivity to the rail residual stresses, and site-specific calibration requirements. To address these problems, a new technique has been recently developed by VNTSC and Foster-Miller and a prototype test fixture has been used to validate the technique through field tests. The technique is founded on a well-known principle of mechanics and it provides the absolute force without site-specific calibration. It is not "destructive," but requires removal of spikes and anchors from the test section rail.

E.2 Rail Uplift Method

If the rail is freed from ties over some length, restrained vertically at the ends of the freed portion and subjected to a concentrated uplift load at the center, the resulting deflection depends on the magnitude of the rail longitudinal force. Clearly, longitudinal compressive load will increase the deflection of the "beam-column," and tensile force will reduce it. For a given length of rail, the vertical force required to produce a specified deflection is a measure of these rail forces. The

implementation of the concept is based on the fact that the rail can be conveniently held at the two end points by the wheels of a rail car. This automatically fixes the length of the rail and boundary conditions at the ends of the rail beam. The spikes and anchors between the inner wheels of the two trucks of the car must be removed. Figure E-1 shows schematically the rail uplift method.

An analytical model has been developed as indicated in Figure E-2 to calculate the vertical deflection produced by different levels of rail force. This model proved that the deflection is measurably sensitive within the range of longitudinal forces of interest in buckling safety assessment. Results from the model were used to conduct parametric studies required to plan the tests, design the test fixture and assess measurement sensitivity. Figure E-3 shows the influence of rail size on the uplift force required for different levels of longitudinal force.

E.3 Test Results

Tests were conducted at TTC on a tangent and a 5-deg curved track. A special instrumentation car with inner wheel spacing of 340 in. was adapted to provide a maximum central vertical force of 30 kips. The test sections were instrumented with strain gauges to measure the rail force. The variation in the rail force was achieved through destressing at reasonably high neutral temperatures for tensile loads and by means of artificial rail heating for compressive force levels. The rail force was correlated with the required vertical load for a 2-in. rail uplift.

Figure E-4 shows the mean regression line for all the test data and also the theoretical prediction. Good agreement between the theory and the test is seen from the figure. It is concluded that the

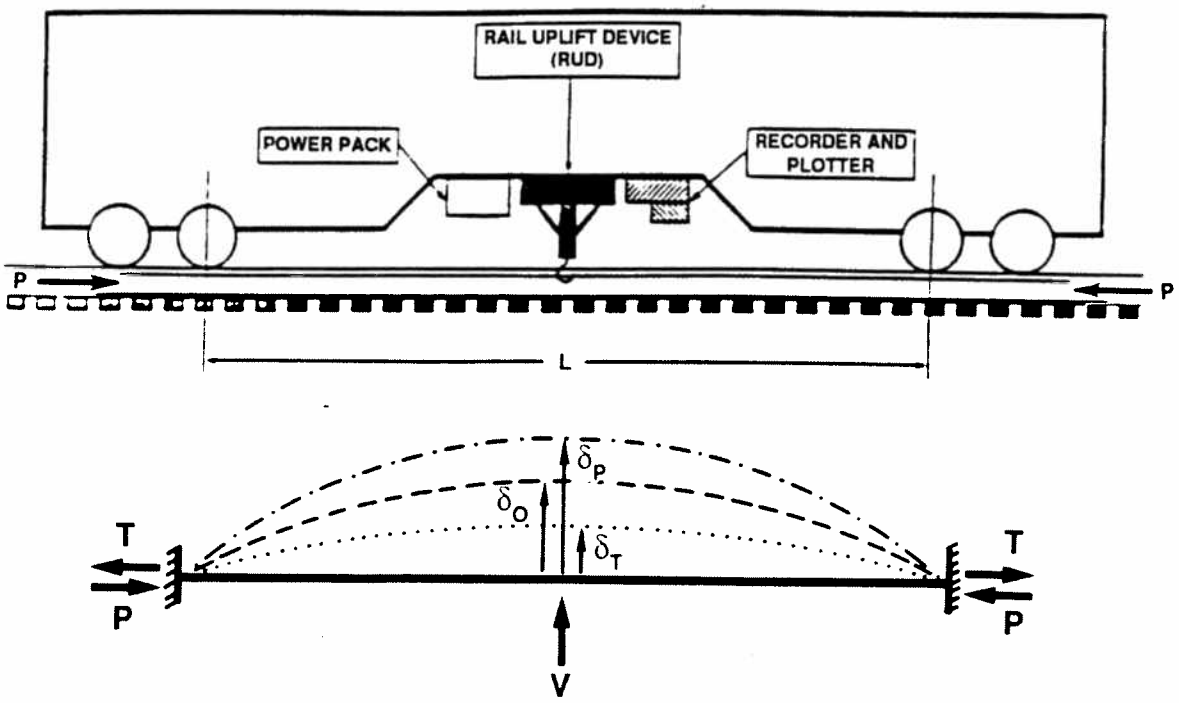

Figure E-1. Schematic of Rail Uplift Concept

MAJOR PARAMETERS:

* RAIL SIZE AND MOMENT OF INERTIA
* VERTICAL AND LONGITUDINAL TRACK STIFFNESS
* CAR PARAMETERS:
  (i) TRUCK CENTER SPACING
  (ii) AXLE SPACING
  (iii) VERTICAL WHEEL LOAD

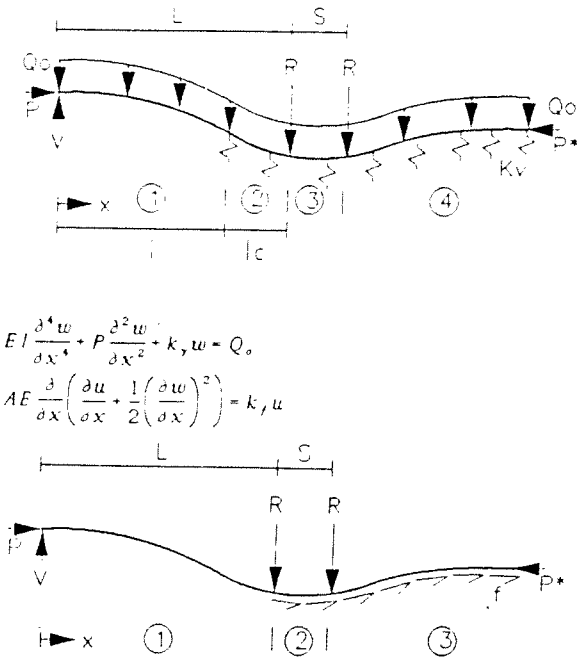

Figure E-2. Beam Bending - Rail Uplift Analysis

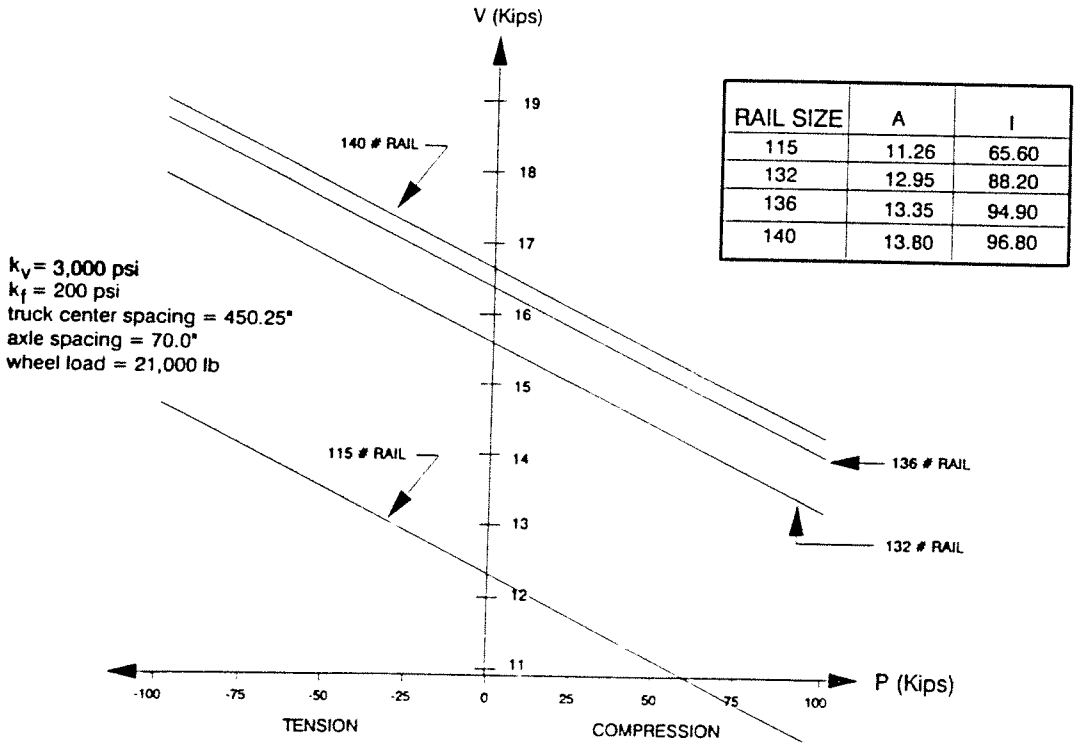

RAIL SIZE	A	I
115	11.26	65.60
132	12.95	88.20
136	13.35	94.90
140	13.80	96.80

Figure E-3. Rail Size Influence on Uplift Force versus Longitudinal Force (605 RFC Car) - 2-in. Deflection

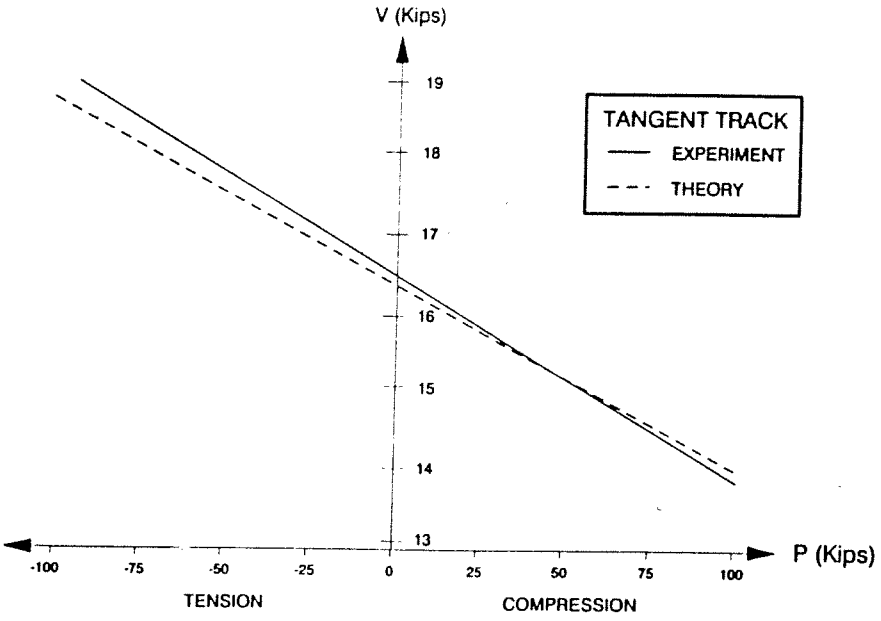

Figure E-4. Comparison of Theoretical and Experimental V versus P Behavior

technique is capable of determining the rail force within an error band of ±12.5 kips, which is tolerable in the buckling safety assessment.

Test data has also been collected on a 5-deg curve. The responses of high and low rails differ from one another and from that of the tangent, as seen in Figure E-5. Differences are attributed to the wheel load variations in high and low rails as well as difference in the "effective lengths" of the rail beam under the wheels. After theoretical allowance was made for the variations, there was good agreement with the recorded data on the curves. *Thus, the proposed technique is universal in application and does not need site-specific calibration for curves*, provided the super elevation is known. Some correction may also be needed in cases of excessive rail wear. The rail uplift concept has been recently incorporated into the Track Loading Vehicle (TLV) of the Association of American Railroads. This vehicle has been used on revenue service track successfully to map the rail neutral temperature variations on tangent and curved segments [9].

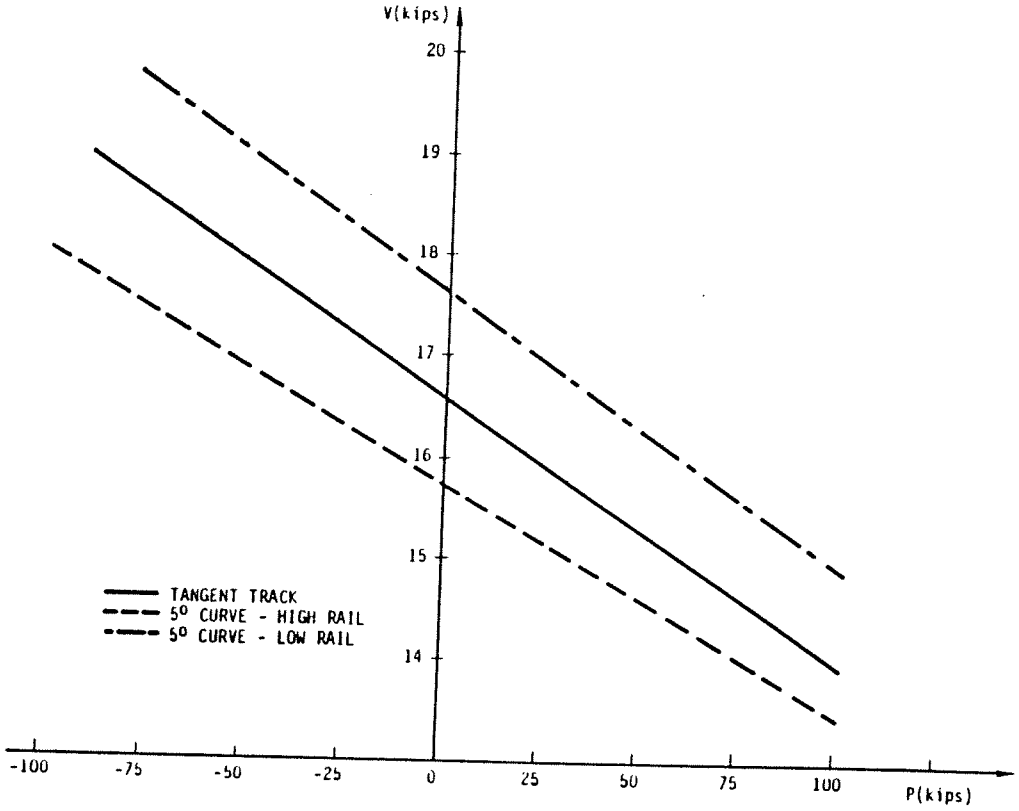

Figure E-5. Comparison of V versus P Regression Lines for Tangent and 5-deg Curve

PROPERTY OF FRA
RESEARCH & DEVELOPMENT
LIBRARY